# SMA-Induced Deformations in Unsymmetric Cross-Ply Laminates

by

Marie-Laure Dano

Thesis submitted to the Faculty of the
Virginia Polytechnic Institute and State University
in partial fulfillment of the requirements for the degree of
MASTER OF SCIENCE
in
Engineering Mechanics

APPROVED:

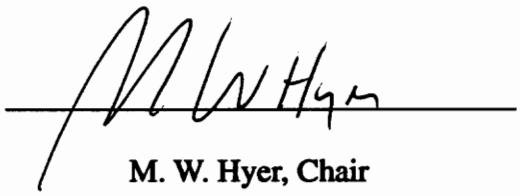

M. W. Hyer, Chair

E. R. Johnson

O. H. Griffin, Jr.

June, 1993

Blacksburg, Virginia

c.2

**SMA-Induced Deformations in Unsymmetric Cross-Ply Laminates**

by

Marie-Laure Dano

M. W. Hyer, Committee Chair

Engineering Mechanics

(ABSTRACT)

Presented is a model for predicting SMA-induced deformations in an unsymmetric cross-ply laminate. A previously developed theory is used to predict the room-temperature shape of the cross-ply laminate by minimizing its total potential energy. Then, using the principle of virtual work, equations relating the shape of the laminate to a force applied on supports fastened to the laminate are derived. Induced strains and displacements are predicted as a function of the applied force. Experiments where the force is generated by known weights are conducted. Good correlations are established between the experimental results and the predictions. The developed theory is able to predict with good accuracy the shape, strains and, displacements of an unsymmetric cross-ply laminate to the force applied on the laminate. This theory is then used to develop a model relating the laminate response to forces produced by a SMA actuator, the actuator being a SMA wire. To describe the mechanics of the SMA actuator, constitutive equations derived by other researchers are used. These constitutive equations relate the temperature of the wire to forces generated in it. Experiments where a SMA wire is used as an actuator are

conducted. These experiments consist of resistively heating a SMA wire attached to supports fastened to the laminate. During these experiments, laminate deformations are measured as a function of the applied voltage. Comparisons with the temperature-based constitutive model predictions are not made since the relation between the applied voltage and the SMA temperature is very difficult to establish. However, the experiments show that a SMA used in conjunction with cross-ply unsymmetric laminates can induce very large changes in the laminate shapes. Thus, the concept of using a SMA actuator to control the shape of cross-ply unsymmetric laminates is validated.

# Acknowledgments

The author would like to thank her advisor, Dr. M. W. Hyer, for direction and support throughout this work, and Dr. O. H. Griffin and Dr. E. R. Johnson, for their time and interest. Special thanks are due to Dr. Z. Chaudry and Dr. C. Liang, for their help in dealing with shape memory alloys. The author wishes to express her gratitude to Dr. J. R. Mahan, coordinator of the exchange program between Virginia Tech and the Université de Technologie de Compiègne, France, that permitted the author to enroll the Master's program of the Engineering Science and Mechanics Department. The partial financial support of grant NAG-1-901 with the NASA Langley Research Center is also appreciated. Finally, the author would like to thank her parents for their encouragement and support throughout her graduate studies.

# Table of content

# List of Illustrations

# List of Tables

# 1.0 Introduction and literature review

## *1.1 Introduction*

To date, unsymmetric laminates have rarely been made for structural purposes. They change shapes with temperature and moisture, and exhibit bending-stretching coupling. For these reasons, they are difficult to work with and are generally not used. However, it would be interesting from a structural point of view to use the shape of unsymmetric laminates to advantage. More especially, controlling their shape by controlling the residual thermal stresses could be an important issue in the use of unsymmetric laminates. In addition, their shapes may be further controlled by the use of smart materials like shape memory alloys (SMA) fastened on the surface of the composite.

The present work focuses on the use of SMA in conjunction with the inherent shape characteristics at room temperature of cross-ply unsymmetric laminates. The combination of SMA and unsymmetric laminate results in a structural configuration that can exhibit large changes in geometry.

Cross-ply unsymmetric laminates have different shapes, depending on their size and on temperature. At curing temperature, they are flat. By cooling them to room temperature, differences in thermal expansion in the different lamina cause the laminate to warp out of

plane. Depending on its length, the laminate takes a saddle shape or one of two cylindrical shapes. For example, a square $(0_2/90_2)_T$ laminate of sufficient length L has two stable cylinder shapes, one with curvature in x direction and one with curvature in y direction, as shown, respectively, in Fig. 1-1(a) and in Fig. 1-1(b). The laminate can be changed from one configuration to the other by a simple snap-through action initiated through the application of forces or moments. These forces or moments could be applied by SMA wires fastened to the top and bottom surface of the laminate and used as actuators. This is depicted in Fig. 1-2.

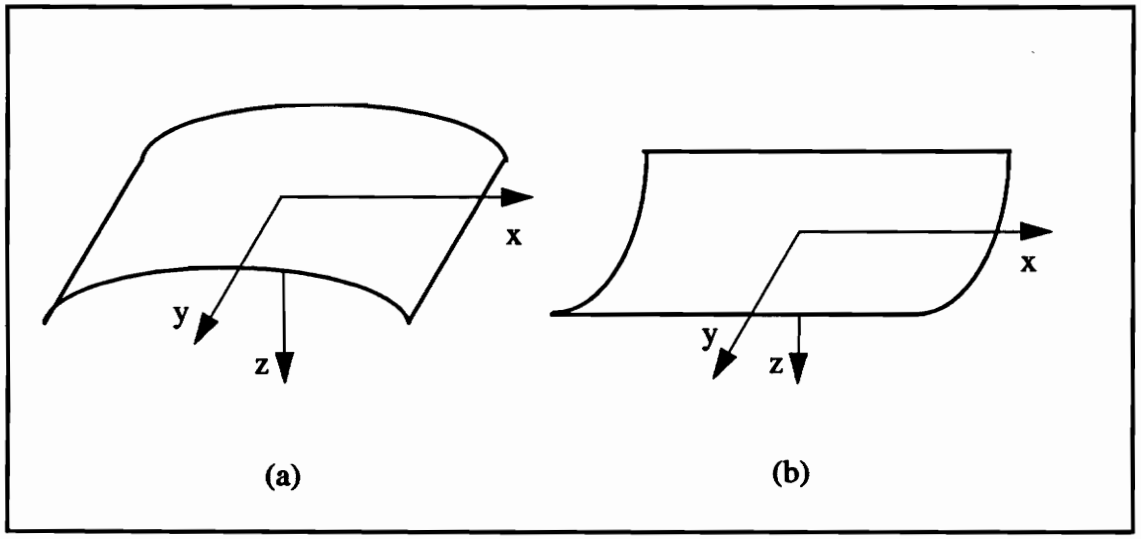


**FIG. 1-1. Shapes of a $(0_2/90_2)_T$ laminate**

Figure 1-2 shows two pairs of supports attached to the unsymmetric laminate, one pair on the top surface and one pair on the bottom surface. Each support is attached to the laminate and is oriented perpendicular to the surface of the laminate. In Fig. 1-2 the top pair of supports are in the x-z plane. SMA wires are plastically stretched parallel to the x-axis, and fastened to each pair of supports. When resistively heated by applying voltage, the plastically deformed SMA wire tries to recover its original shape and shrinks. Since the wire is restrained it is not able to contract freely and thus forces are generated into the wire.

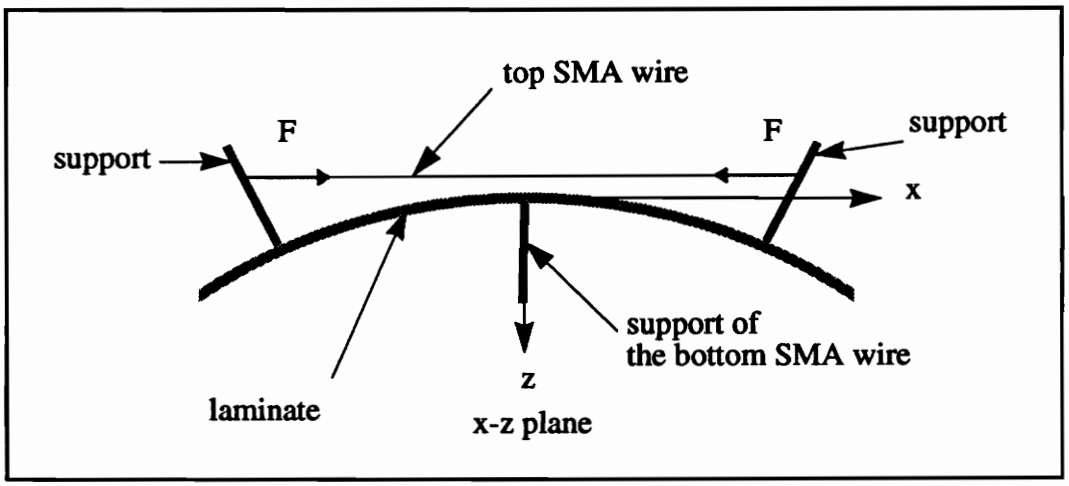


**FIG. 1-2. System description**

Thus, starting with a laminate with the curvature in the x direction, Fig. 1-3(a), the SMA wire fastened on the top surface of the laminate can be activated to generate a force F. The force produces a moment M which makes the laminate curvature decrease. For a great enough voltage, the laminate will snap to another cylinder with the curvature in the y direction, as depicted in Fig. 1-3(b). Then, by activating the SMA wire fastened on the bottom surface of the laminate, the laminate will snap back to its initial shape, Fig. 1-3(b).

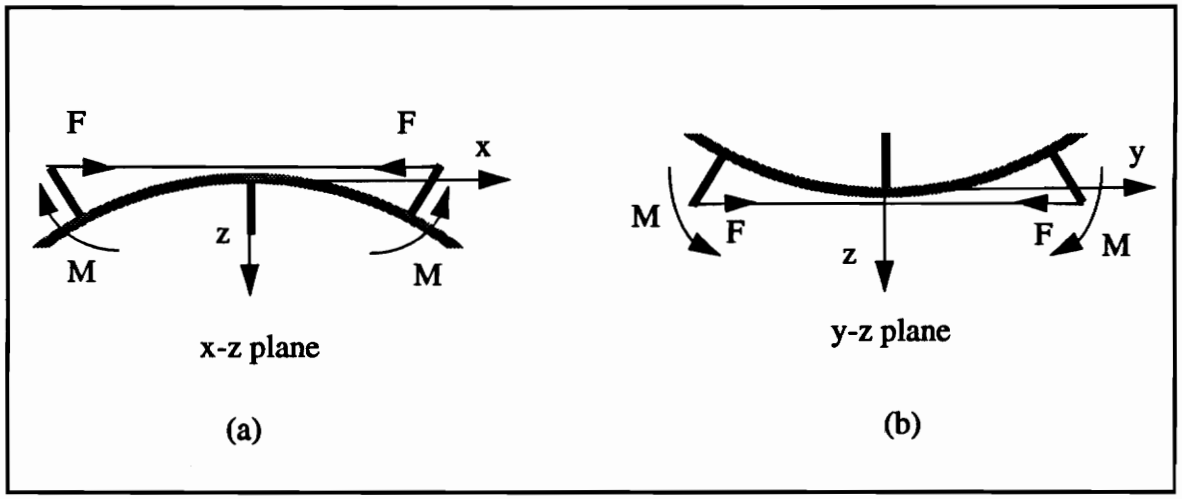


**FIG. 1-3. Concept description**

The objective of this work is to develop a constitutive model of the mechanical system consisting of a laminate and SMA wires to be able to predict the room-temperature shape of unsymmetric laminates as a function of the temperature the SMA wires are heated to. A previously-developed theory is used to describe the mechanics of the cross-ply laminates due to a temperature change. This theory, presented in chapter 2, predicts the room-temperature shape of cross-ply laminate by minimizing the total potential energy of the laminate. In chapter 3, equations relating the shape of the laminate to an applied force are derived, using the principle of virtual work. The force level which makes the laminate snap is determined. Induced strains and displacements are predicted as a function of the force F. Chapter 4 describes an experiment used to check the predicted strains and displacements. In these experiments the forces are applied by using known weights. This setup offers the advantage of knowing exactly the force level applied and having only the mechanics of the laminate involved. Then, in chapter 5, equations describing the mechanics of the laminate subjected to a SMA-induced force are presented. Constitutive equations derived by researchers working in the area of SMA's are used to describe the mechanics of SMA wires. Though the SMA wires are generally attached to the laminate as shown in Fig. 1-2, limits on the capabilities of SMA materials require that the concept shown in Fig. 1-2 must be somewhat modified. This is discussed in chapter 5. Since existing models relate force to temperature, relations are established between the force generated in the wire and the temperature in the SMA wire, and between the shape of the laminate and the temperature in the SMA wire. Experiments, where the force is generated by a SMA wire, are described in chapter 6. However, measuring temperature is difficult and thus relations between voltage in the SMA wire and the force would be desirable. Limited knowledge of heat transfer coefficients and other important data prevent such a relationship from being established for the application being studied here. Thus, in the final analysis, though empirical relations between laminate curvature and voltage applied to the SMA wire are presented, it is not possible to correlate the theory developed with observations. However, if temperature, and thus force, is considered to be proportional to

the voltage, then the general concept of controlling laminate shape with SMA materials is validated, and it becomes clear where further efforts must be focused. These and other details are discussed in chapter 6. Finally, the last chapter will present a summary of this work and recommendations for future work.

## *1.2 Literature review*

### 1.2.1 Unsymmetric laminates

To date unsymmetric laminates are mostly used to evaluate the stress-free temperature of a material system, or the influence of environmental factors like moisture or temperature on material behavior. For example, Pagano and Hahn [1] used the shape of unsymmetric laminates to evaluate curing stresses.

The most common theory to predict the shape of unsymmetric laminates is the classical lamination theory. This is a linear theory using the following assumptions:

- continuous displacement throughout the laminate
- undeformed normal (Kirchhoff hypothesis)
- linear strain-displacement relationship
- linearly elastic material
- small through-the-thickness stresses compared to the inplane stresses (plane stress assumption)

This theory was used by several researchers [2-4] to study the response of unsymmetric laminates in static, dynamic, bending and buckling. In many cases the theory outlined above is not always able to predict the correct room-temperature curvature of

unsymmetric laminates. Classical lamination theory predicts two equal and opposite curvatures, namely, a saddle shape. In contrast, the room-temperature shapes of unsymmetric laminates are often cylindrical. Moreover, most of them can take a second cylindrical shape by a way of simple snap-through action. Thus, in general, classical lamination theory can not be applied to unsymmetric laminates to predict the correct shape. The most obvious reason why classical lamination theory can not be used is that the assumption of linear strain-displacement relationship is not valid with unsymmetric laminates. Indeed, unsymmetric laminates involve geometric nonlinearities which must be taken into account. Thus, classical lamination theory has to be extended to include these nonlinearities. Hyer [5-8] did this by developing a nonlinear theory which predicted the correct shape of cross-ply laminates. This theory is used in the present study and is explained in chapter 2.

Dang [9] generalized Hyer's theory, which was restricted to cross-ply unsymmetric laminates, to more general unsymmetric laminates.

### 1.2.2 Shape memory alloys

Shape memory alloys are special alloys, which after being deformed, can recover their original shape when heated. The strain recovering process is associated with a solid-to-solid martensite phase transformation, which is activated when the temperature reaches the phase transformation temperature. Plastic strains up to 8% can be recovered by heating the shape memory alloy. In the recovery process, very large stress can be generated by the SMA, which is often used as an actuator.

One of the most common shape memory alloys is Nitinol. Nitinol is a Nickel Titanium alloy developed at the Naval Ordinance Laboratory in the late 1950's. In the name Nitinol,

Ni stands for Nickel, Ti for Titanium, NOL for Naval Ordnance Laboratory. Nitinol exhibits phenomenal recovery of plastic strains. Moreover, Nitinol exhibits high corrosion resistance and excellent fatigue behavior. Thus, Nitinol is an excellent mechanical actuator. However, when mechanical performance is not a priority and cost is important, copper based-shape memory alloys are used. Their cost is one-tenth of the cost of Nitinol, but their maximum recovery strain is only about 4%.

Since the discovery of Nitinol, numerous efforts have been made to explain and describe shape memory behavior. Müller [10] proposed in1979 a model based on shape memory effect phenomenology, thermodynamics, and statistical physics. A few years later, in 1982, Tanaka [11] derived a model based on Müller's in which the minimization of the free energy governs the martensite transformation. These models provide a satisfying explanation of the physical nature of shape memory alloys but are limited since they can not quantitatively predict shape memory behavior.

Based on Tanaka's work, Liang and Rogers [12-13] derived a thermomechanical constitutive model of shape memory effect. The proposed equation, relating the stress, strain, temperature and martensite fraction, accurately describe the martensite-temperature relation and therefore can correctly predict the stress-strain relation and SMA behavior.

Liang and Rogers' model is used in this work to quantify the shape memory wires' effects on the unsymmetric laminate. Details of SMAs will be discussed more in chapter 5.

# 2.0 Mechanics of cross-ply unsymmetric laminate under temperature change

This chapter presents a nonlinear theory, developed by Hyer [5-8], which is able to predict the shape of cross-ply unsymmetric laminates. The theory accounts for the laminate characteristics (stacking sequence, elastic and thermal properties, length and thickness) and the environmental conditions (temperature, moisture). The theory is based on a minimization of the laminate's total potential energy. The total potential energy will be written in terms of laminate displacements. Since the problem is nonlinear, laminate displacements are approximated, using a Rayleigh-Ritz approach, by polynomials with unknown coefficients. Then, by taking the first variation of the approximate energy expression, equilibrium equations are obtained in terms of the unknown coefficients. Finally, by taking the second variation of the approximate energy expression, stability equations are derived and stability of equilibrium can be examined.

## 2.1 *Problem formulation*

Consider a square cross-ply unsymmetric laminate of dimension L by L, as shown in Fig. 2-1. The thickness of the laminate is denoted by H, and the thickness of a single ply, by h.

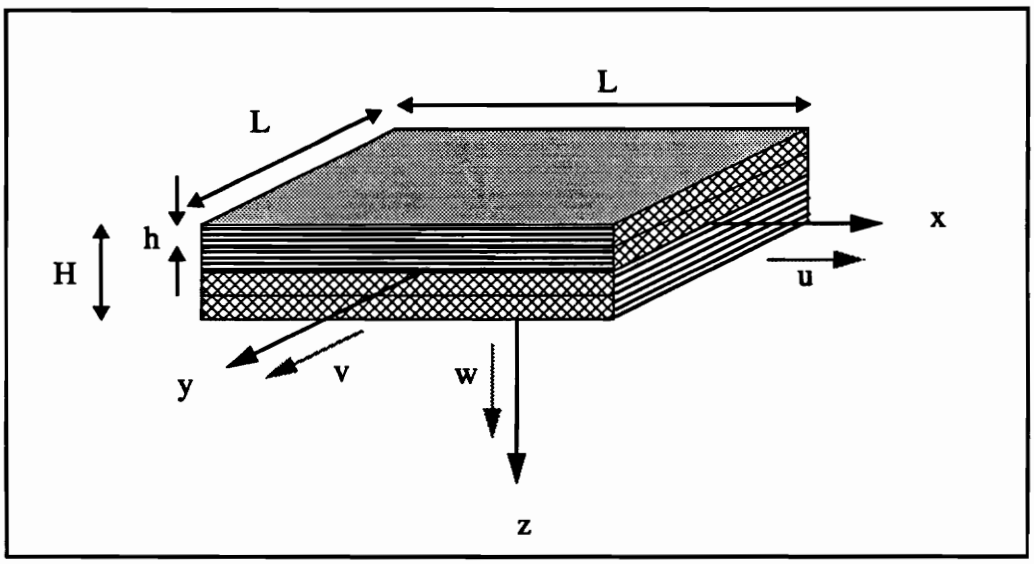


**FIG. 2-1. Laminate's dimensions and coordinate systems**

Upon cooling to room temperature, the laminate does not remain flat, but rather will have different shape configurations, as shown in Fig. 2-2. At the curing temperature, the laminate is flat, as shown in Fig. 2-2(a). By cooling it to room temperature, differences in thermal expansion in the different lamina cause the laminate to warp out of the plane. Depending on its length, the laminate takes a saddle shape, like classical lamination theory predicts, Fig. 2-2(b), or one of two cylindrical shapes, Fig.2-2(c) or Fig. 2-2(d). In fact, the laminate takes the shape which minimizes its total potential energy. Thus, by computing the total potential energy of the laminate and by looking for its minimum, the correct shape can be predicted.

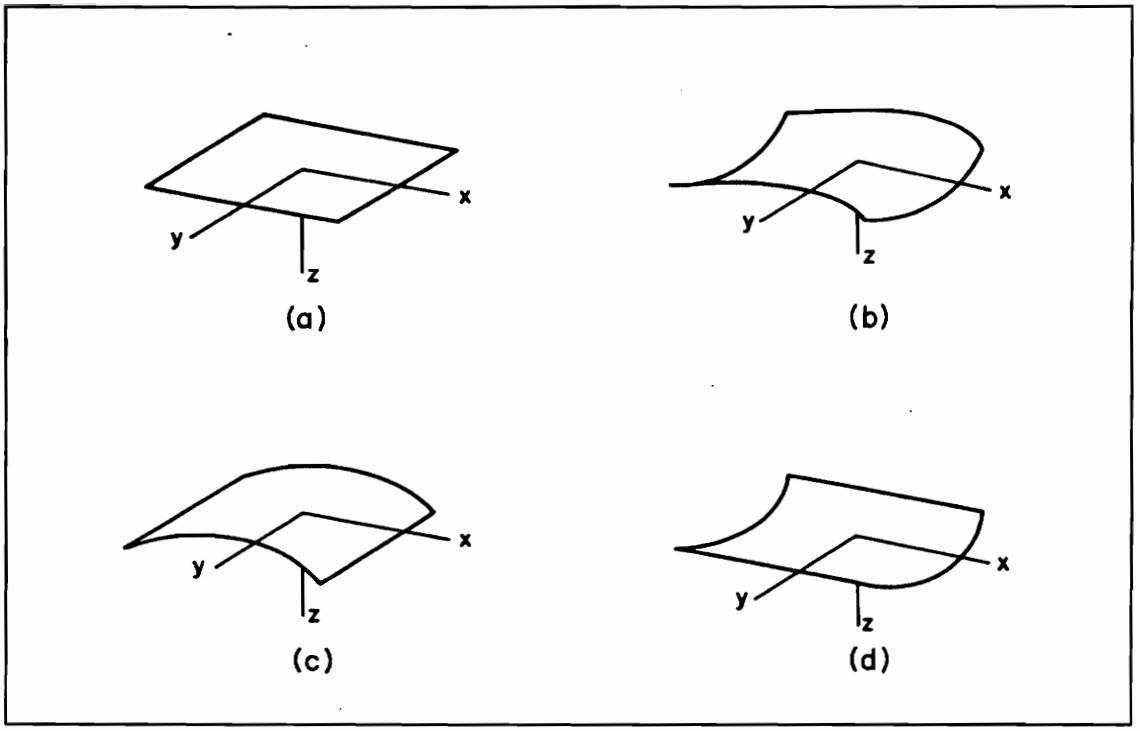


**FIG. 2-2. Shape of cross-ply unsymmetric laminates**

The x-y-z coordinate system which is used to compute the total potential energy and analyze the laminate is the one shown in Figs. 2-1 and 2-2. The z-axis is associated with the out-of-plane direction and x and y are in the plane of the laminate when it is flat at its cure temperature. The displacements in the x, y, z directions are, respectively, denoted u, v, w.

## 2.2 *Total potential energy*

For a square unsymmetric laminate of length L and thickness H, the total potential energy of the laminate is expressed by

$$\Pi = \frac{1}{2}\int_{-\frac{L}{2}}^{\frac{L}{2}}\int_{-\frac{L}{2}}^{\frac{L}{2}}\int_{-\frac{H}{2}}^{\frac{H}{2}} \{ (\sigma_x - \sigma_x^T)\,\varepsilon_x + (\sigma_y - \sigma_y^T)\,\varepsilon_y + (\tau_{xy} - \tau_{xy}^T)\,\gamma_{xy} \}\, dxdydz, \tag{2.1}$$

where $\sigma_x$, $\sigma_y$, $\tau_{xy}$ are the mechanical stresses and $\sigma_x{}^T$, $\sigma_y{}^T$, $\tau_{xy}{}^T$ the equivalent thermal stresses. Hooke's Law can be stated as

$$\{\sigma\} = [Q]\begin{Bmatrix} \varepsilon_x - \varepsilon_x^T \\ \varepsilon_y - \varepsilon_y^T \\ \gamma_{xy} - \gamma_{xy}^T \end{Bmatrix}$$
$$\{\sigma^T\} = [Q]\begin{Bmatrix} \varepsilon_x^T \\ \varepsilon_y^T \\ \gamma_{xy}^T \end{Bmatrix}, \tag{2.2}$$

where $\varepsilon_x$, $\varepsilon_y$, $\gamma_{xy}$ are the total strains and are given by

$$\begin{aligned} \varepsilon_x &= \varepsilon_x^o + z\kappa_x^o \\ \varepsilon_x &= \varepsilon_x^o + z\kappa_x^o \\ \gamma_{xy} &= \gamma_{xy}^o + z\kappa_{xy}^o, \end{aligned} \tag{2.3}$$

and $\varepsilon_x{}^T$, $\varepsilon_y{}^T$, $\gamma_{xy}{}^T$ are the equivalent thermal strains and are given by

$$\{\varepsilon^T\} = \{\alpha\}\,\Delta T, \tag{2.4}$$

where $\{\alpha\}$ is the thermal deformation coefficient vector and $\Delta T$ is the temperature change.

The quantities $\varepsilon_x^o$, $\varepsilon_y^o$, $\gamma_{xy}^o$, $\kappa_x^o$, $\kappa_y^o$, $\kappa_{xy}^o$ are defined as

$$\begin{aligned}
\varepsilon_x^o &= \frac{\partial u^o}{\partial x} + \frac{1}{2}\left(\frac{\partial w^o}{\partial x}\right)^2 \\
\varepsilon_y^o &= \frac{\partial v^o}{\partial y} + \frac{1}{2}\left(\frac{\partial w^o}{\partial y}\right)^2 \\
\gamma_{xy}^o &= \frac{\partial u^o}{\partial y} + \frac{\partial v^o}{\partial x} + \frac{\partial w^o}{\partial x}\frac{\partial w^o}{\partial y} \\
\kappa_x^o &= -\frac{\partial^2 w^o}{\partial x^2} \\
\kappa_y^o &= -\frac{\partial^2 w^o}{\partial y^2} \\
\kappa_{xy}^o &= -2\frac{\partial^2 w^o}{\partial x \partial y},
\end{aligned} \tag{2.5}$$

where $u^o$, $v^o$, $w^o$ are the midplane field displacements. Here these quantities are evaluated using approximations based on observations of the cooled laminate shapes shown in Fig. 2-2. These approximations are

$$\begin{aligned}
u^o(x,y) &= cx - a^2\frac{x^3}{6} - ab\frac{xy^2}{4} \\
v^o(x,y) &= dx - b^2\frac{y^3}{6} - ab\frac{yx^2}{4} \\
w^o(x,y) &= \frac{1}{2}(ax^2 + by^2),
\end{aligned} \tag{2.6}$$

where the coordinates x and y are measured from the geometric center of the laminate, as shown in Figs. 2-1 and 2-2. In the expressions of the field displacements, a and b represent, respectively, the curvatures in the x and y directions. The parameters c and d represent, respectively, the portion of the strains in the x and y directions that are

independent of spatial location in the laminate. These strains are associated with the laminate coefficients of thermal deformation. These four variables define completely the shape of the laminate. Thus, the total potential energy of the laminate can be expressed as a function of a, b, c, d. That is,

$$\Pi = \Pi(a, b, c, d). \tag{2.7}$$

As the temperature is decreased from the curing temperature, $\Delta T<0$, the laminate assumes the shape that minimizes its potential energy. That shape can be predicted by determining the minimum of the potential energy and its associated variables values a, b, c, d. To determine the minimum of the energy function, the first variation of the total potential energy is computed and set to zero to obtain equilibrium equations.The equilibrium equations are written in terms of a, b, c, d. By solving them, a, b, c, d can be evaluated and the shape of the laminate predicted as a function of $\Delta T$.

## *2.3 Minimization of the total potential energy*

### 2.3.1 Variation of the total potential energy

By using small increments $\varepsilon a_1$, $\varepsilon b_1$, $\varepsilon c_1$, $\varepsilon d_1$, $\varepsilon$ being a small scalar and $a_1$, $b_1$, $c_1$, $d_1$ being increments in the value of a, b, c, d, in the expression of the total potential energy, the increment in energy can be obtained.This increment can be expressed as

$$\Pi(a+\varepsilon a_1, b+\varepsilon b_1, c+\varepsilon c_1, d+\varepsilon d_1) = \Pi(a, b, c, d) + \Delta\Pi, \tag{2.8}$$

where $\Pi$(a, b, c, d) is the original energy and $\Delta\Pi$ the variation of the total potential energy.

The variation $\Delta\Pi$ can be written as

$$\Delta\Pi = \varepsilon\Pi_1 + \varepsilon^2\Pi_2 + \varepsilon^3\Pi_3 + \ldots, \tag{2.9}$$

where $\Pi_1$, $\Pi_2$,and $\Pi_3$ are, respectively, the first, second, and third variation of $\Pi$ with respect to a, b, c, d. The variations are functions of a, $a_1$, b, $b_1$, c, $c_1$, d, $d_1$.

### 2.3.2 Equilibrium equations

The laminate is at equilibrium when the first variation is equal to zero for every increment $a_1$, $b_1$, $c_1$, $d_1$. The first variation can be expressed as

$$\begin{aligned}\Pi_1 = {} & \{f_a(a,b,c,d)\}\, a_1 + \{f_b(a,b,c,d)\}\, b_1 + \\ & \{f_c(a,b,c,d)\}\, c_1 + \{f_d(a,b,c,d)\}\, d_1 \cdot\end{aligned} \tag{2.10}$$

Thus, having $\Pi_1$=0 for every possible increment $a_1$, $b_1$, $c_1$, $d_1$, implies

$$\begin{aligned} f_a(a,b,c,d) &= 0 \\ f_b(a,b,c,d) &= 0 \\ f_c(a,b,c,d) &= 0 \\ f_d(a,b,c,d) &= 0 \cdot \end{aligned} \tag{2.11}$$

The above equations are the equilibrium equations of the laminate. They are functions of laminate geometry, laminate material properties, and the temperature change. By solving them, a, b, c, d, can be determined for a given laminate and the equilibrium shapes of the laminate can be predicted. Moreover, it is possible from Eq. (2.11) to find expressions for c and d in term of a and b.

Symbolically,

$$\begin{aligned} f_a(a,b,c,d) &= 0 \\ f_b(a,b,c,d) &= 0 \\ f_c(a,b,c,d) &= 0 \\ f_d(a,b,c,d) &= 0 \end{aligned} \quad \longleftrightarrow \quad \begin{aligned} f_a(a,b) &= 0 \\ f_b(a,b) &= 0 \\ c &= c(a,b) \\ d &= d(a,b)\,. \end{aligned} \tag{2.12}$$

Then, by substituting the expressions for c and d in terms of a and b into in the total potential energy function, the energy function becomes only a function of a and b. Plotting the energy as a function of a and b, it is possible to visually localize the minimums of the energy function. It turns out that, depending on the geometry of the laminate, either one or three real solutions are found from the equilibrium equations, corresponding to either one or three different shapes. As depicted in Fig. 2-2, one shape is a saddle and the other two are cylindrical. Thus, as unsymmetric laminates are observed to have either a saddle shape or one of two cylindrical shapes, the stability of these solutions need to be studied.

### 2.3.3 Stability

An equilibrium configuration is considered to be stable if the second variation of the total potential energy ($\Pi_2$ in Eq. (2.9)) is positive definite. For the present problem, $\Pi_2$ can be expressed in quadratic form as

$$\Pi_2 = \frac{1}{2}\begin{bmatrix} a_1 & b_1 & c_1 & d_1 \end{bmatrix} \begin{bmatrix} k_{11} & k_{12} & k_{13} & k_{14} \\ k_{12} & k_{22} & k_{23} & k_{24} \\ k_{13} & k_{23} & k_{33} & k_{34} \\ k_{14} & k_{24} & k_{34} & k_{44} \end{bmatrix} \begin{bmatrix} a_1 \\ b_1 \\ c_1 \\ d_1 \end{bmatrix}. \tag{2.13}$$

The second variation $\Pi_2$ is positive definite if the principal minors of the K matrix are all positive. Using this criterion, it is indeed found that some solutions are unstable. Depending on the size of the laminate, the saddle shape is stable and the two cylindrical shapes do not exist. Alternatively, for laminates of other sizes, the saddle shape and the two cylindrical shapes exist, but the saddle shape is unstable.

## *2.4 Numerical example*

Consider a square $(0_2/90_2)_T$ graphite-epoxy laminate with the following typical properties

$$
\begin{aligned}
&0 \le L \le 12 \text{ in.} \\
&h = 0.006 \text{ in.} \\
&E_1 = 20.0 \text{ Msi} \\
&E_2 = 1.3 \text{ Msi} \\
&G_{12} = 1.03 \text{ Msi} \\
&\nu_{12} = 0.3 \\
&\alpha_1 = -0.167\ 10^{-6}\ /^{o}\text{F} \\
&\alpha_2 = 15.6\ 10^{-6}\ /^{o}\text{F}.
\end{aligned}
\tag{2.14}
$$

By solving Eq. (2.12), in terms of a and b for a length L varying from 0 to 12 in., relations between the curvatures a and b and the laminate length L can be obtained. Such a relationship is illustrated in Fig. 2-3. In Fig. 2-3 it is important to note the existence of length $L_b$. For $L<L_b$, where b stands for bifurcation, only one solutions exists. For this solution the curvatures a and b are unique and a=-b Fig. 2-2(b). The shape of the laminate

can only be a saddle and it is stable.

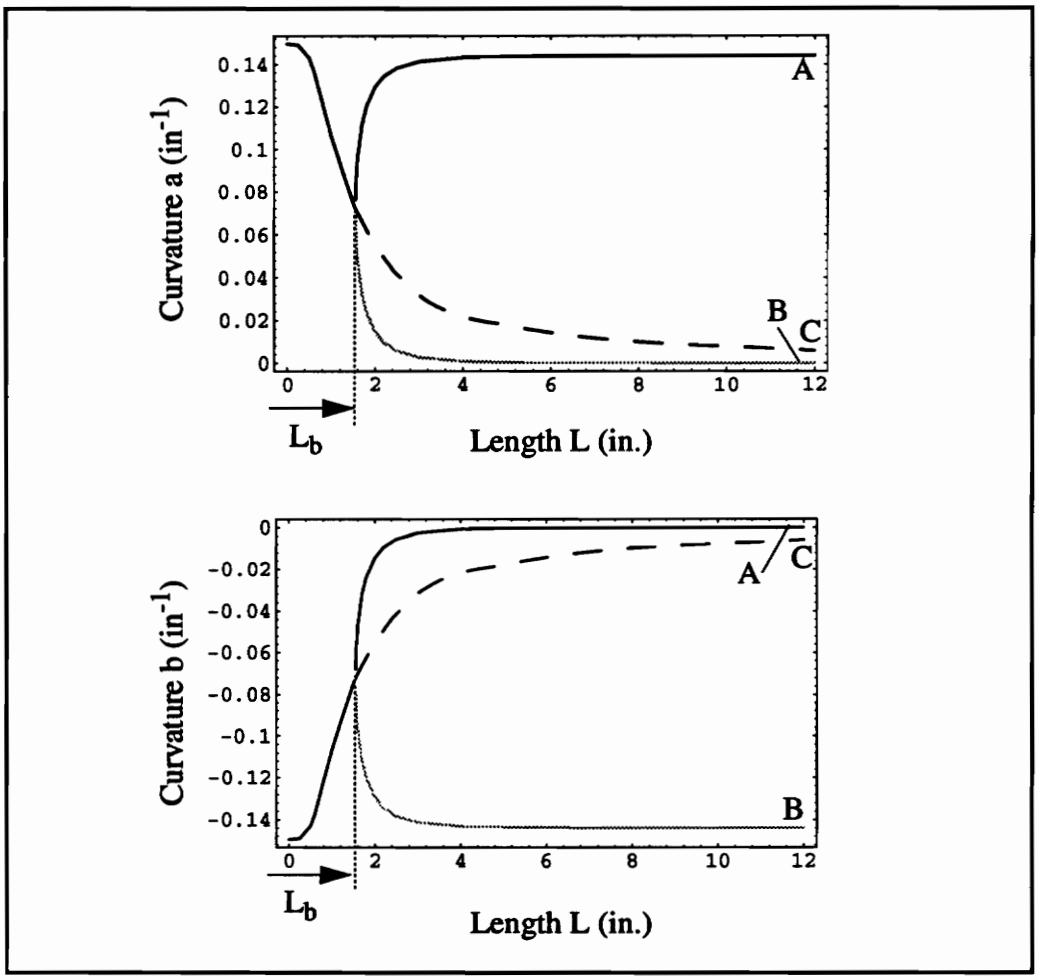


**FIG. 2-3. Curvatures in the x and y direction as a function of the length of the laminate**

For $L>L_b$, three solutions are found. Two solutions correspond to two cylindrical shapes. One is a cylinder with the curvature in x direction, Fig. 2-2(c) and the solid black line, and the other is a cylinder with the curvature in the y direction, Fig. 2-2(d) and the solid grey line. Another solution exists and it corresponds to a saddle shape, Fig. 2-2(b) and the dashed line. By studying stability, it is found that the saddle shape is unstable and the cylindrical shapes are stable. In Fig. 2-3, the points A, B, and C are for purposes of a

discussion to be presented in chapter 3.

In case L is exactly equal to $L_b$, L=1.5535 in., stability analysis shows that the unique saddle shape is unstable!

Considering the total potential energy function, it is interesting to plot Π vs. a and b for the three cases just discussed, i.e., $L<L_b$, $L>L_b$, $L=L_b$.

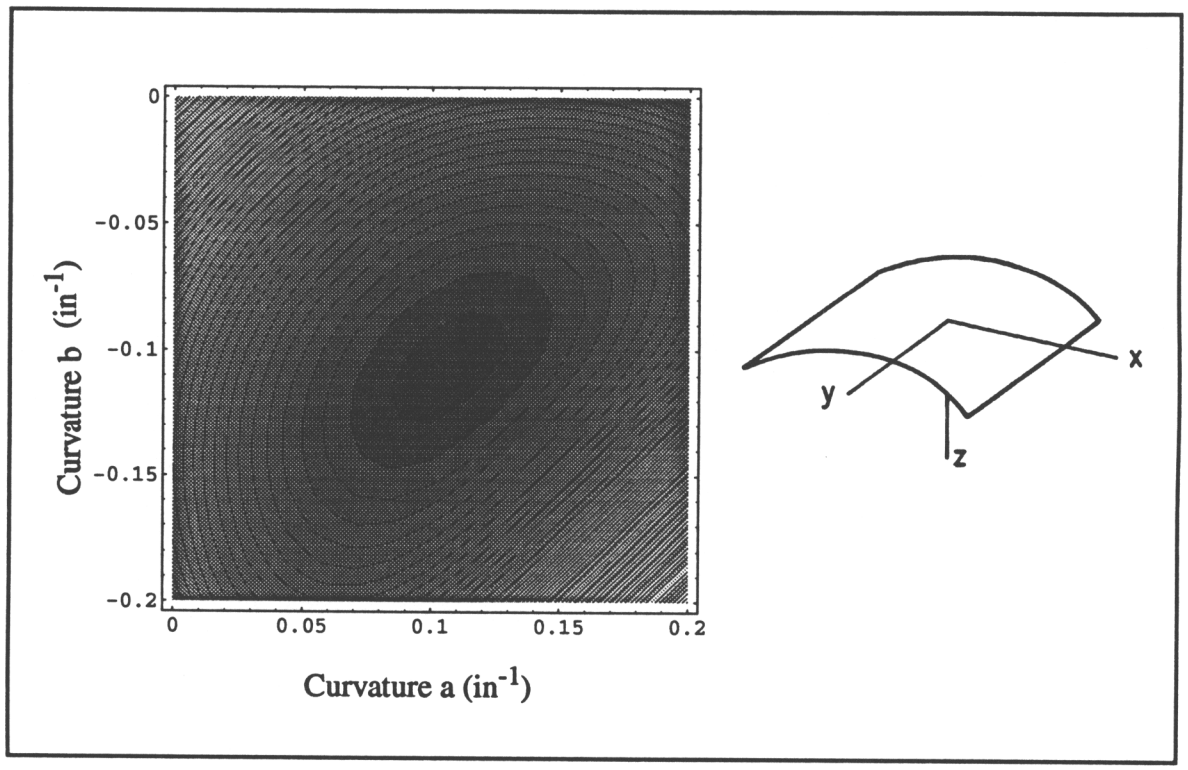


**FIG. 2-4. Contour plot of the energy function for L=1 in.**

Figure 2-4 shows a contour plot of the total potential energy for $L<L_b$, specifically, L=1 in. The figure confirms the existence of a unique minimum.The potential energy has a minimum at a=-b=0.11 in$^{-1}$. This corresponds to a stable saddle shape.

As shown in Fig. 2-5(a) and 2-5(b), respectively, for a 12 in. by 12 in. unsymmetric laminate, the total potential energy function shows two minimums, one at a=0.1439 $in.^{-1}$, b~0, and the other at a~0, b=-0.1439 $in.^{-1}$.This 12 in. by 12 in. laminate has also a saddle point at a=0.0057$in.^{-1}$, b=-0.0057$in.^{-1}$, as illustrated in Fig. 2-6. Each minimum corresponds to a different stable cylinder shape, the first with curvature in x direction and the second with curvature in the y direction. The laminate can go from one cylinder shape to the other by a simple snap-through action. It is interesting to note that to make the laminate change shape, the laminate's total potential energy has to be increased by the action of external forces. At some point during the application of the forces, the laminate attains an unstable equilibrium configuration and moves suddenly away from this configuration to another stable configuration, which is the other cylindrical shape.

For the very special case where $L=L_b$, the total potential energy, Fig. 2-7, does not seem to have a distinct minimum, but rather a cylindrical shaped minimum. This cylindrical minimum is shown more clearly in Fig. 2-8. Figure 2-8 shows the variation in the potential energy function along the F and G planes, the planes being indicated in Fig. 2-7.

In the F plane, the energy function does have a unique minimum. However, in the G plane, the energy function has no distinct minimum (straight line). Thus, for $L=L_b$, the potential energy function has a cylindrical shape and it can be said that the laminate has no stable shape.

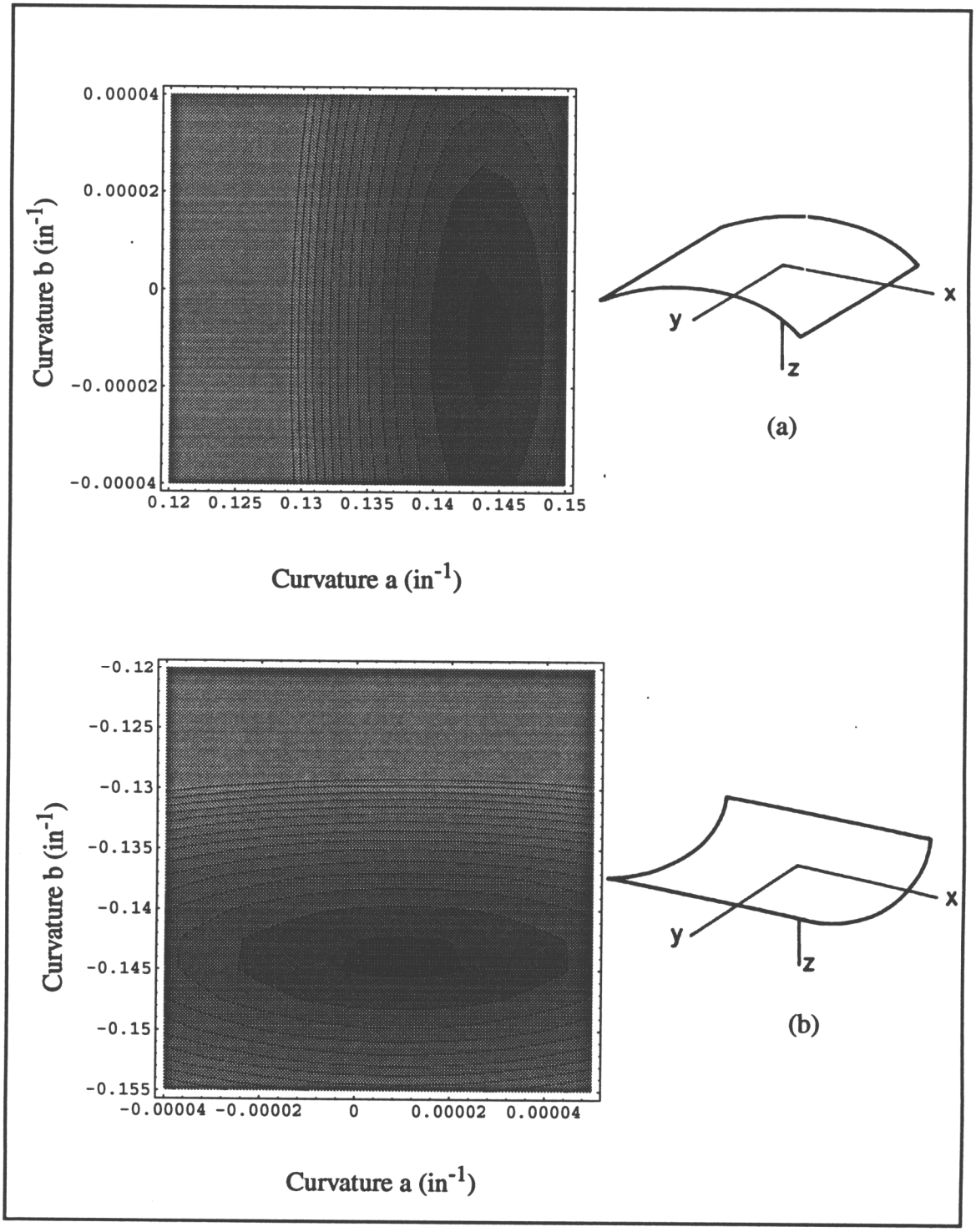


**FIG. 2-5. Minimums of the potential energy for L=12 in.**

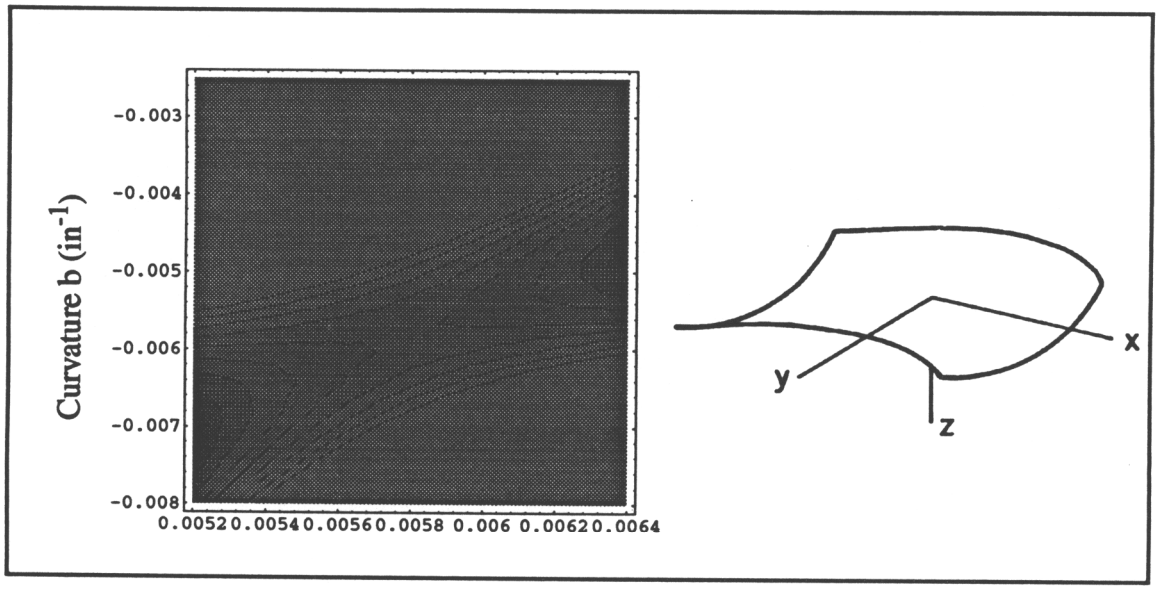


**FIG. 2-6. Saddle point of the potential energy function for L=12 in.**

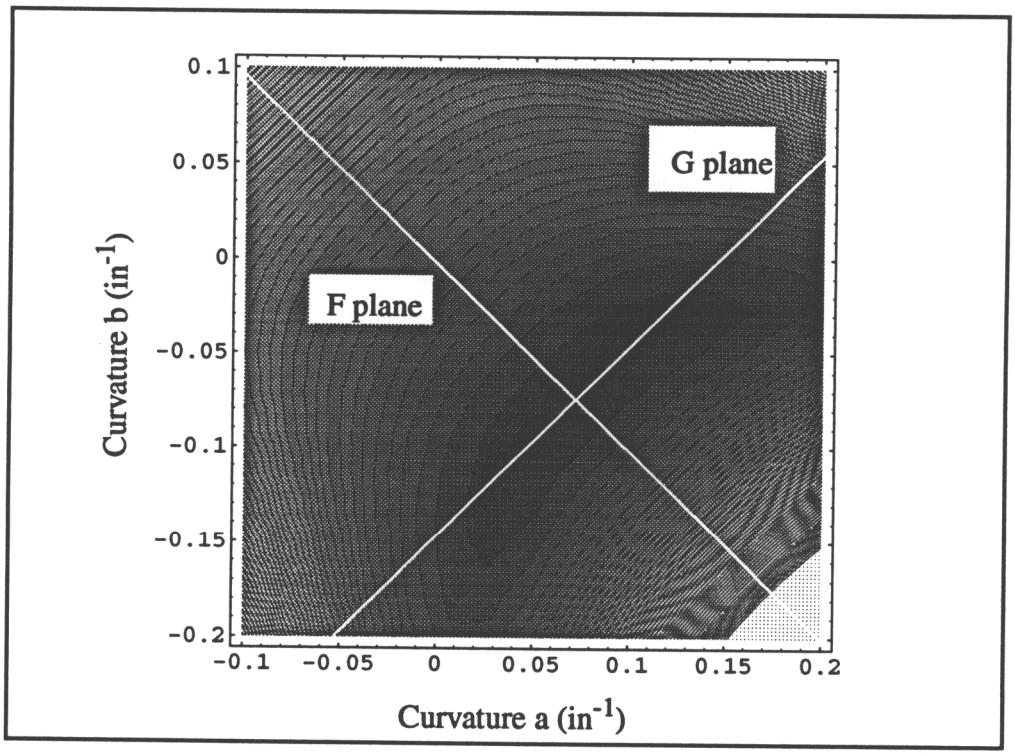


**FIG. 2-7. Potential energy for $L=L_b$**

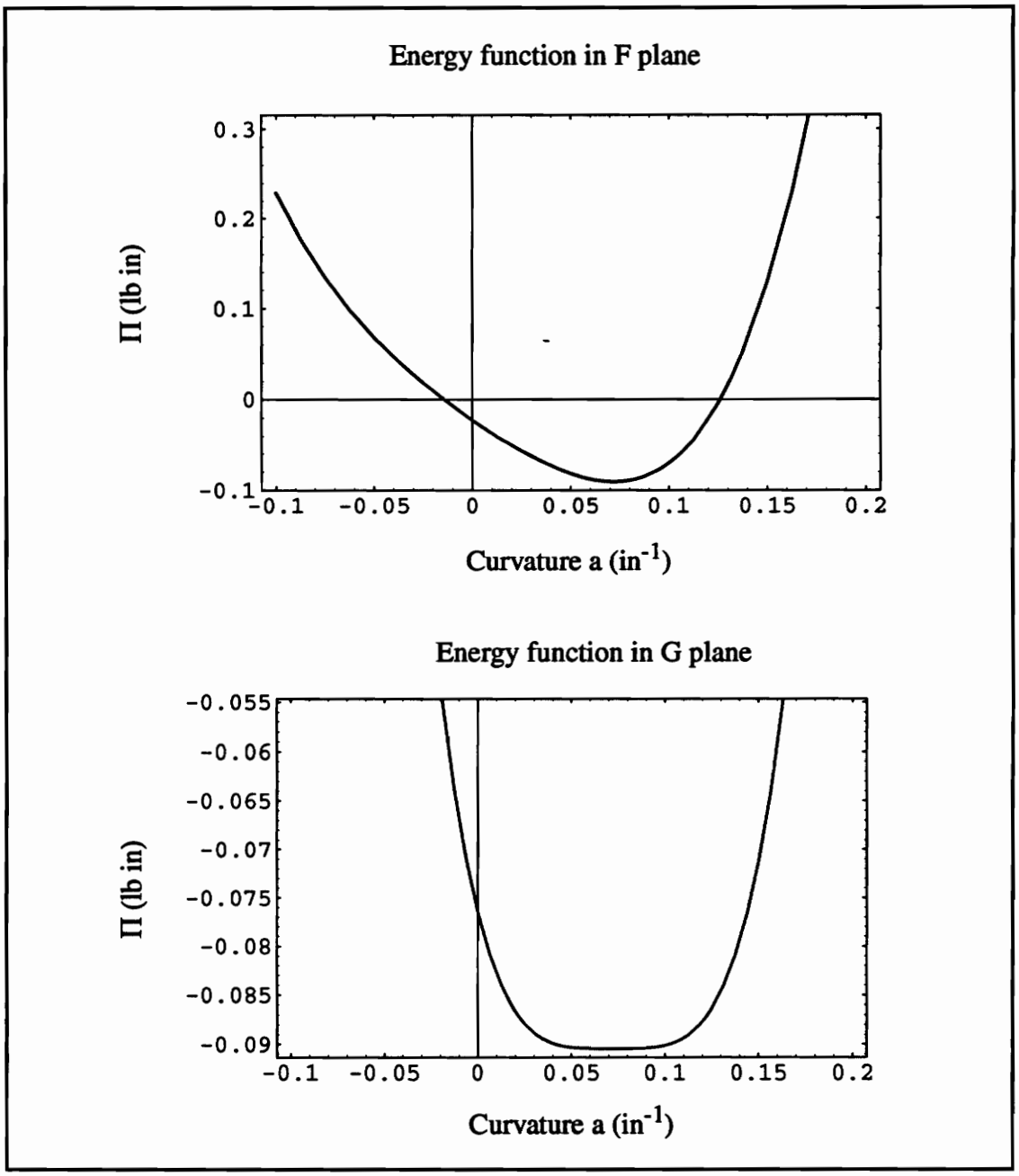


**FIG. 2-8. Cylindrical bottom of the potential energy function for $L=L_b$**

Thus, in summary, using the nonlinear theory derived by Hyer, the shape of a cross-ply unsymmetric laminate can be predicted. The laminate, depending on its size, takes either a

saddle shape or cylindrical shapes. More specifically, a square $(0_2/90_2)_T$ laminate with side length L greater than $L_b$ has two stable cylinder shapes, one with curvature in x-direction and one with curvature in y direction. The laminate can go from one configuration to the other by a simple snap-through action. This snap-through could be accomplished by moments applied on the edges of the laminate. However, it may be more realistic to apply forces on supports attached to the laminate, as was discussed in chapter 1. To study the influence of these forces on laminate shape, the work done by the forces has to be accounted for in the energy expression. Then, the deflection of the laminate can be computed as a function of the force level. This is done in the next chapter. The applied forces may be generated by a shape memory alloy wire, as shown in chapter 5, or by another mechanism. In chapter 4, the forces will be applied in a laboratory setup by a weight to verify the predictions of the theory of the next chapter.

In the work to follow, the laminate will have a side length of approximately 10 in., thus exhibiting the double cylinder phenomenon.

# 3.0 Mechanics of cross-ply unsymmetric laminate with applied forces

This chapter deals with predicting the response of a cylindrical cross-ply unsymmetric laminate subjected to forces applied on supports attached to the laminate, as shown in Fig. 3-1. It is assumed that the direction of the forces remains always parallel to the x direction. The forces, acting at a distance e out the support, then produce a moment proportional to the magnitude of F and e.

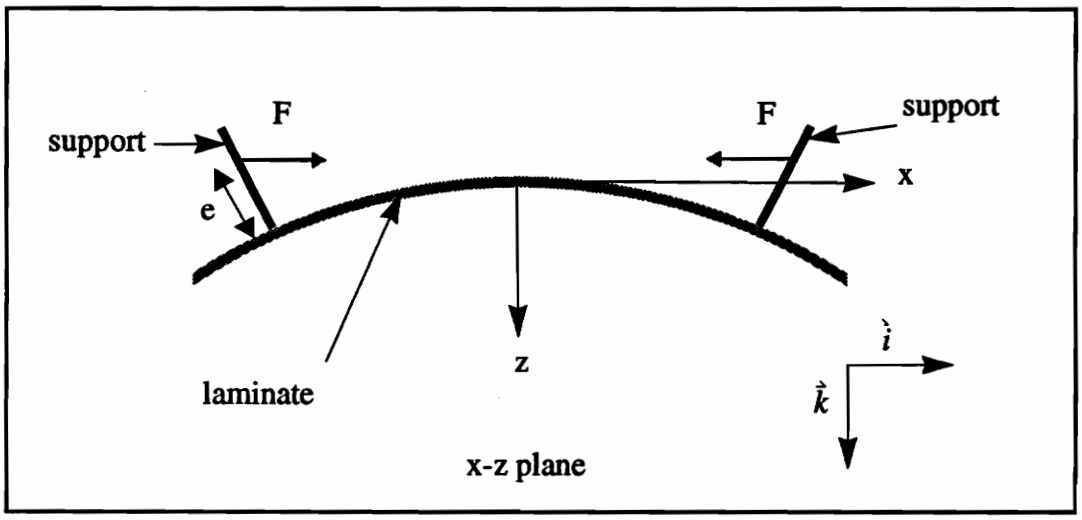


**FIG. 3-1. Force system description**

The supports are located at a distance $L_{xp}$ from the center of the laminate, in the x direction, as illustrated in Fig. 3-2. Strictly speaking, $L_{xp}$ is a straight-line distance measured along the x-axis with the laminate flat.

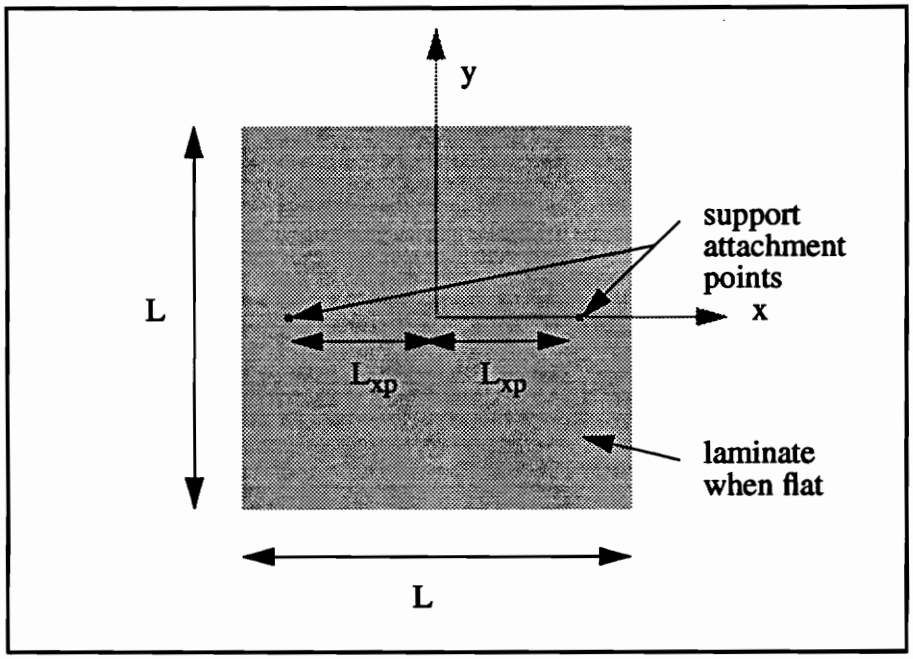


**FIG. 3-2. Supports location**

Using the principle of virtual work, equilibrium equations are derived relating the laminate's room-temperature shape to the applied force F. By solving these equations, for an increasing force level, relations between the curvature and the force can be derived and the force level at which the laminate snaps can be determined. Moreover, laminate strains and displacements can be determined as a function of F.

## 3.1 *Problem formulation*

To use the principle of virtual work, the virtual work of the applied forces and the virtual work of the internal forces within the laminate must be computed. The virtual work of the internal forces is just the first variation of the strain energy of the laminate. That was derived in the last chapter. In the nomenclature of the last chapter,

$$\delta\Pi = \varepsilon\Pi_1, \tag{3.1}$$

where $\delta\Pi$ is the notation for the variation of the internal strain energy. Thus, if the virtual work of the applied force F is denoted as $\delta W_F$, the virtual work is given by

$$\delta W_T = \delta\Pi - \delta W_F \tag{3.2}$$

and the principle of virtual work stipulates that

$$\delta W_T = \delta\Pi - \delta W_F = 0. \tag{3.3}$$

## 3.2 *Virtual work of the applied force*

Recall, the virtual work must be computed with the laminate in a deformed configuration, and by assuming the force level remains constant during the virtual displacement. With this in mind, consider a cross-ply unsymmetric laminate that has been cooled to room temperature and has assumed a cylindrical shape with the curvature in the x direction. Assume the laminate is subjected to the force system of Fig. 3-1. (In what follows, just one support is considered. The effects at the other support are very similar). Due to the force F,

the curvature in the x direction changes relative to its room-temperature value. Now suppose the laminate is given a virtual displacement, as shown in Fig. 3-3. The virtual displacement of the force F can be written as

$$\delta\vec{r} = \delta u\vec{i} + \delta w\vec{k}. \tag{3.4}$$

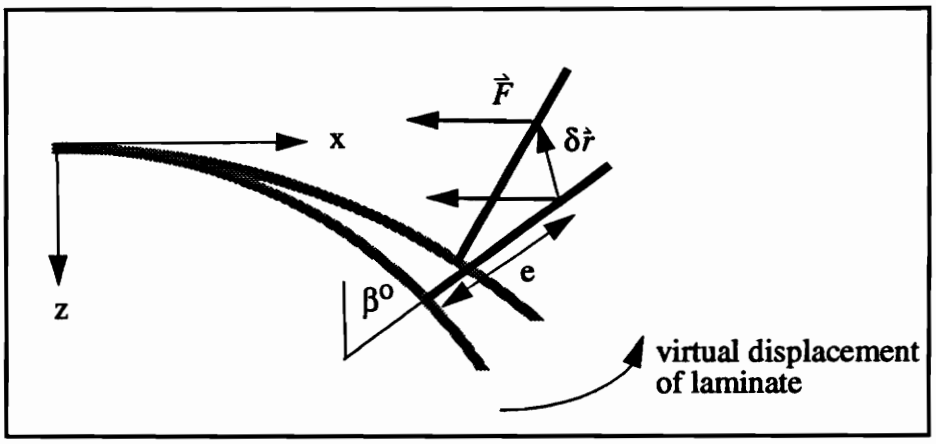


**FIG. 3-3. Virtual displacement of laminate**

Since the force direction remains always parallel with the x direction

$$\vec{F} = -F\vec{i}. \tag{3.5}$$

Thus,

$$\begin{aligned} \delta W_F &= \vec{F} \cdot \delta\vec{r} \\ &= -F\vec{i}\,(\delta u\vec{i} + \delta w\vec{k}) \\ &= -F\delta u \cdot \end{aligned} \tag{3.6}$$

Then, only the virtual displacement in the x direction, $\delta u$, is needed. This displacement can be decomposed into a translation due to $\delta u^o$ and a rotation due to $\delta\beta^o$, where,

$$\beta^o = \frac{\partial w^o}{\partial x}. \tag{3.7}$$

The virtual displacement due to translation, $\delta u^o$, is illustrated in Fig. 3-4. The virtual displacement due to rotation, $\delta\vec{\Delta}$, is illustrated in Fig. 3-5. From that figure,

$$\delta\vec{\Delta} = (e + \frac{H}{2})\,\delta\beta^o \cos\beta^o \vec{i}\,. \tag{3.8}$$

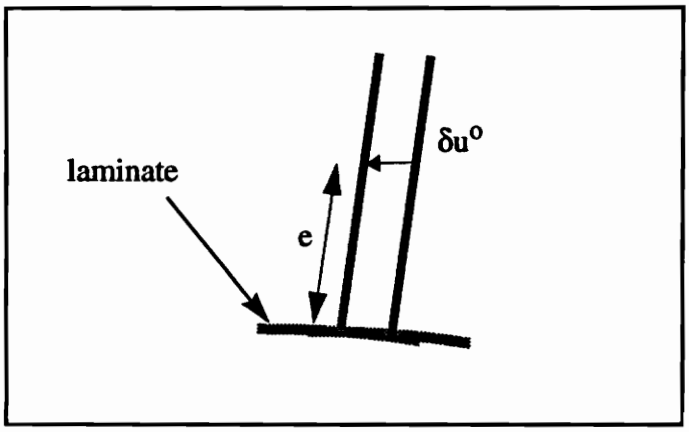


**FIG. 3-4. Virtual displacement due to translation**

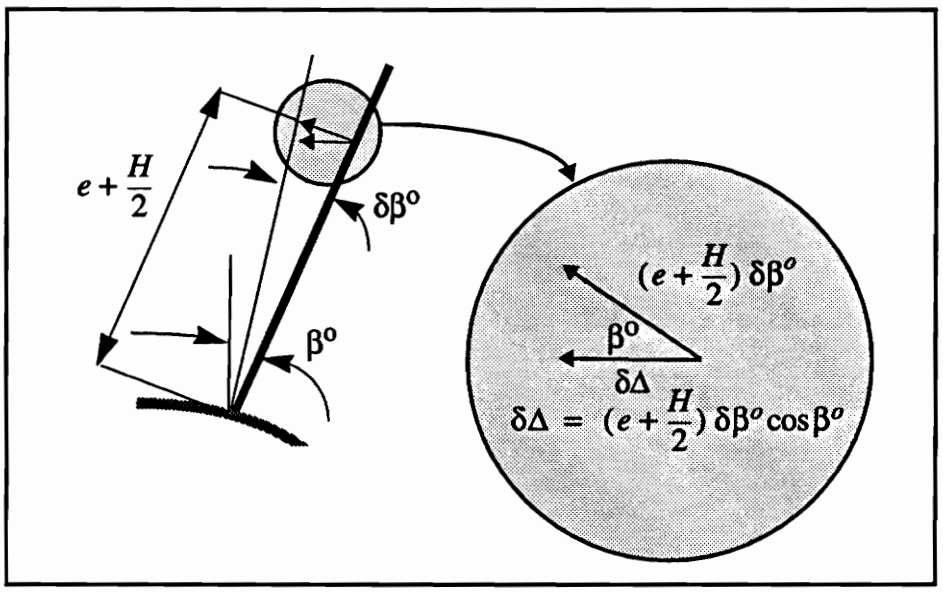


**FIG. 3-5. Virtual displacement due to rotation**

Combining the above,

$$\delta\vec{u} = (\delta u^o + (e + \frac{H}{2})\,\delta\beta^o \cos\beta^o)\,\vec{i}. \tag{3.9}$$

From Eq. (2.6), since the support is located at x=$L_{xp}$,y=0,

$$\delta u^o = L_{xp}\delta c - \frac{L_{xp}^3}{3} a\delta a. \tag{3.10}$$

Similarly, from Eq. (2.6),

$$\beta^o = \frac{\partial w^o}{\partial x} = aL_{xp}, \tag{3.11}$$

and

$$\delta\beta^o = L_{xp}\delta a. \tag{3.12}$$

The virtual displacement $\delta\vec{u}$, Eq. (3.9), becomes

$$\delta\vec{u} = \left(L_{xp}\delta c - \frac{L_{xp}^3}{3} a\delta a + (e + \frac{H}{2})\,L_{xp}\cos(aL_{xp})\,\delta a\right)\vec{i}. \tag{3.13}$$

To be consistent with the small displacements denoted $\varepsilon a_1$, $\varepsilon b_1$, $\varepsilon c_1$, $\varepsilon d_1$, used to compute the first variation of the strain energy $\delta\Pi$ in the last chapter, $\delta a$ and $\delta c$ are, respectively, replaced by $\varepsilon a_1$ and $\varepsilon c_1$. Thus, the virtual displacement becomes

$$\delta\vec{u} = \left(L_{xp}c_1 - \frac{L_{xp}^3}{3} a a_1 + (e + \frac{H}{2})\,L_{xp}\cos(aL_{xp})\,a_1\right)\varepsilon\vec{i}. \tag{3.14}$$

Then, from Eq. (3.6), the virtual work of the applied force is

$$\delta W_F = -F\delta u$$
$$= -F\varepsilon\left(L_{xp}c_1 - \frac{L_{xp}^3}{3}aa_1 + (e+\frac{H}{2})L_{xp}\cos(aL_{xp})a_1\right). \tag{3.15}$$

The total virtual work of the system can now be computed and, according to Eq. (3.2), is equal to

$$\delta W_T = \delta\Pi - \delta W_F$$
$$= \delta\Pi(a, a_1, b, b_1, c, c_1, d, d_1, \varepsilon)$$
$$+ 2F\varepsilon\left(L_{xp}c_1 - \frac{L_{xp}^3}{3}aa_1 + (e+\frac{H}{2})L_{xp}\cos(aL_{xp})a_1\right), \tag{3.16}$$

where the 2 factor represents the effect of both supports. To have algebraic equations rather than transcendental ones, the cosine term is expanded in Taylor series,

$$\cos(aL_{xp}) \cong \left(1 - \frac{a^2L^2_{xp}}{2}\right), \tag{3.17}$$

and the total virtual work can be expressed by

$$\delta W_T = \delta\Pi(a, a_1, b, b_1, c, c_1, d, d_1, \varepsilon)$$
$$+ 2F\varepsilon\left(L_{xp}c_1 - \frac{L_{xp}^3}{3}aa_1 + (e+\frac{H}{2})L_{xp}\left(1 - \frac{a^2L^2_{xp}}{2}\right)a_1\right). \tag{3.18}$$

Now, the principal of virtual work can be applied and the equilibrium equations obtained.

## *3.3 Derivation of the equilibrium equations*

According to the principle of virtual work, the virtual work has to vanish for every admissible virtual displacement. Thus,

$$\delta W_T = \delta\Pi(a, a_1, b, b_1, c, c_1, d, d_1, \varepsilon)$$
$$+ 2F\varepsilon\left(L_{xp}c_1 - \frac{L_{xp}^3}{3}aa_1 + ((e + \frac{H}{2})L_{xp})\cos(aL_{xp})a_1\right) = 0 \tag{3.19}$$

for every increment $\varepsilon a_1$, $\varepsilon b_1$, $\varepsilon c_1$, $\varepsilon d_1$.

The virtual work can be written as

$$\delta W_T = f_a^v(a, b, c, d)\varepsilon a_1 + f_b^v(a, b, c, d)\varepsilon b_1 + f_c^v(a, b, c, d)\varepsilon c_1 + f_d^v(a, b, c, d)\varepsilon d_1 \cdot \tag{3.20}$$

This is the analog to Eq. (2.10).

Thus, having $\delta W_T=0$ for every $a_1$, $b_1$, $c_1$, $d_1$, implies that

$$\begin{aligned} f_a^v(a, b, c, d) &= 0 \\ f_b^v(a, b, c, d) &= 0 \\ f_c^v(a, b, c, d) &= 0 \\ f_d^v(a, b, c, d) &= 0. \end{aligned} \tag{3.21}$$

The above equations are the equilibrium equations of the laminate with a temperature decrease $\Delta T$ and subjected to a force F. By solving them, a, b, c, d are determined for a given force level and the shape of the laminate can be predicted as a function of the force. Moreover, the strains and displacements induced by the force can be computed.

## *3.4 Prediction of laminate deformation*

By solving the equilibrium equations for an increasing value of the force, the curvature of the laminate, the laminate strains, and the movement of the support can be computed as a

function of F.

### 3.4.1 Prediction of laminate curvature

Starting with F=0, the shape of the laminate due to a temperature decrease ΔT is obtained. As with the just-completed derivation, assume this shape is cylindrical with a nonzero curvature in the x direction. By increasing the force F, the curvature of the laminate decreases. At some level of force, the laminate configuration reaches an unstable configuration and the laminate snaps to the other cylinder shape, a cylinder with the curvature in the y direction. A numerical example will be presented in a next section showing the curvatures as a function of the force level. However, it is very difficult experimentally to measure the curvature when a force is applied. Thus, other variables, ones which can be measured more easily, can be predicted and compared to experimental results. For this reason, the strains induced by the applied force are predicted. Strains can be measured experimentally by using strain gages.

### 3.4.2 Prediction of laminate strains

Using the values of a, b, c, d found by solving the equilibrium equation for increasing F, the mechanical strains induced in the laminate can be evaluated. The expression for the strain induced by the force is

$$\{\varepsilon^F\} = \{\varepsilon\} - \{\varepsilon^{\Delta T}\}, \tag{3.22}$$

where $\varepsilon^F$ is the strain induced by the force only, ε is the total strain induced by both the

force and the temperature change, and $\varepsilon^{\Delta T}$ is the thermal-induced strain, due only to $\Delta T$. Since the force is acting in the x direction, it induces mostly strain in the x direction. Thus, only the induced strain in the x direction need be studied. It is expressed by

$$\varepsilon_x^F = \frac{\partial u^o}{\partial x} + \frac{1}{2}\left(\frac{\partial w^o}{\partial x}\right)^2 - z\frac{\partial^2 w^o}{\partial x^2} - \left(\frac{\partial u^o}{\partial x} + \frac{1}{2}\left(\frac{\partial w^o}{\partial x}\right)^2 - z\frac{\partial^2 w^o}{\partial x^2}\right)\Bigg|_{F=0}. \tag{3.23}$$

By expressing $u^o$ and $w^o$ in term of a, b, c, d, as done in chapter 2, and considering the strain in the center of the laminate (x=0, y=0), Eq. (3.23) becomes

$$\varepsilon_x^F = c + za - (c + az)\,|_{F=0}. \tag{3.24}$$

When F=0 the laminate has its initial shape due to $\Delta T$ only and $a=a_i$, $c=c_i$, the subscript i denoting initial values. The strain expression becomes

$$\varepsilon_x^F = c - c_i + z(a - a_i). \tag{3.25}$$

Considering the strains induced on the top and bottom surface of the laminate, $z = \pm\frac{H}{2}$, Eq. (3.25) becomes

$$\varepsilon_x^F = c - c_i \pm \frac{H}{2}(a - a_i). \tag{3.26}$$

Then, the induced strains can be determined as a function of the force and can be compared to experimental strains. This will be done in chapter 4.

Another way to check the theory is to measure the displacement of the force support as a function of the applied force and compare the measurements with predictions. This prediction is discussed next.

### 3.4.3 Prediction of support displacements

When a force is applied on the support and the curvature of the laminate decreases, the distance between the two supports becomes shorter, as shown in Fig. 3-6.

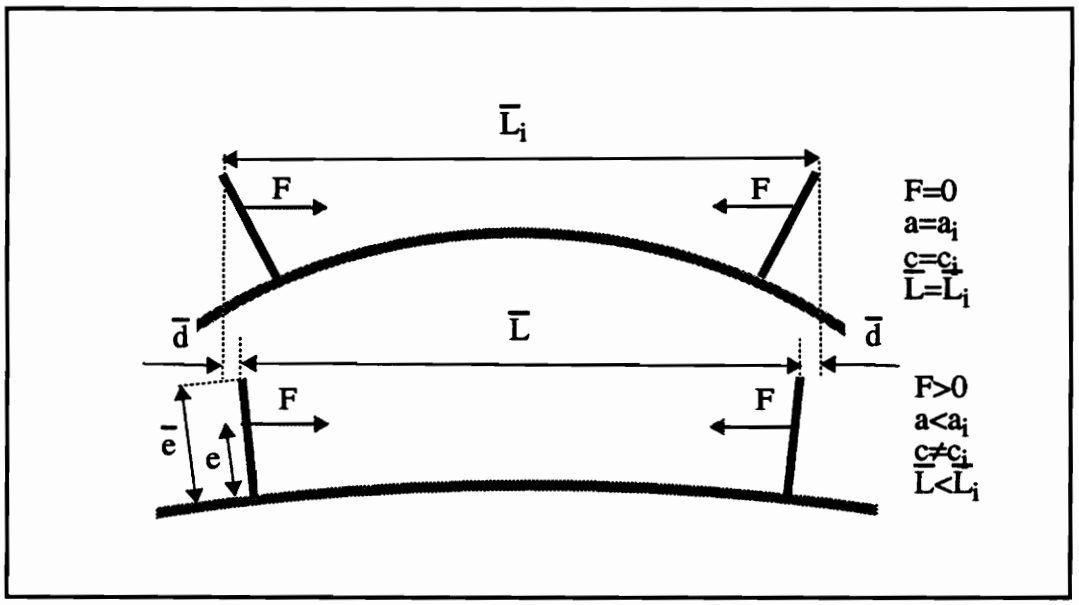


**FIG. 3-6. Displacement of the support due to the applied force**

The change in the distance between the two supports, denoted by $\Delta\bar{L}$, can be expressed by

$$\Delta\bar{L} = \bar{L} - \bar{L}_i = 2\bar{d}, \tag{3.27}$$

where $\bar{L}_i$ is the initial distance between the two supports and $\bar{d}$ is the displacement of each support due to the applied force. The change in length $\Delta\bar{L}$ can be easily measured in an experiment. Thus, it is interesting to derive a theoretical relation between $\Delta\bar{L}$ and the force level F.

The computation of $\Delta\bar{L}$ follows somewhat the same line as the computation of the virtual displacement of the point where the force is applied. Due to the temperature change $\Delta T$, the displacement of a point a distance $\bar{e}$ out the support consists of a component due to translation and a component due to rotation, as shown in Fig. 3-7.

The component due to translation is given by Eq. (2.6) and since $x=L_{xp}$ and $y=0$, the component due to translation, $u^T$, is

$$u^T = u^o = cL_{xp} - a^2\frac{L_{xp}^3}{6}. \tag{3.28}$$

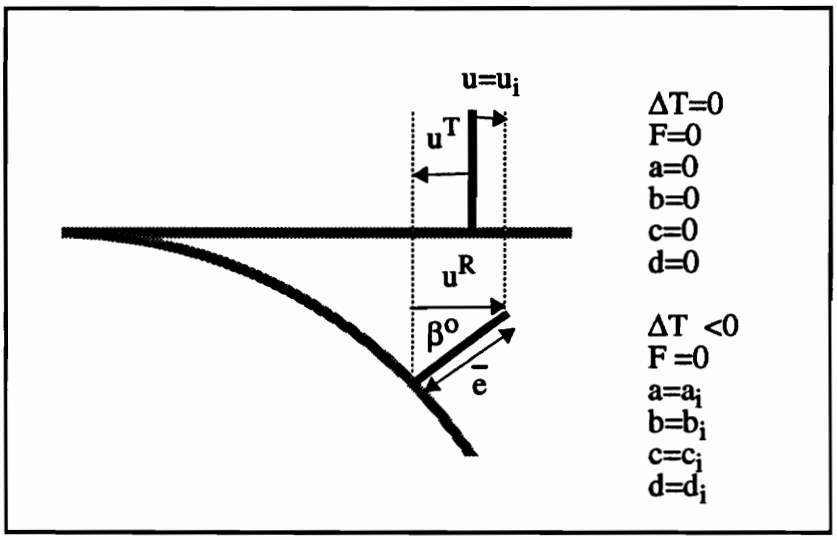


**FIG. 3-7. Displacement due to the temperature change**

The component due to rotation, $u^R$, is

$$u^R = \bar{e}\sin\beta^o = \bar{e}\sin(aL_{xp}), \tag{3.29}$$

where Eq. (3.7) has been used. Adding these two components,

$$u_i = c_iL_{xp} - a_i^2\frac{L_{xp}^3}{6} + \bar{e}\sin(a_iL_{xp}), \tag{3.30}$$

where the subscript i signifies the displacement is due to only a temperature change.

When the force is applied, the configuration of the laminate changes relative to its configuration due only to a temperature change. However, the form of Eqs. (3.28)-(3.30) are still valid. Consequently, when due to a temperature change and an applied force ($\Delta T<0$, $F>0$), as shown in Fig. 3-8, the displacement of a point a distance $\bar{e}$ out the support is given by

$$u = cL_{xp} - a^2\frac{L_{xp}^3}{6} + \bar{e}\sin(aL_{xp}). \tag{3.31}$$

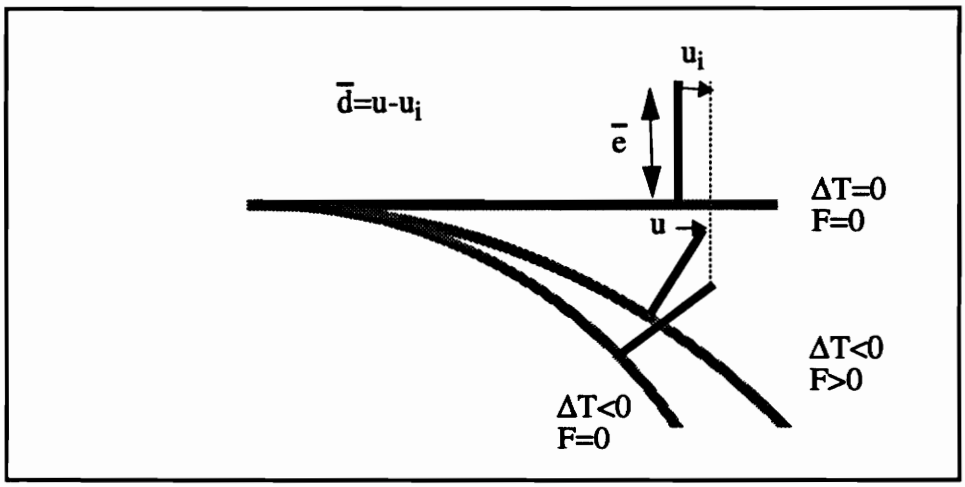


**FIG. 3-8. Displacement due to the force**

Consequently, the displacement of a point a distance $\bar{e}$ out the support and due only to the force is obviously

$$\bar{d} = u - u_i. \tag{3.32}$$

Thus, the change in the distance between the two supports is

$$\Delta\bar{L} = 2(u - u_i)$$
$$= 2\left(L_{xp}(c - c_i) - \frac{L_{xp}^3}{6}(a^2 - a_i^2) + \bar{e}(\sin(aL_{xp}) - \sin(a_iL_{xp}))\right). \quad (3.33)$$

Then, $\Delta\bar{L}$ can be computed for increasing force level and compared to experimental results.

### 3.4.4 Numerical example

Consider a $(0_2/90_2)_T$ unsymmetric laminate, on which supports are fastened, with the following properties

L=12 in.
h=0.006 in.
$E_1$=20.0 Msi
$E_2$=1.3 Msi
$G_{12}$=1.03 Msi
$\nu_{12}$=0.3 (3.34)
$\alpha_1$=-0.167 10-6 /°F
$\alpha_2$=15.6 10-6 /°F
$L_{xp}$=4 in.
e=1.25 in.
$\bar{e}$=2 in.

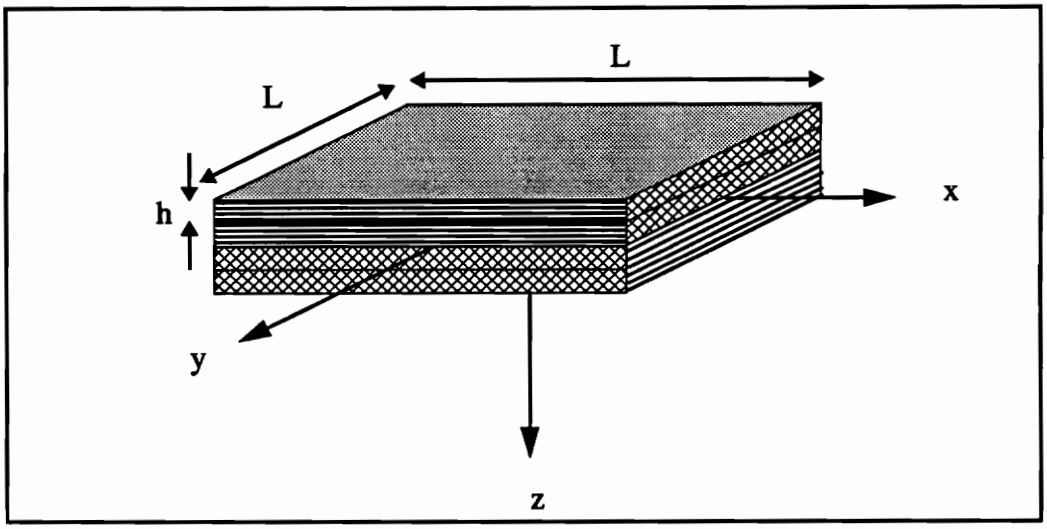


**FIG. 3-9. Laminate's geometrical characteristics**

By solving the equilibrium equations, Eq. (3.21), the curvatures of the laminate in the x and y direction are computed for increasing force level. These can be as a function of F, as presented in Fig. 3-10.

Fig. 3-10(a) presents the curvature in the x direction, a, whereas Fig. 3-10(b), presents the characteristics of the curvature in the y direction, b. In both graphs, the black line represents the stable curvature of one cylindrical shape, the dotted line the curvature of the unstable saddle shape, and the grey line the curvature of the other stable cylindrical shape. When no force is applied, the initial shape of the laminate is a cylinder with the curvature in the x direction, a=0.1439 $in.^{-1}$, b~0. This is denoted by the 'A's in the Fig. 3-10. The other possible shapes when F=0 are the other stable cylindrical shape, point B, and the unstable saddle shape, point C. Points corresponding to configurations A, B, and C correspond to similar points in Fig. 2-3. By increasing F, the curvature in the x direction, a, decreases, following the black line, in Fig. 3-10(a). With F=9.83 lb, point D in Fig. 3-10,

an unstable configuration is reached and the laminate snaps to the other cylinder shape which has no curvature in the x direction. This snapping is indicated by the arrow from D to E.

Fig. 3-10(b) represents the evolution of the curvature in the y direction, b. With F=0, the curvature in the y direction, b, is equal to zero. While the force increases, curvature b increases slightly, as indicated by the black line of Fig. 3-10(b). When F=9.83 lb curvature b changes immediately to -0.1439 $in.^{-1}$. This curvature corresponds to the other cylindrical shape of the laminate. Thus, for F=9.83 lb the laminate has changed its shape. Further increases in force results in minimal curvature change.

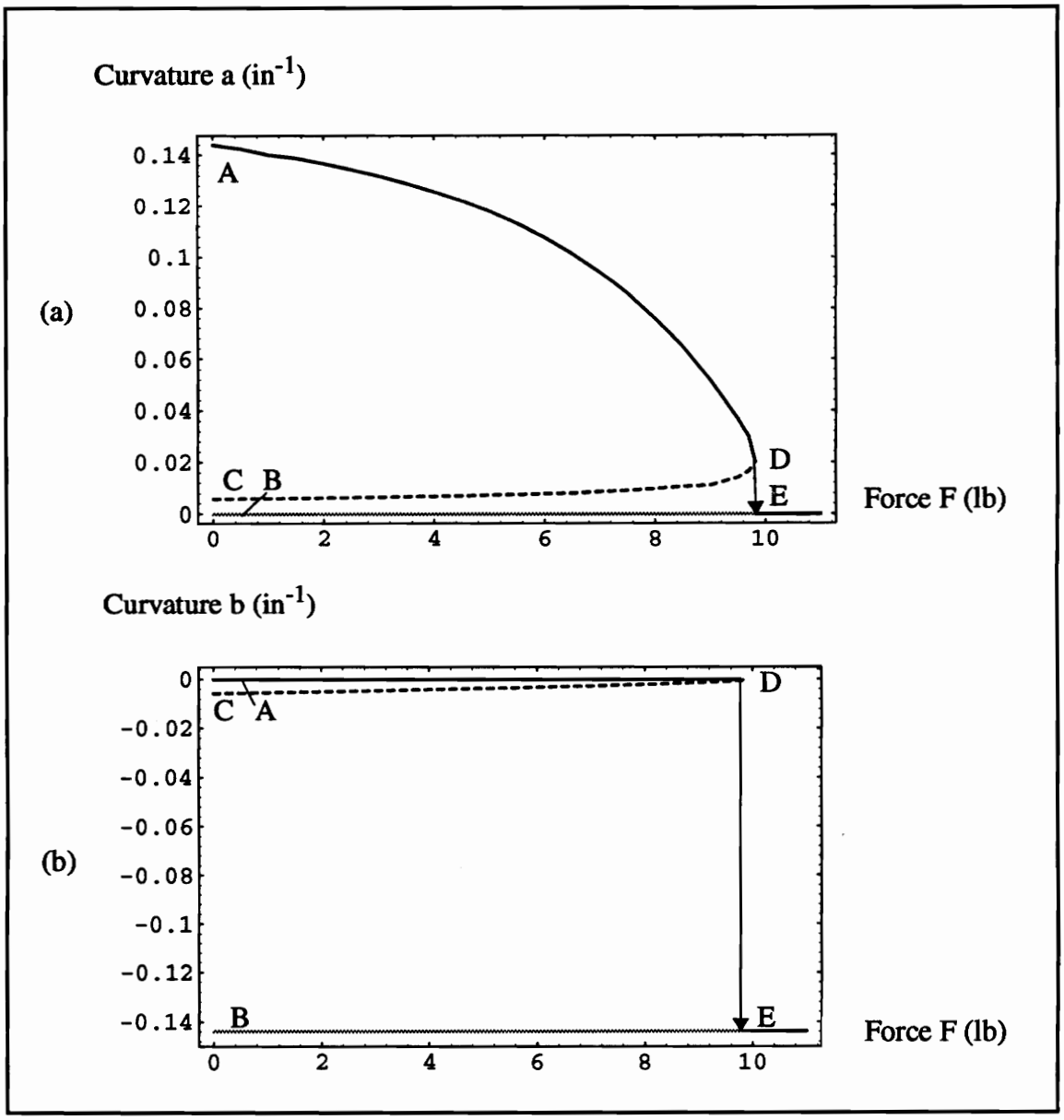


**FIG. 3-10. Laminate curvature in the x and y direction as a function of the applied force F**

Now, using the solutions a, b, c, d, found by solving the equilibrium equations, the induced strains are evaluated as a function of the force F. Figure 3-11 represents the strain

at the center of the top surface, z=-H/2 and Fig. 3-12 represents the strain at the center of the bottom surface, z=H/2.

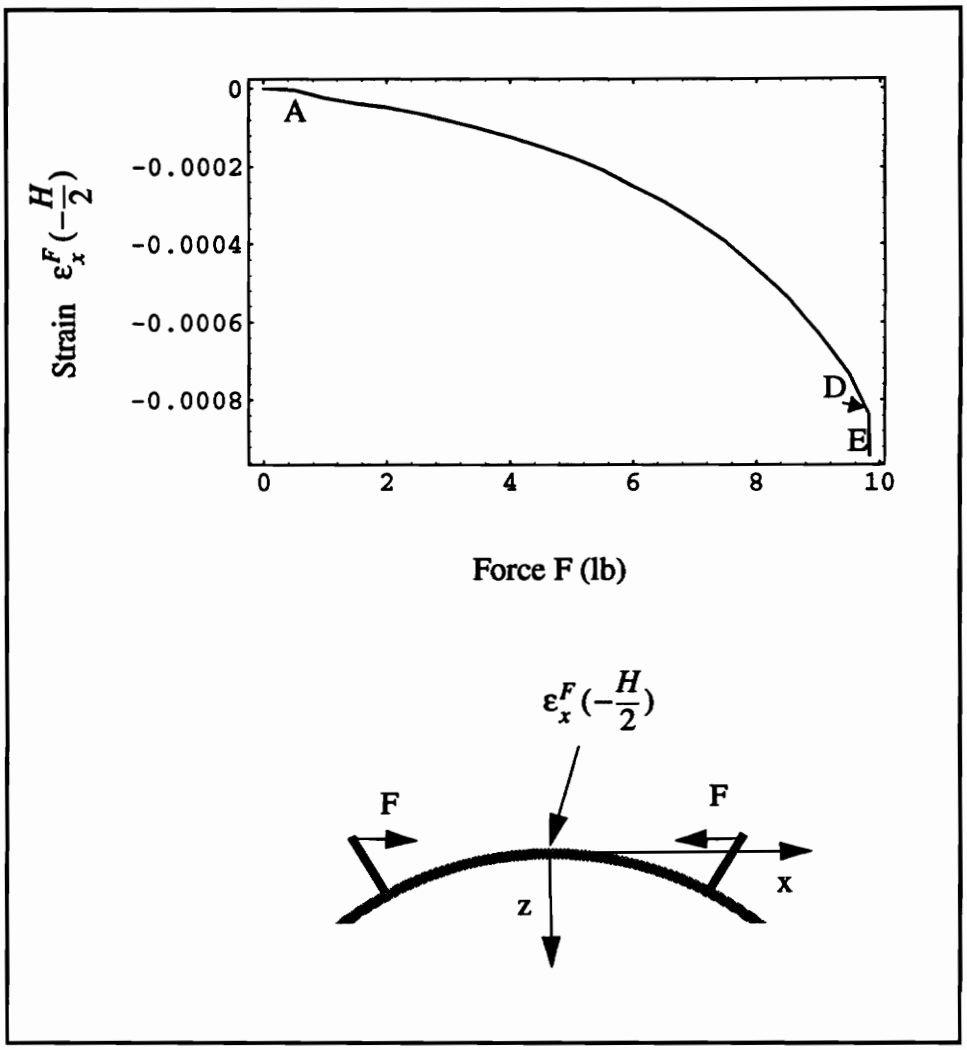


**FIG. 3-11. Force-induced strain in the center of the top surface of the laminate**

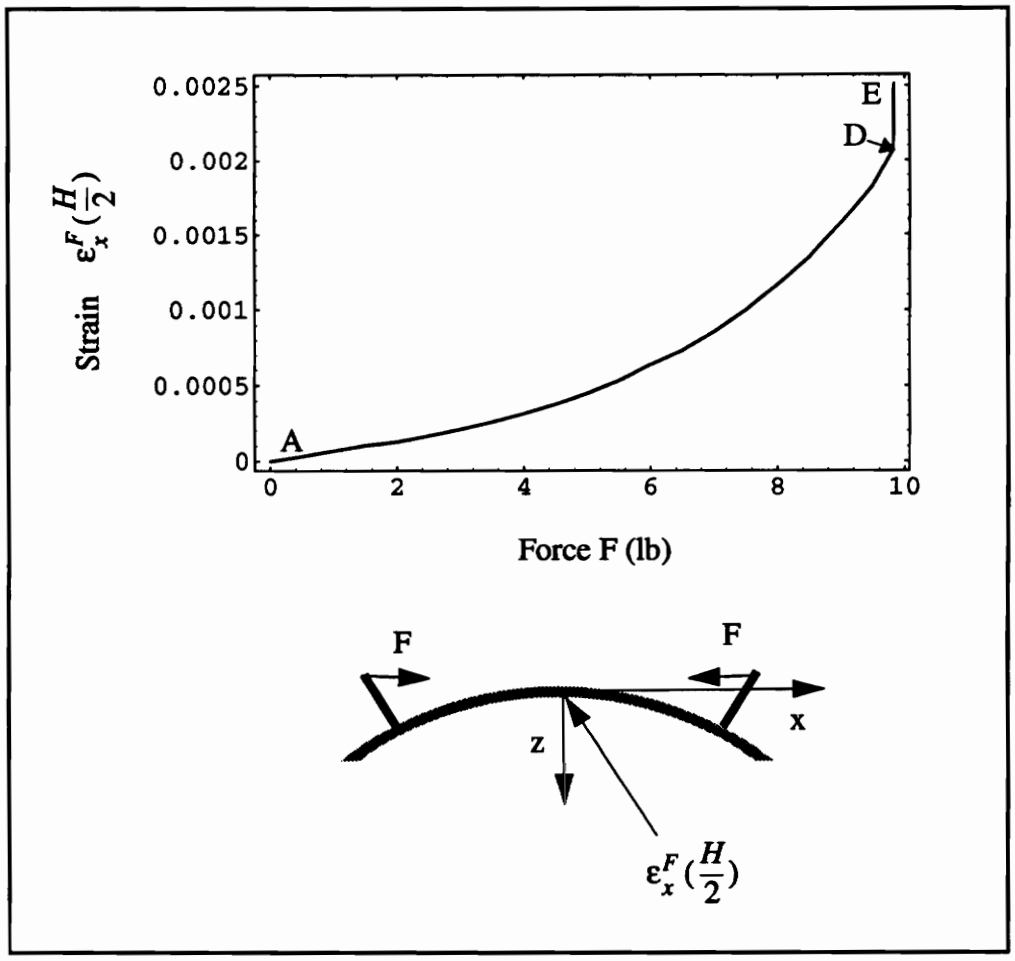


**FIG. 3-12. Force-induced strain in the center of the bottom surface of the laminate**

Note that the strains induced on the top surface, $\varepsilon_x^F(-\frac{H}{2})$, is negative, since the top surface is in compression. The bottom strain, $\varepsilon_x^F(\frac{H}{2})$, is positive, since the bottom surface is in tension, as shown in Fig. 3-13. Note, however, due to the $B_{ij}$ terms, the force-induced strains are not equal in magnitude. Points A, D and E of Fig. 3-10 are noted in Figs. 3-11 and 3-12.

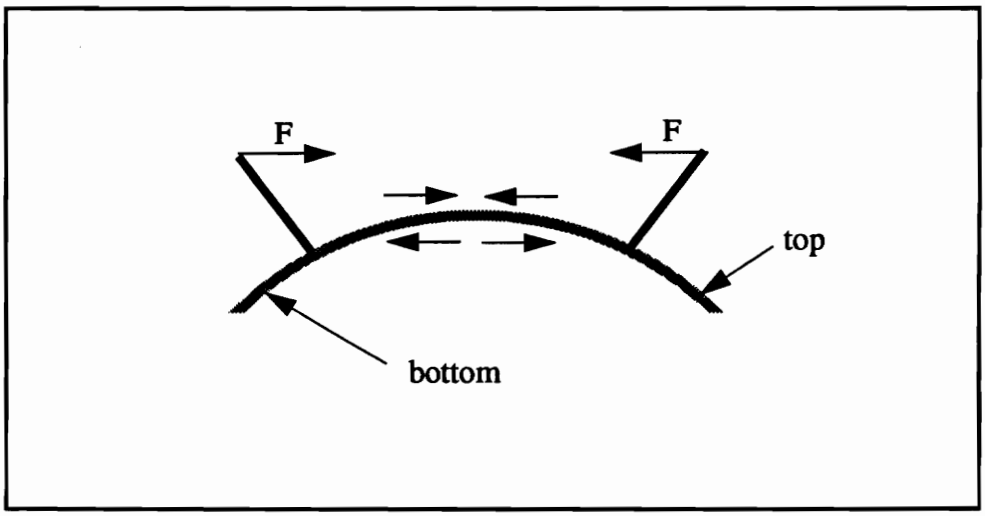


**FIG. 3-13. Sign of the force induced strains**

Consider now the change in the distance between the two supports, as developed in Eq. (3.33). As a and c are already known as a function of F, the change in length $\Delta\overline{L}$ is very easy to compute and to plot as a function of F. Figure 3-14 represents the prediction of the change in length $\Delta\overline{L}$ as a function of the applied force F. The quantity $\Delta\overline{L}$ has negative values since the distance between the two supports shortens. Points A, D, and E are also denoted in Fig. 3-14.

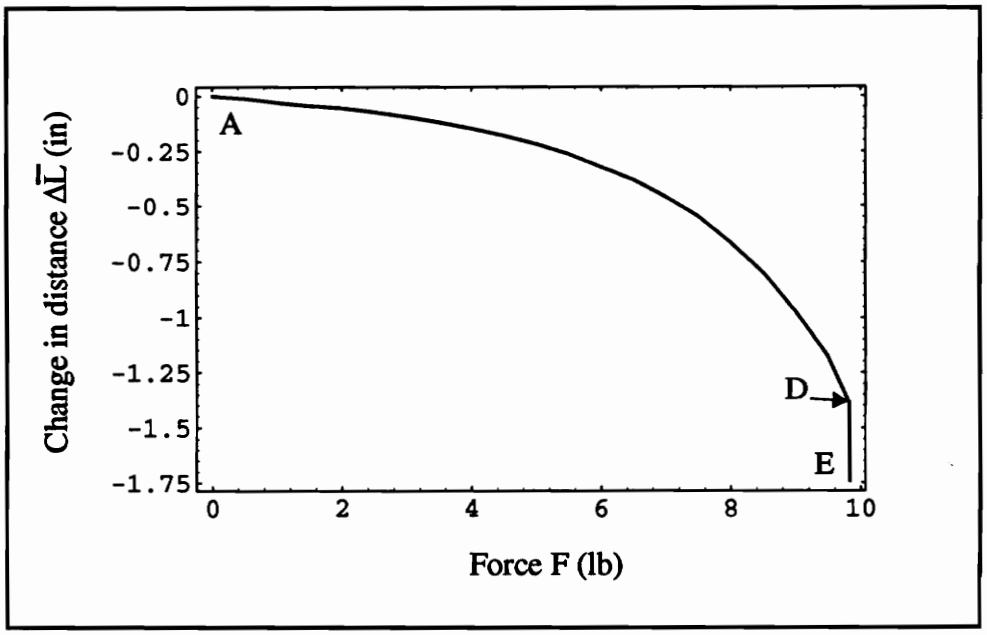


**FIG. 3-14. Change in the distance between the two supports versus the applied force F**

Thus, governing equations, describing the mechanics involved when the laminate is subjected to an applied force, have been derived. The deformation of the laminate induced by the force can be predicted. More specifically, force-induced strains at the center of the laminate, as well as the displacement of the support, have been computed. Thus, the theory can now be checked by conducting experiments.

# 4.0 Experiments with known weights to produce the force

To check the theory derived in chapters 2 and 3, a $(0_2/90_2)_T$ cross-ply unsymmetric laminate is tested. First, the initial curvature of the laminate, as determined by the temperature decrease $\Delta T$, is measured and compared to the curvature predicted theoretically. Then, supports are attached to the laminate, and a force is applied. The strains on the top and bottom surface of the laminate, and the distance between the two supports are measured as a function of the force F. Comparisons are made with the results predicted by the theory of chapter 3.

## *4.1 Unsymmetric laminate properties*

The laminate tested is a graphite-epoxy $(0_2/90_2)_T$ unsymmetric laminate. The material used is IM7/8551-7A. The laminate geometrical properties are

$$\begin{aligned} L_x &= 10.750 \text{ in.} \\ L_y &= 10.626 \text{ in.} \\ h &= 0.0048125 \text{ in.} \end{aligned} \tag{4.1}$$

where $L_x$ is the length of the laminate and $L_y$ the width. The elastic and thermal properties

are evaluated experimentally. Tensile tests are conducted on composite specimens to measure the elastic modulus in the fiber direction, $E_1$, the elastic modulus in the matrix direction, $E_2$, and the Poisson's ratio, $\nu_{12}$. The testing and the results are explained in Appendix A. The inplane shear modulus is not evaluated since its value does not effect the computation of the stiffness matrix for a $(0_2/90_2)_T$ laminate. The specimens are then heated in an oven. The strains are measured as a function of the temperature to determine the coefficients of thermal expansion $\alpha_1$ and $\alpha_2$. This is discussed in Appendix B. The results of the testing described in Appendix A and B lead to

$$\begin{aligned} E_1 &= 24.77 \text{ Msi} \\ E_2 &= 1.27 \text{ Msi} \\ \nu_{12} &= 0.335 \\ \alpha_1 &= 0.3435\ 10^{-6}\ /^{o}\text{F} \\ \alpha_2 &= 15.34\ 10^{-6}\ /^{o}\text{F}. \end{aligned} \tag{4.2}$$

## *4.2 Initial curvature measurement*

The initial curvature of the laminate is computed using the following expression derived in Appendix C,

$$a = \frac{2\rho}{\rho^2 + \lambda^2}, \tag{4.3}$$

where $\rho$ and $\lambda$ are represented in Fig. 4-1.

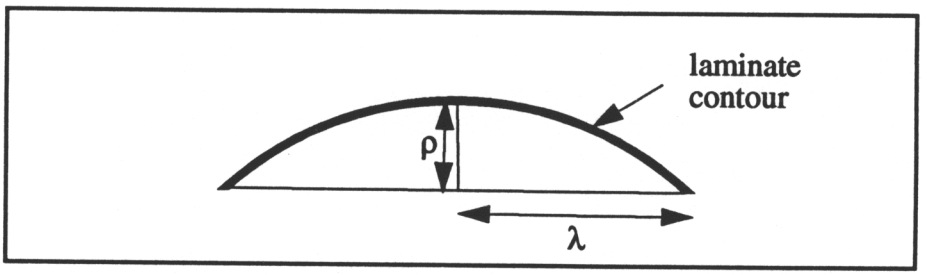


**FIG. 4-1. Definitions of the parameters ρ and λ**

Figure 4-1 represents a drawing executed directly from the laminate. To obtain drawings as in Fig. 4-1, the laminate is put on a sheet of paper and its contour drawn, as shown in Fig. 4-2.

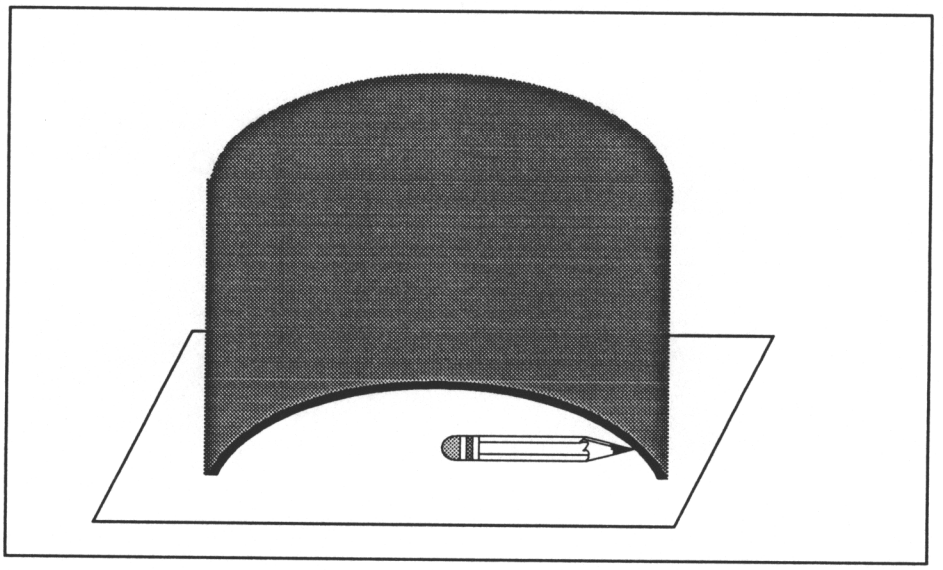

**FIG. 4-2. Drawing of the curvature of the laminate**

The values of ρ and λ measured for the experimental laminate are

ρ=2.086 in.

λ=4.705 in.

Then, substituting these values in the expression (4.1), the value for the initial curvature is found to be 0.1575 $in.^{-1}$. Now, using the theory derived in chapter 2, the initial curvature can be predicted. In particular, Eq. (2.12) is solved for the curvatures of the experimental laminate. The solutions are

$$a=0.1591\ in.^{-1},\ b=-8.575\ 10^{-6}\ in.^{-1}$$

$$a=8.575\ 10^{-6} in.^{-1},\ b=-0.1591\ in.^{-1} \qquad (4.4)$$

$$a=0.005878\ in.^{-1},\ b=-0.005878\ in.^{-1},$$

which correspond, respectively, to a cylindrical shape with the curvature in the x direction, a cylindrical shape with the curvature in the y direction, and a saddle shape. Studying stability, it is found that only the two cylindrical shapes of the experimental laminate are stable. As the predicted curvature is 0.1591 $in.^{-1}$ and the experimental curvature is 0.1575 $in.^{-1}$, there is a very good correlation between the theory and the experiment.

Next, a force is applied to the supports attached to the laminate. The laminate strains and the displacement of the supports are measured as a function of the force and are compared to the predictions of chapter 3, paragraph 3.4.4.

## *4.3 Experimental setup*

### 4.3.1 Description

Two supports are fastened to the laminate simply by using screws passing through holes in the laminate. One of the supports is used to fasten the laminate to a table, as shown in Fig. 4-3. This is accomplished by a clamp. The other support is free to move.

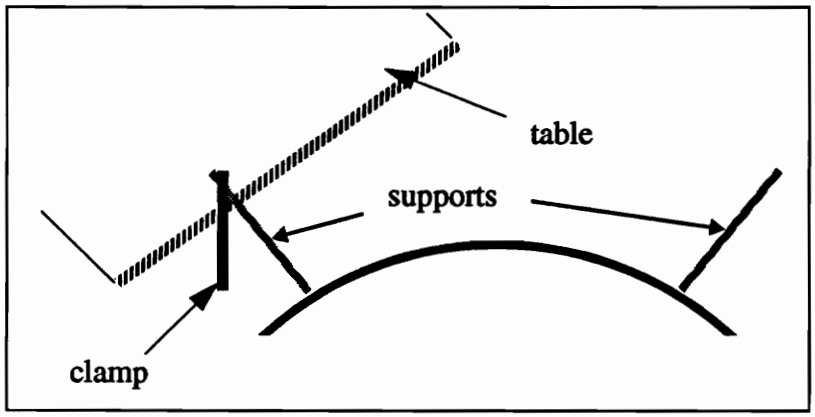


**FIG. 4-3. Setup description**

To generate the force F, a known weight is hung to a wire which is fastened to the support free to move and which passes through a hole in the clamped support, as shown in Fig. 4-4. Thus, the weight makes only one support move. Furthermore, this approach applies an equal force F on each support, and the force level is known exactly.

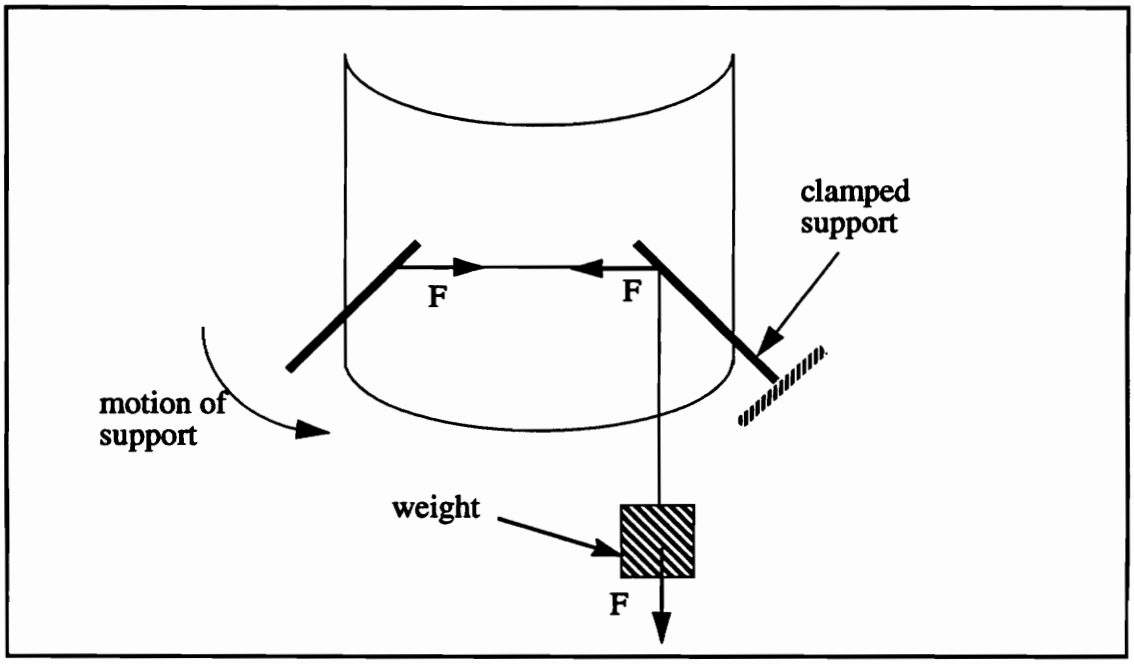


**FIG. 4-4. Laminate with an applied force generated by a weight**

### 4.3.2 Measurements

As just mentioned, the force is generated by a weight hung on a string. In fact, the weight is due to water poured into a container hanging on the string. The water is first weighed on a scale and then it is poured into the container. Thus, at any time the applied force is known and can be controlled with a great deal of accuracy. When the laminate is about to snap, the water is poured very slowly into the container until the shape change occurs. The remaining water is weighted and the force to make the laminate snap can be evaluated. This system offers the advantage of having a very precise value of the snapping force.

To measure the strains, strain gages are used. One strain gage is bonded to the center (x=0,

y=0) of each surface of the laminate. Thus, strains induced on the surfaces of the laminate can be measured every time additional water is poured into the container.

The change in the distance between the two supports is measured directly. To measure this change in distance, a transparent plexiglas ruler is fastened to the clamped support, at point A, located at a distance $\bar{e}$ from the laminate, as shown in Fig. 4-5. The ruler simply extends to the other support. A X-mark is scribed on the free support, at point B, located at a distance $\bar{e}$ from the laminate. Thus, by pivoting the ruler around A, so that the scribe mark comes just under the graduation of the ruler, the distance AB is precisely measured.

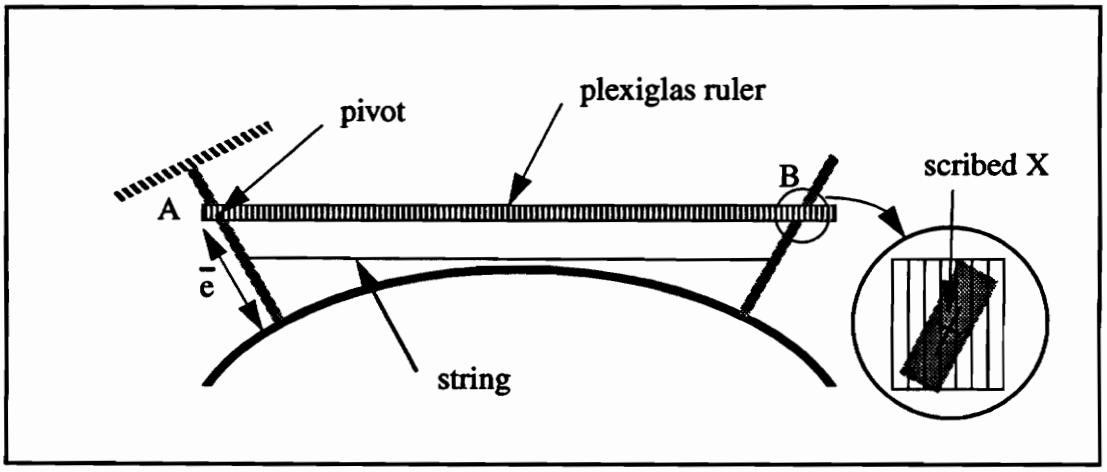


**FIG. 4-5. Setup to measure the support displacement**

For increasing force level, the distance AB is measured until the laminate snaps. Since it is interesting to obtain the change in the distance to be able to compare it with the theoretical results from chapter 3, the initial distance AB is subtracted from the other measured distances.

Photos taken during the experiment are presented in Figs. 4-6 to 4-9. The first one, Fig. 4-6 represents a top view of the laminate subjected only to the weight of the container hanging on a string. Thus, the force applied on the supports is close to zero and the

curvature is almost the same as with no force applied. Visible in the photograph are the laminate, the clamped and free supports, the container for the water, the plexiglas ruler for measuring support motion, the string which transmits the force, and wires from the strain gages to the strain gage equipment. Water is poured into the container, Fig. 4-7. Enough force is generated to induce a large curvature decrease, associated with a substantial support displacement. Figure 4-8 presents a side view of the laminate with the load level as in Fig. 4-7. It can be noticed that local deformations are occurring at the support location. By pouring more water into the container, a force great enough to make the laminate snap is generated. This is shown in the photo of Fig. 4-9.

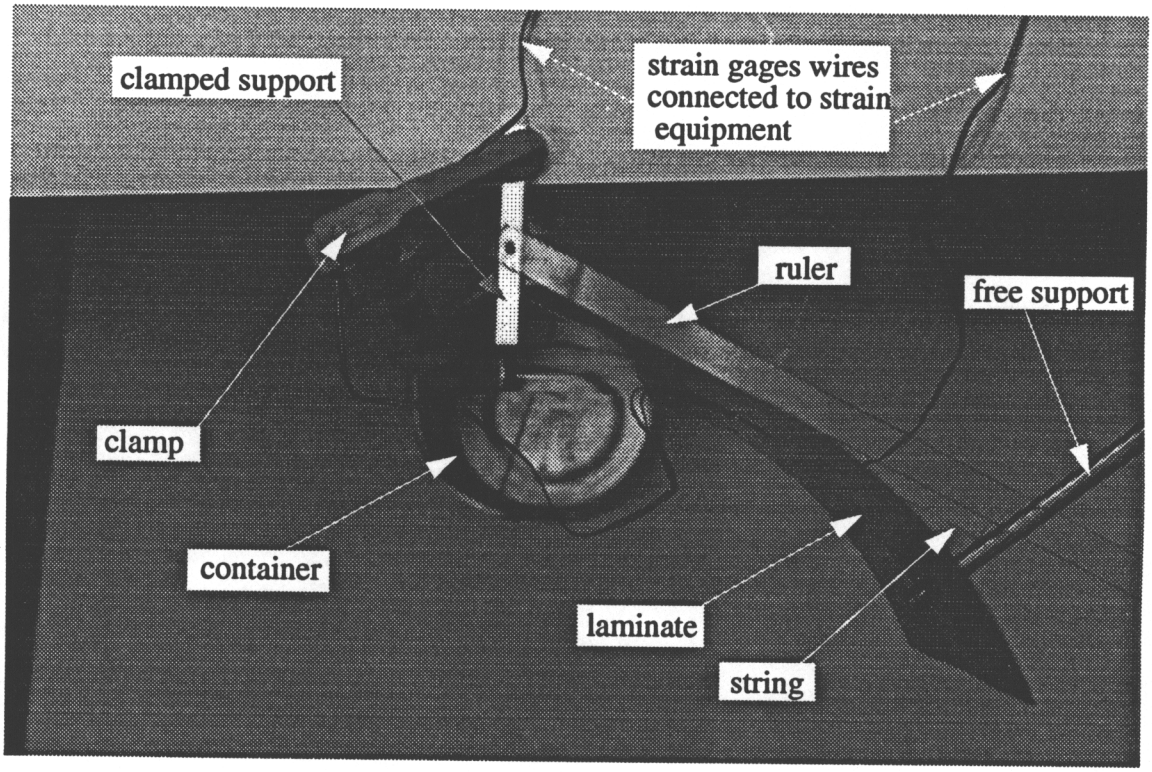


**FIG. 4-6. System configuration with a very low applied force**

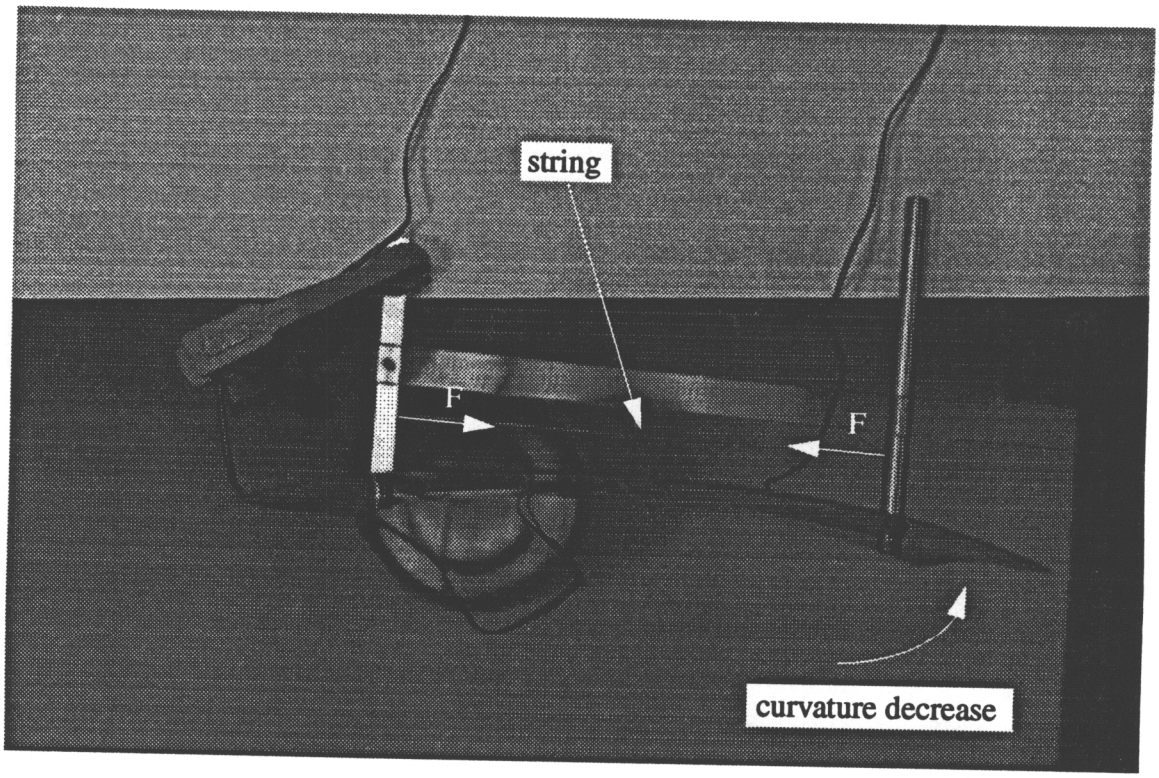


**FIG. 4-7. System configuration with an important applied force**

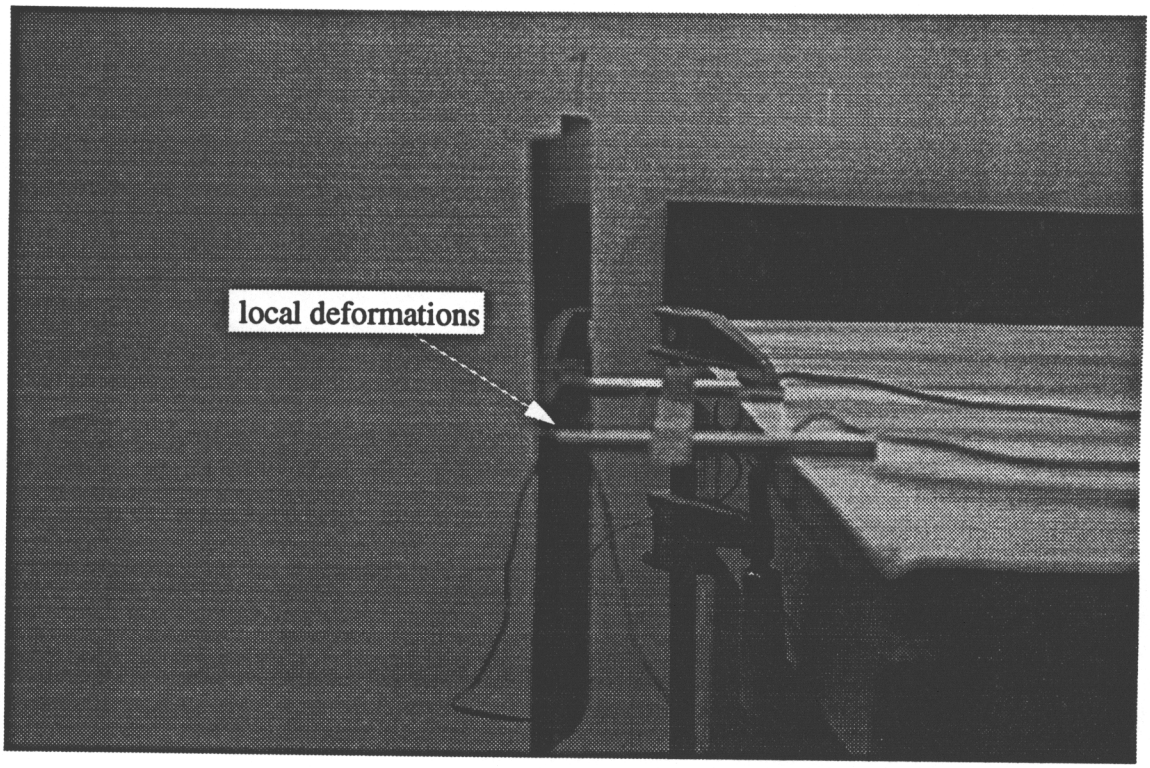


**FIG. 4-8. Side view of the system configuration with an important applied force**

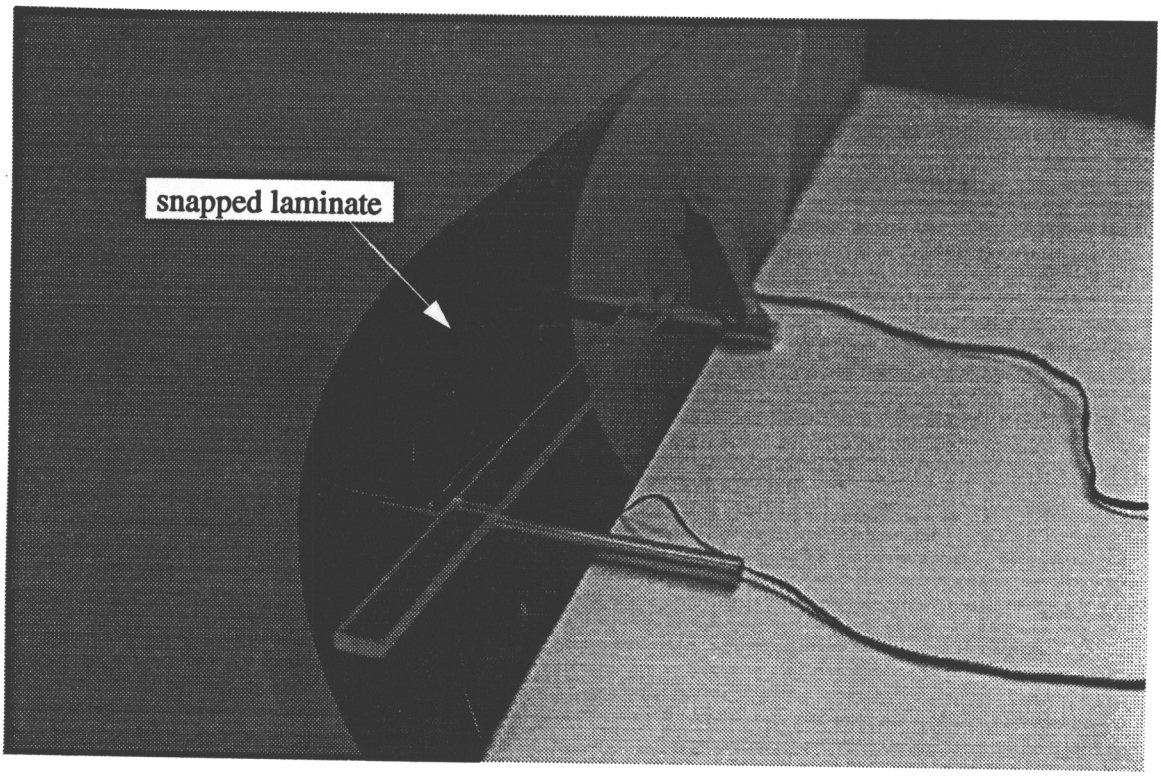


**FIG. 4-9. System configuration after snapping**

## *4.4 Comparison of the experiment with the theory*

### 4.4.1 Strain comparison

Proceeding as previously explained to measure the force and the strain level, the strains on the surfaces at the center of the laminate are measured as a function of the applied force F.

Figures 4-10 (a) and Fig. 4-10 (b) represent, respectively, the corresponding relations for the strains $\varepsilon_x^F(-\frac{H}{2})$ and $\varepsilon_x^F(\frac{H}{2})$. These correspond, respectively, to the top and bottom surface strains as shown in Figs. 3-11 and 3-12. The theoretical strains are represented by a black line, whereas the experimental strains are represented by black dots.

Very good correlations can be observed for force level up to 4 lb. For a force greater than this value, the experimental strains are less than the predicted strains. These differences are thought to be due to the local deformations which occur at the support locations. These local deformations are not accounted for in the theory, a theory which uses an approximate overall shape for the laminate. Another source of error is thought to be due to the highly unstable nature of the laminate as the force reaches the level for snapping. Near this level the laminate configuration is unstable. In fact, since the configuration is unstable, laminate imperfections, small movements of the hanging weight, slight misalignment of the supports attached to the laminate, or any one of a number of unwanted perturbations could cause the laminate shape to deviate significantly from any particular configuration. Thus, it is not entirely surprising that near the snapping force level, but with the laminate in the unsnapped configuration, there are deviations between experiment and predictions.

Additional correlation between prediction and experiment can be found in Appendix D. The results presented in this appendix were taken from a laminate that was found to have absorbed an unknown amount of moisture. Thus, the initial curvature, and possible the material properties, were affected by the presence of moisture, and correlation with prediction would not be valid. However, the empirical data are presented to illustrate the good repeatability of the results.

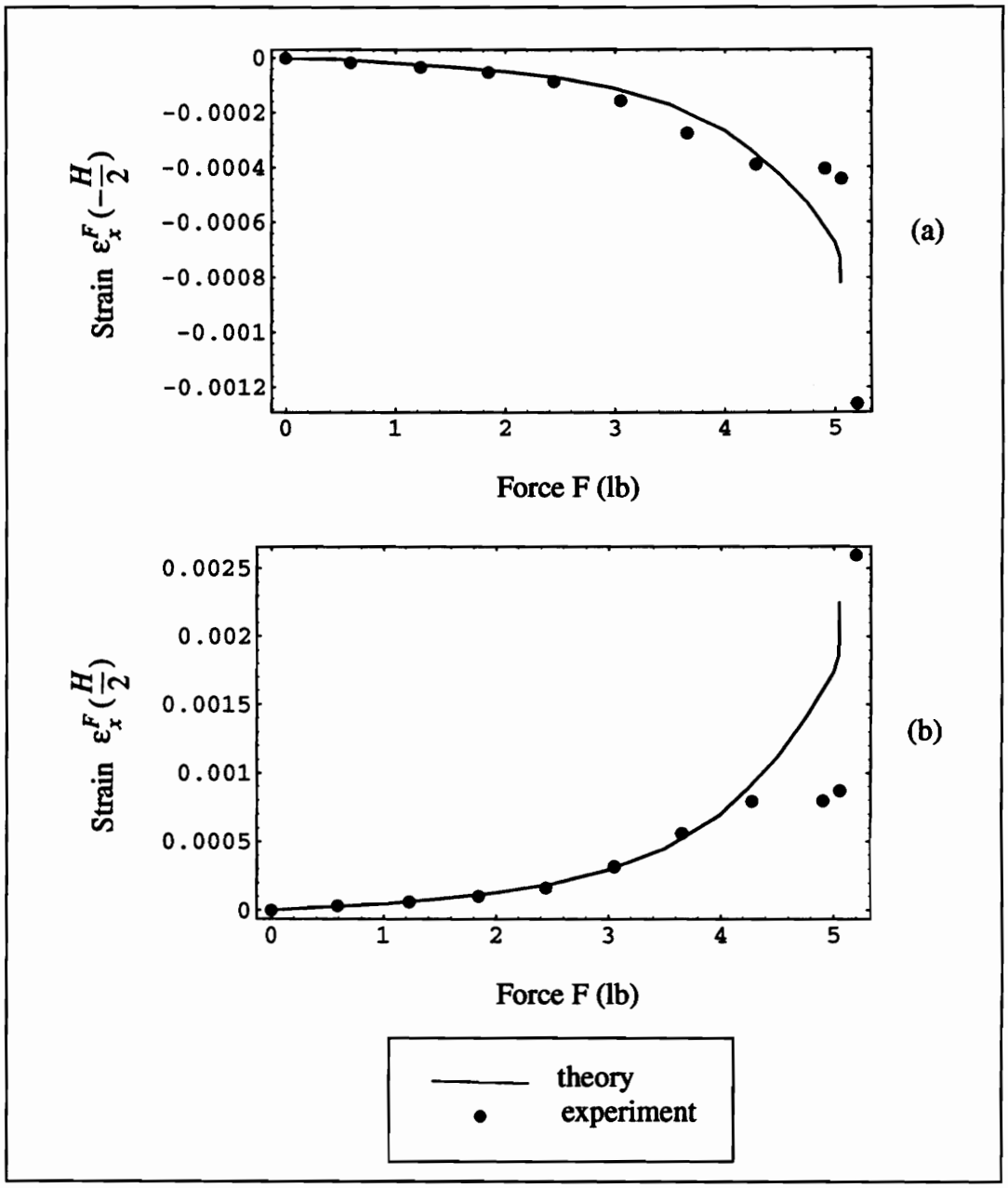


**FIG. 4-10. Comparison of experimental strains with theoretical strains**

### 4.4.2 Support displacement comparison

The support displacement is experimentally determined as a function of the applied force by measuring the change in length $\Delta\bar{L}$, as discussed in paragraph 4.3.2. Figure 4-11 represents the relation between the support displacement and the applied force. The predictions are illustrated by a black line, whereas the experimental data are represented by the dots.

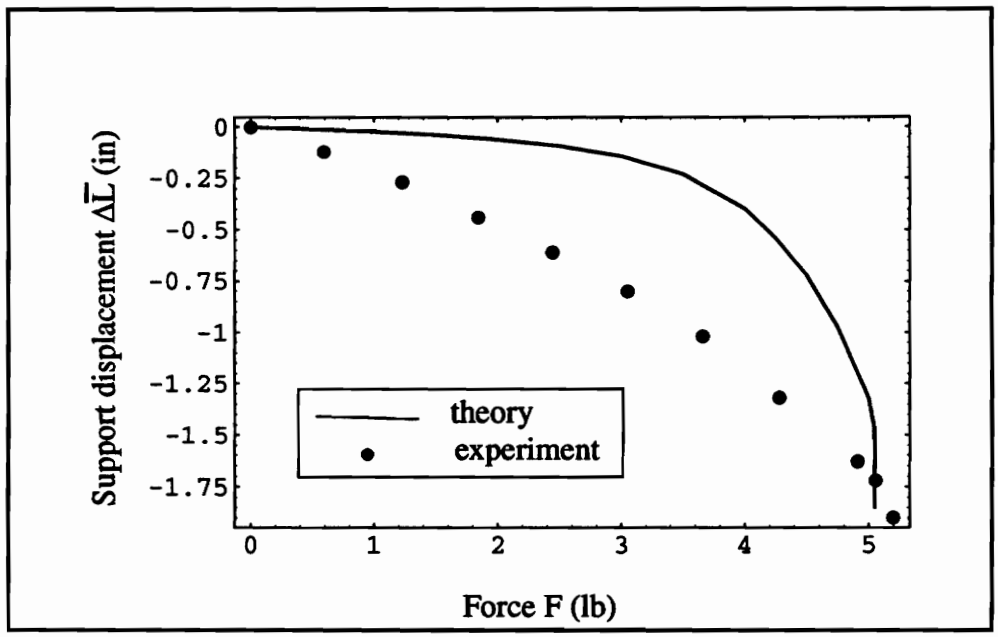


**FIG. 4-11. Support displacement as a function of the applied force**

Obviously the experimental results do not correlate well with the theoretical relation between the support displacement and the applied force. For a force level less than 5 lb the

displacements are much larger. This difference can also be explained by local laminate deformations occurring at the supports locations and affecting the support displacement. These local laminate deformations were quite obvious during the experiments and, in fact, can be seeing in Fig. 4-8. However, when the laminate has snapped, since the local deformations have disappeared, the experimental displacement is very close to the predicted one.

Overall, it is felt that the ability to predict the response of this particular class of cross-ply laminates to forces applied in the manner described is in hand. Attention now turns to using SMA to produce the forces.

# 5.0 Mechanics of cross-ply unsymmetric laminate subjected to SMA actuators

## *5.1 Constitutive Modeling of SMA*

### 5.1.1 Phenomenological approach

Shape memory alloys are metals which when plastically strained and then heated undergo reversible martensite transformation which allow them to recover these plastic strains. At low temperature martensite conditions, shape memory alloys, presumable in some particular shape, can be plastically deformed quite easily, Fig. 5-1 (a). When heated, Fig. 5-1 (b), martensite transforms into austenite and the shape memory alloy regains its original shape. While the SMA cools, Fig. 5-1 (c), austenite transforms into martensite and the SMA is able to go through other plastic strain and recovery processes. Thus, the process of regaining the original shape is strongly associated with the change of deformed low-temperature martensite phase to high-temperature austenite phase.

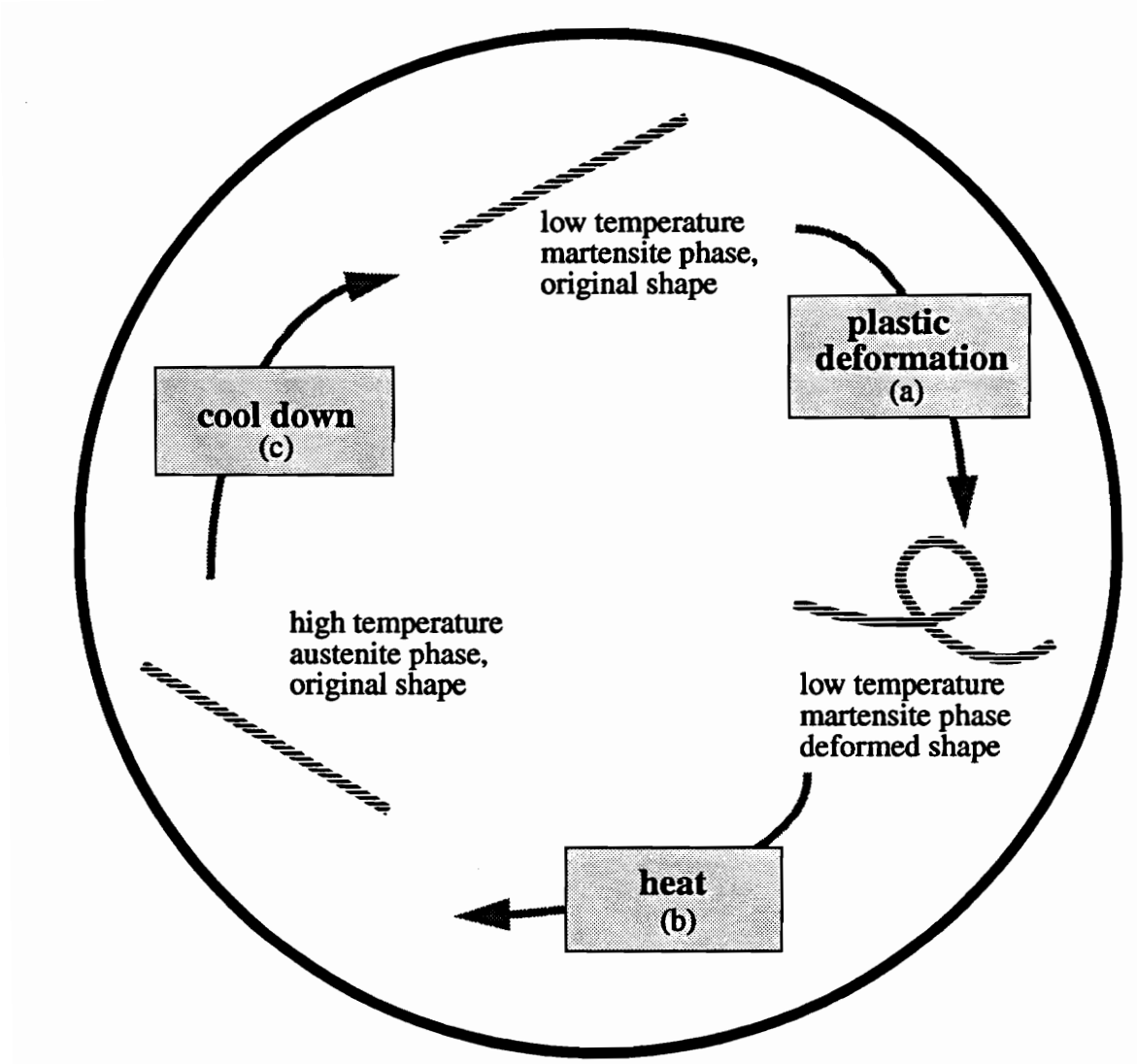


**FIG. 5-1. Shape memory effect principle**

### 5.1.2 Phase transformation relations

It is important to characterize phase transformation relations since they govern the strain recovery in shape memory effects. The martensite fraction-temperature relation can be approximated as Liang and Rogers do in their paper [12] by a cosine function. Using their results, then, for a martensite-to-austenite-transformation, the martensite fraction, $\xi$, can be evaluated by

$$\xi = \frac{1}{2}\{\cos a_A (T - A_s) + 1\}, \tag{5.1}$$

whereas for a austenite-to-martensite-transformation, the martensite fraction is given by

$$\xi = \frac{1}{2}\{\cos a_M (T - M_f) + 1\}. \tag{5.2}$$

In the above, $a_A$ and $a_M$ are material constants and are determined from

$$\begin{aligned} a_A &= \frac{\pi}{(A_f - A_s)} \\ a_M &= \frac{\pi}{(M_s - M_f)} \end{aligned} \cdot \tag{5.3}$$

The four parameters $M_f$, $M_s$, $A_s$, $A_f$ characterize the $\xi$-T relation and are, respectively, the martensite finish temperature ($M_f$), the martensite start temperature ($M_s$), the austenite finish temperature ($A_f$) and the austenite start temperature ($A_s$). Thus, starting with a 100% martensite phase-SMA, point A in Fig. 5-2, and heating it, the martensite begins to transform into austenite when the temperature reaches $A_s$ (black path). The transformation ends at $T=A_f$, a temperature at which all the martensite has become austenite, point B in

Fig. 5-2. The SMA is then 100% austenite (0% martensite). By cooling it, the transformation can be reversed. Austenite begins to transform into martensite at $M_s$ and finishes at $M_f$ (grey path).

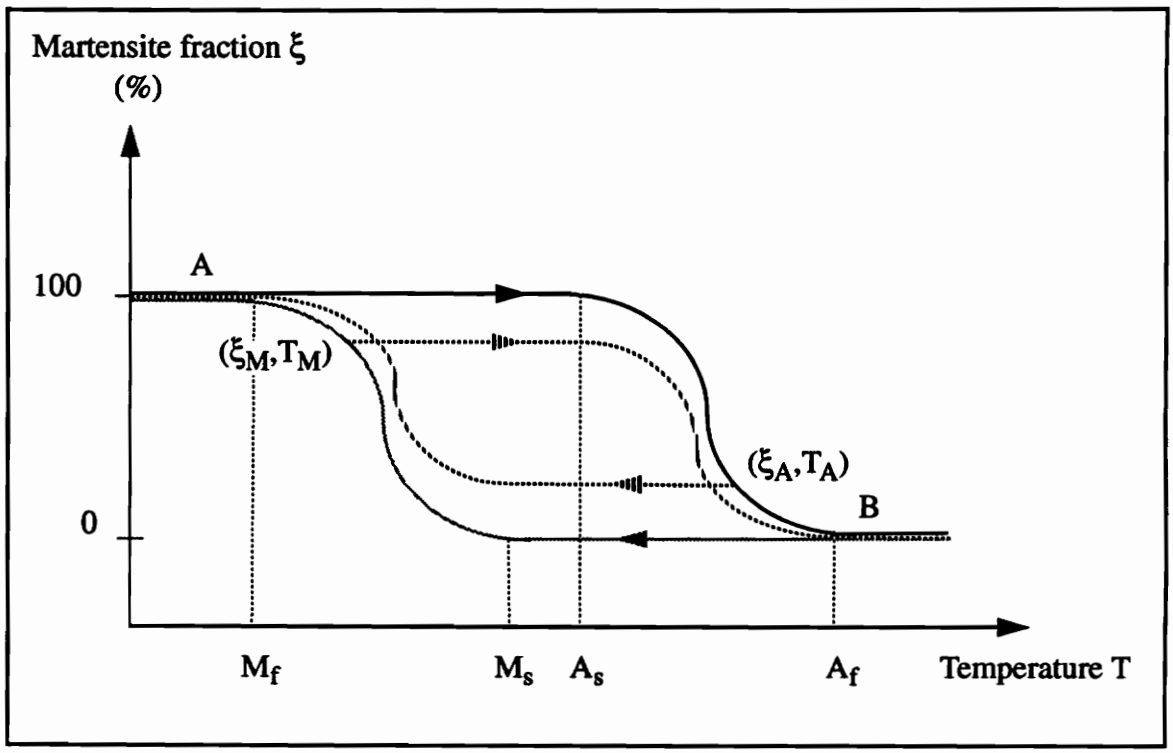


**FIG. 5-2. Martensite transformation versus temperature**

In case the SMA is composed initially with both martensite and austenite, i.e., $\xi=\xi_M$, $T=T_M$, the phase transformation starts only when the temperature is higher than $A_s$ and is described by the given relation

$$\xi = \frac{\xi_M}{2}\{\cos a_A (T - A_s) + 1\}. \tag{5.4}$$

Similarly, in a cooling process and starting with a mixed-phase SMA, i.e., $\xi=\xi_A$, $T=T_A$,

the austenite begins to transform into martensite only when the temperature becomes less than $M_s$. For this temperature range, the transformation can be derived by

$$\xi = \frac{1-\xi_A}{2}\{\cos a_M (T-M_f) + 1\} + \frac{1+\xi_A}{2} \quad . \tag{5.5}$$

Since stress induces an increase of $M_s$, $M_f$, $A_s$, $A_f$, the relation describing the phase transformation needs to be modified. The hysteresis loop of Fig. 5-2 is consequently translated to the right. To account for stress effect, a term is added to equations (5.1) and (5.2). These relations become

- for a martensite-austenite transformation

$$\xi = \frac{\xi_M}{2}\{\cos [a_A (T-A_s) + b_A \sigma] + 1\}, \tag{5.6}$$

- for a austenite-martensite transformation

$$\xi = \frac{1-\xi_A}{2}\cos [a_M (T-M_f) + b_M \sigma] + \frac{1+\xi_A}{2}, \tag{5.7}$$

where $b_A$ and $b_M$ are material constants.

### 5.1.3 Constitutive equation

The basic governing stress-strain relation for SMA is expressed by

$$\sigma^r - \sigma_o^r = D(\varepsilon^r - \varepsilon_o^r) + \Theta(T-T_o) + \Omega(\xi - \xi_o), \tag{5.8}$$

where D is the elastic modulus, $\Theta$ the thermoelastic tensor and $\Omega$ the transformation

tensor. The subscript "o" corresponds to the initial conditions.

Eq. (5.8) is general and has to be modified according to strain recovery conditions.

First, in free recovery case, there is no external load. For this case $\sigma^r = \sigma_o^r = 0$ and Eq. (5.8) becomes

$$D(\varepsilon^r - \varepsilon_o^r) + \Theta(T - T_o) + \Omega(\xi - \xi_o) = 0. \tag{5.9}$$

In the fully restrained recovery, where the SMA wire is restrained from regaining its original length, the strain does not change and $\varepsilon^r = \varepsilon_o^r$. The recovery stress $\sigma^r$ is only a function of the temperature T and the martensite fraction $\xi$ and is expressed by

$$\sigma^r - \sigma_o^r = \Theta(T - T_o) + \Omega(\xi - \xi_o). \tag{5.10}$$

At the initial temperature, $T=T_o$, with $T_o<A_s$, the martensite fraction is equal to the initial martensite fraction $\xi_o$, and the stress $\sigma^r$ is consequently equal to $\sigma_o{}^r$ which is assumed to be zero. Until the temperature T reaches the austenite start temperature, the martensite fraction does not change and the stress-temperature relation is

$$\sigma^r = \Theta(T - T_o). \tag{5.11}$$

As stress induces an increase in the austenite start temperature, a new austenite start temperature, $A_s{}^m$, needs to be computed to know at which temperature martensite will transform into austenite. At $T=A_s{}^m$, the martensite fraction $\xi$ is still equal to $\xi_o$. Thus,

$$\xi = \xi_o = \frac{\xi_o}{2}\{\cos[a_A(A_s^m - A_s) + b_A\sigma^r] + 1\}. \tag{5.12}$$

After some computations, Eq. (5.12) can be written as

$$\begin{aligned} \cos[a_A(A_s^m - A_s) + b_A\sigma^r] &= 1 \\ a_A(A_s^m - A_s) + b_A\sigma^r &= 0 \cdot \end{aligned} \tag{5.13}$$

Substituting $\sigma^r$ by Eq. (5.11), Eq. (5.13) becomes

$$a_A (A_s^m - A_s) + b_A \Theta (T - T_o) = 0 \cdot \tag{5.14}$$

Thus, the new austenite start temperature is

$$A_s^m = \frac{C_A A_s - \Theta T_o}{C_A - \Theta}. \tag{5.15}$$

The corresponding stress, $\sigma_{As}^r$, is obtained by substituting $A_s^m$ into Eq. (5.11) and is expressed by

$$\sigma_{As}^r = \Theta (A_s^m - T_o). \tag{5.16}$$

As soon as temperature T is above $A_s^m$, Eq. (5.10) can be used but with others initial conditions for the stress and temperature which are,

$$\begin{aligned} T_o &= A_s^m \\ \sigma_o^r &= \sigma_{As}^r \cdot \end{aligned} \tag{5.17}$$

Thus, Eq. (5.10) becomes

$$\sigma^r - \sigma_{As}^r = \Theta (T - A_s^m) + \Omega (\xi - \xi_o), \tag{5.18}$$

with

$$\xi = \frac{\xi_o}{2} \{ \cos [a_A (T - A_s) + b_A \sigma^r] + 1 \}. \tag{5.19}$$

This relation is not explicit and iteration is needed to converge. If the temperature reaches the austenite finish temperature, all the martensite has been transformed into austenite and $\xi$=0. Like the temperature $A_s$, the austenite finish temperature $A_f$ has increased due to the presence of stresses. The new austenite finish temperature, $A_f^m$, needs to be computed. At $T=A_f^m$, the martensite fraction $\xi$ is zero. Thus, from Eq. (5.18),

$$\sigma^r = \Theta (A_f^m - A_s^m) - \Omega \xi_o + \sigma_{As}^r, \tag{5.20}$$

and from Eq. (5.6)

$$\frac{\xi_o}{2}\{\cos[a_A(A_f^m - A_s) + b_A\sigma^r] + 1\} = 0$$
$$\cos[a_A(A_f^m - A_s) + b_A\sigma^r] + 1 = -1 \tag{5.21}$$
$$a_A(A_f^m - A_s) + b_A\sigma^r = \pi\,.$$

Substituting Eq. (5.20) into Eq. (5.21), the new austenite finish temperature is determined.

$$a_A(A_f^m - A_s) + b_A(\Theta(A_f^m - A_s^m) - \Omega\xi_o + \sigma_{As}^r) = \pi$$
$$A_f^m(a_A + b_A\Theta) = \pi + a_A A_s + b_A\Theta A_s^m + b_A\Omega\xi_o - b_A\sigma_{As}^r \tag{5.22}$$
$$A_f^m = \frac{\pi + a_A A_s + b_A\Theta A_s^m + b_A\Omega\xi_o - b_A\sigma_{As}^r}{a_A + b_A\Theta}$$

For $T>A_f^m$, the stress-temperature relation is

$$\sigma^r - \sigma_{Af}^r = \Theta(T - A_f^m)\,, \tag{5.23}$$

with $\sigma^r_{Af}$ being the stress at $T=A_f^m$, and given by Eq. (5.20),

$$\sigma_{Af}^r = \Theta(A_f^m - A_s^m) - \Omega\xi_o + \sigma_{As}^r\,. \tag{5.24}$$

Thus, the stress-temperature relation to use for a restrained recovery case can be summarized by

$$\sigma^r = \begin{cases} \Theta(T - T_o) + \sigma_o^r & T_o \le T \le A_s^m \\ \Theta(T - A_s^m) + \Omega(\xi - \xi_o) + \sigma^r{}_{As} & A_s^m \le T \le A_f^m \\ \Theta(T - A_f^m) + \sigma_{Af}^r & A_f^m \le T\,. \end{cases} \tag{5.25}$$

In controlled recovery case, the SMA wire is under some tension, which allows it to recover some strain but prevents it from full recovery. In this case, the constitutive equation is given by Eq. (5.8),

$$\sigma^r - \sigma_o^r = D(\varepsilon^r - \varepsilon_o^r) + \Theta(T - T_o) + \Omega(\xi - \xi_o)\,. \tag{5.26}$$

Two categories can be distinguished in controlled recovery. The first category assumes that a constant stress is applied ($\sigma^r = \sigma_o^r$). Eq. (5.8) becomes

$$D(\varepsilon^r - \varepsilon_o^r) + \Theta(T - T_o) + \Omega(\xi - \xi_o) = 0, \tag{5.27}$$

where the stress appears in the fraction of material in the martensite phase. Using the same procedure as for the restrained recovery case, the new transitions temperatures, $A_s^m$ and $A_f^m$ need to be computed.

The second category assumes that the stress is proportional to the recovery strain and can be modeled as an SMA-spring system, the SMA and the spring being in series.

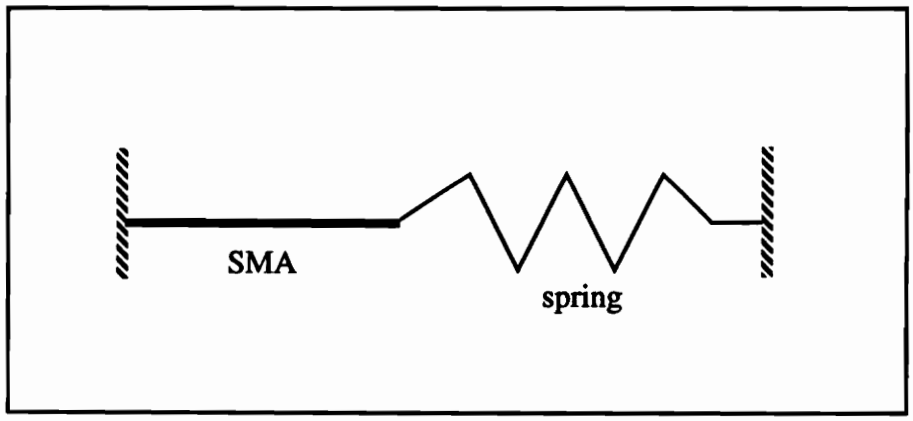


**FIG. 5-3. SMA-spring structure model**

Consider a SMA-spring structure as shown in Fig. 5-3. The SMA is a wire of length L and cross-section area s attached in series with a spring of constant stiffness K. The stress in the SMA wire can be expressed as a function of strain as

$$\sigma^r - \sigma_o^r = \frac{KL}{s}(\varepsilon_o^r - \varepsilon^r). \tag{5.28}$$

Substituting Eq. (5.28) in Eq. (5.8), the constitutive equation becomes

$$(1+\frac{s}{KL}D)\ (\sigma^r-\sigma_o^r)\ =\ \Theta(T-T_o)+\Omega(\xi-\xi_o)\,. \tag{5.29}$$

This equation can be handled the same way as for the restrained recovery case. Eq. (5.29) is only valid for a linear spring. A nonlinear spring would involve different results. It is important to note that the above constitutive equation for SMA describes with a good accuracy the SMA behavior for strains up to 5%. Thus, to be able to obtain good correlations between theory and experiment, the SMA should not be deformed more than 5%.

In essence, as will be seen, the unsymmetric laminate is a nonlinear spring so the SMA-unsymmetric laminate behaves as a SMA wire and nonlinear spring in parallel.

## *5.2 Cross-ply unsymmetric laminate subjected to SMA actuators*

### 5.2.1 Principle

Since shape memory alloys, when plastically deformed, can recover these deformations when heated and in the process generate stresses, they may be used as actuators to make a laminate snap, much as the weight-generated force did in chapter 4. Figures 1-2 and 1-3 illustrated how these force actuators may be utilized to cause the laminate to snap from one cylindrical shape to another. However, since SMA can recover only up to 5% strain in a predictable fashion, to be predictable, an appropriate actuator configuration has to be found to utilize SMA. The configuration has to allow the SMA strains to stay within 5%, and generate enough force to be able to snap the laminate. If the support distance for the

SMA wire, e of Fig. 3-1, is too far from the surface of the laminate, strains greater than 5% are generated. However, if the support distance is too small, large forces are required to produce the snapping moment, which is proportional to e. Furthermore, if the support distance is too small, due to the curvature of the laminate, the SMA wire will contact the surface of the laminate. This is shown in Fig. 5-4.

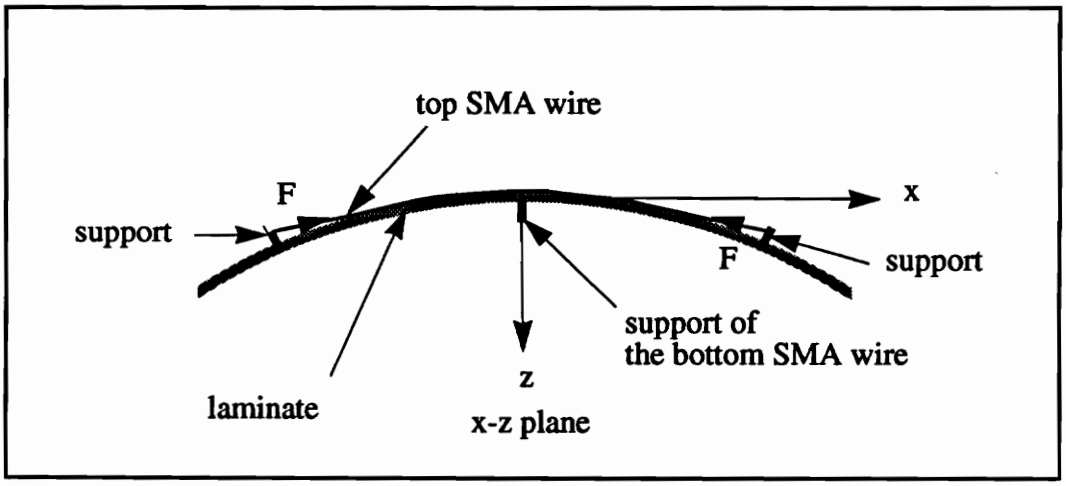


**FIG. 5-4. System description**

For the SMA material used here, and the laminate geometry considered, the support distance used with the weight-generated force experiment was too large. Plastic strains in excess of 15% were required. Thus it was necessary to use SMA wire configurations as shown in Fig. 5-4, with the wire contacting the laminate.

### 5.2.2 Constitutive equation of the SMA wire

With the SMA wire fastened between two supports attached to the laminate, the wire-laminate system can be modeled as a SMA-spring system, as shown in Fig. 5-5 and as

discussed before. The only difference is that for the laminate the spring stiffness K is not constant. Rather the spring stiffness is a function of F. Thus, the force-displacement relation of the laminate needs to be computed. This can be done as follows:

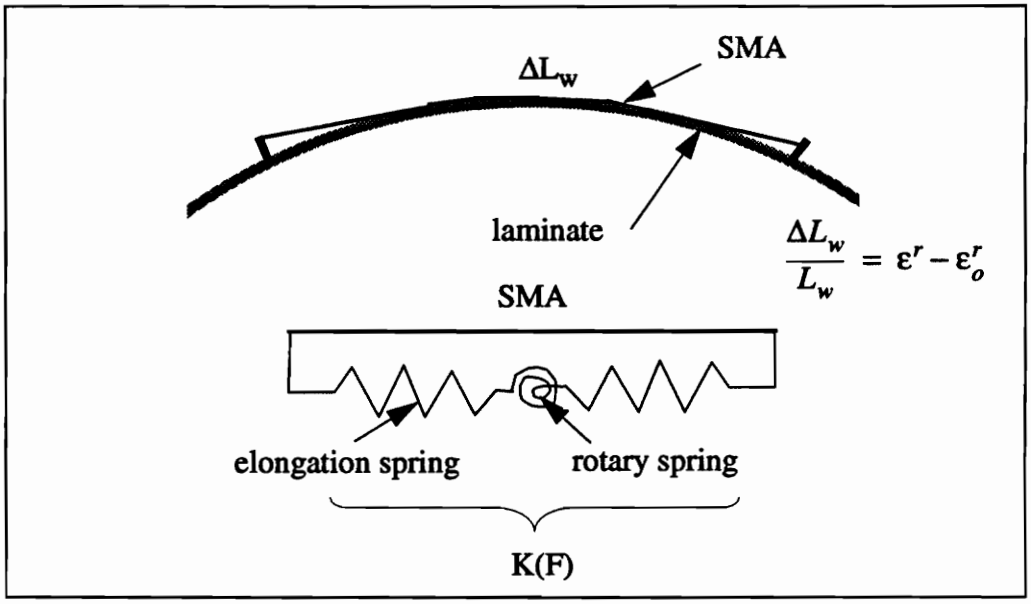


**FIG. 5-5. Modelisation of the SMA wire-laminate system**

As discussed previously, the constitutive equation for the SMA wire is

$$\sigma^r - \sigma_o^r = D(\varepsilon^r - \varepsilon_o^r) + \Theta(T - T_o) + \Omega(\xi - \xi_o). \tag{5.30}$$

The stress and strain can be expressed, respectively, in terms of the force F and the change in length of the SMA wire $\Delta L_w$ by

$$\begin{aligned} \sigma^r &= \frac{F}{s} \\ \sigma_o^r &= \frac{F_o}{s} \\ \varepsilon^r - \varepsilon_o^r &= \frac{\Delta L_w}{L_w}, \end{aligned} \tag{5.31}$$

where

s= cross section area of SMA wire

$L_w$=length of SMA wire.

Thus, substituting these expressions into Eq. (5.30), the constitutive equation becomes

$$\frac{F}{s} - \frac{F_o}{s} = D\frac{\Delta L_w}{L_w} + \Theta(T - T_o) + \Omega(\xi - \xi_o). \tag{5.32}$$

The constitutive equation is now function of the force F, the change in length $\Delta L_w$ and the temperature T. However, the displacement can be related to the force.

### 5.2.3 Computation of the force-displacement relation

Since the SMA wire is partially tangent to the laminate curvature, the force F generated in the SMA wire is no longer parallel to the x-axis, as it was in the case in chapter 3. Thus, the theory derived in that chapter has to be slightly modified. The main change is in the applied force virtual work computation. The virtual work of the applied force is given by

$$\delta W_F = 2\vec{F} \cdot \delta\vec{r}\,, \tag{5.33}$$

where $\delta\vec{r}$ is a virtual displacement and can be written as

$$\delta\vec{r} = \delta u\vec{i} + \delta w\vec{k}\,. \tag{5.34}$$

Since the support height e is small, the force is approximately perpendicular to the support, as shown in Fig. 5-6. There is in fact a small angle $\alpha$, as shown in Fig. 5-6, that is neglected to simplify the computations. This approximation is thought not to involve to

much error.

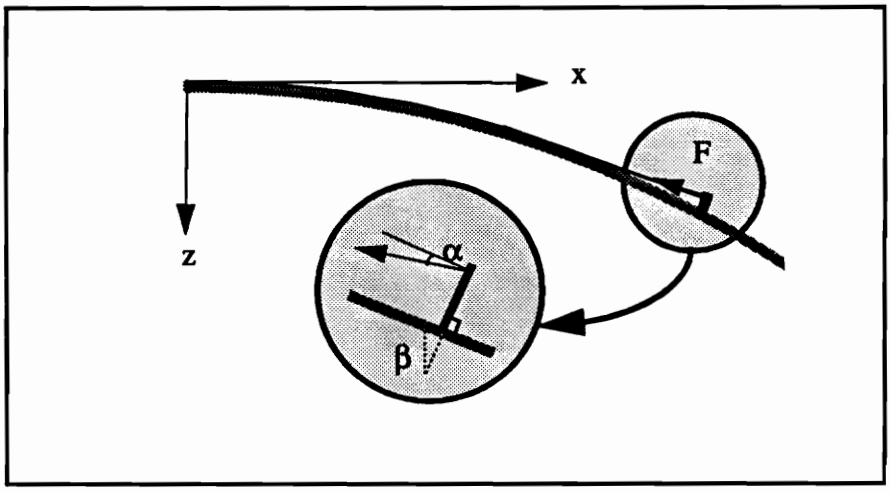


**FIG. 5-6. Direction of the SMA-induced force**

Thus, the force F can be expressed by

$$\vec{F} = -F(\cos\beta\vec{i} + \sin\beta\vec{k}), \tag{5.35}$$

and

$$\delta W_F = -2F(\cos\beta\delta u + \sin\beta\delta w) \cdot \tag{5.36}$$

From Eq. (3.13),

$$\begin{aligned}\delta\vec{u} &= (\delta u^o + (e+\frac{H}{2})\delta\beta\cos\beta)\vec{i} \\ &= \left(L_{xp}c_1 - \frac{L_{xp}^3}{3}aa_1 + (e+\frac{H}{2})L_{xp}\cos(aL_{xp})a_1\right)\varepsilon\vec{i}\cdot\end{aligned} \tag{5.37}$$

Similarly, the component $\delta\vec{w}$ is equal to

$$\begin{aligned}\delta\vec{w} &= (\delta w^o + (e+\frac{H}{2})\delta\beta\sin\beta)\vec{k} \\ &= \left(\frac{L_{xp}^2}{2}\delta a + (e+\frac{H}{2})L_{xp}\delta a\sin(aL_{xp})\right)\vec{k}\cdot\end{aligned} \tag{5.38}$$

As in chapter 3, the displacement $\delta a$ and $\delta c$ are respectively replaced by $\varepsilon a_1$ and $\varepsilon c_1$ to be consistent with the computation of the first variation of the strain energy $\delta\Pi$.

Thus, the virtual work can be expressed by

$$\begin{aligned}\delta W_F = &-2F\cos(aL_{xp})\,\varepsilon\left(L_{xp}c_1 - \frac{L_{xp}^3}{3}aa_1 + (e+\frac{H}{2})L_{xp}\cos(aL_{xp})\,a_1\right)\\ &-2F\sin(aL_{xp})\,\varepsilon\left(\frac{L_{xp}^2}{2}a_1 + (e+\frac{H}{2})L_{xp}a_1\sin(aL_{xp})\right)\\ \cong &-2F\varepsilon\left((e+\frac{H}{2})L_{xp}a_1 + \left(1-\frac{a^2L_{xp}^2}{2}\right)\left(L_{xp}c_1 - \frac{L_{xp}^3}{3}aa_1\right)\right.\\ &\left.+aL_{xp}\left(\frac{L_{xp}^2}{2}\right)a_1\right).\end{aligned} \tag{5.39}$$

Then, the principal of virtual work can be applied and the equilibrium equations obtained following the same procedure as explained in chapter 3. By solving these equilibrium equations, the shape of the laminate is determined for a given force level. It should be noticed that the influence of the SMA touching the surface of the laminate has not been accounted for in the virtual work expression. The tension in the SMA wire exerts a force on the laminate, along the line where the wire touches the laminate, and the force is normal to the surface of the laminate. This effect on the shape of the laminate has been ignored.

Since with an SMA wire the change in length and the force generated are related through Eq. (5.32), the change in length of the SMA wire, $\Delta L_w$, needs to be computed for these shortened supports. Since the SMA wire is partially touching the laminate surface following its contour, as shown in Fig. 5-7, the length of the wire, from one support to the other, is not as simple to determine as in chapter 3. In fact, after having determined the

position of the support end, $(S_x, S_z)$ in Fig. 5-7, the location where the SMA wire becomes tangent to the laminate surface, $(T_x, T_z)$ in Fig. 5-7, has to be computed. These computations are presented in Appendix E.

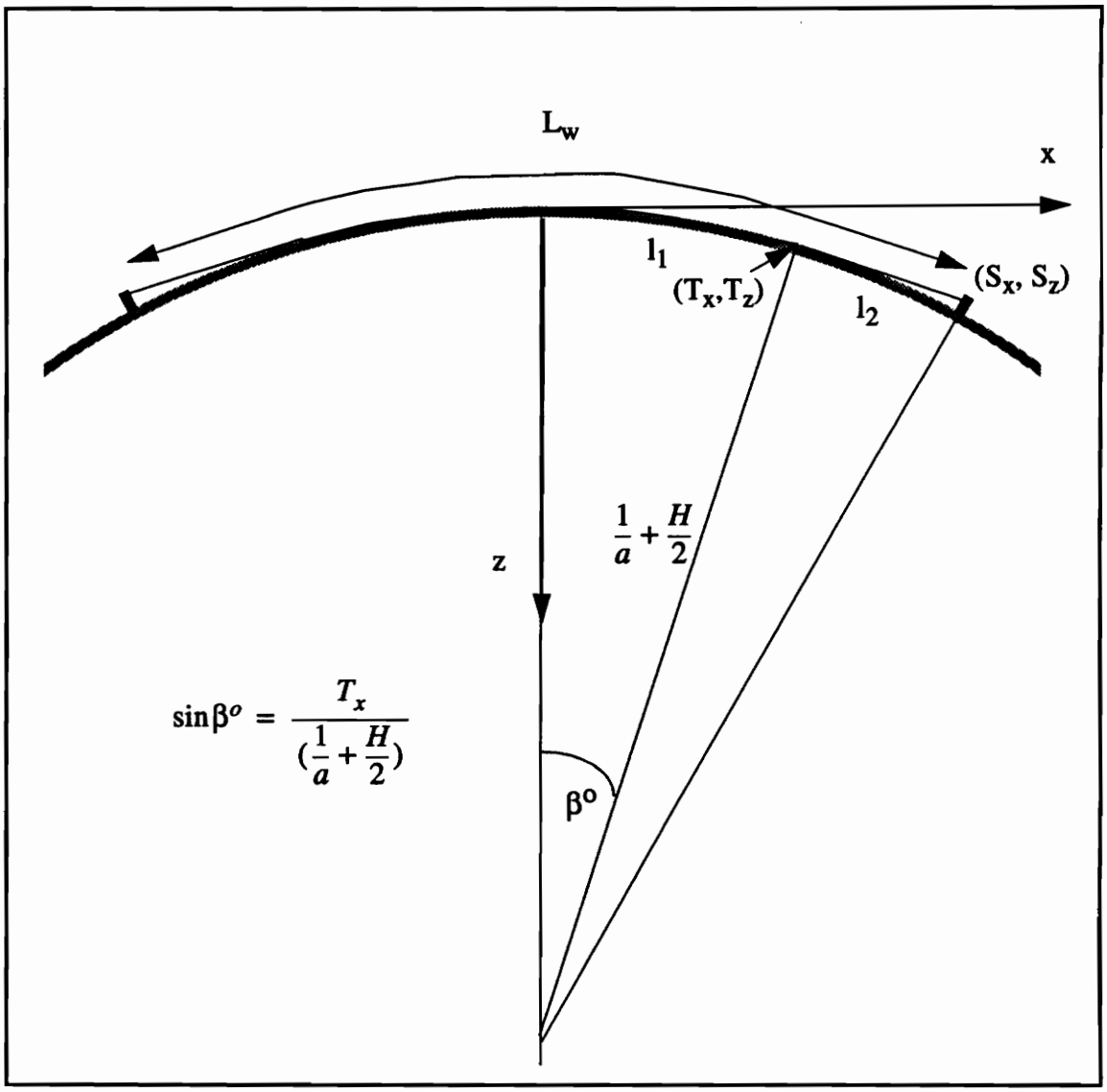


**FIG. 5-7. SMA-wire length computation**

Then, the length $L_w$ of the SMA wire for a given laminate curvature is

$$\begin{aligned} L_w &= 2\,(l_1 + l_2) \\ &= 2\,((\frac{1}{a} + \frac{H}{2})\,\beta^o + \sqrt{(S_x - T_x)^2 + (S_z - T_z)^2}), \end{aligned} \tag{5.40}$$

where

$$\beta^o = \text{asin}\left(\frac{aT_x}{1 + a\frac{H}{2}}\right). \tag{5.41}$$

Thus, the change in length $\Delta L_w$ can be written as

$$\begin{aligned} \Delta L_w &= L_w - L_{wi} \\ &= 2\left[(\frac{1}{a} + \frac{H}{2})\,\text{asin}\left(\frac{aT_x}{1 + a\frac{H}{2}}\right) + \sqrt{(S_x - T_x)^2 + (S_z - T_z)^2}\right] \\ &-2\left[(\frac{1}{a_i} + \frac{H}{2})\,\text{asin}\left(\frac{a_i T_{xi}}{1 + a_i\frac{H}{2}}\right) + \sqrt{(S_{xi} - T_{xi})^2 + (S_{zi} - T_{zi})^2}\right], \end{aligned} \tag{5.42}$$

where the i subscript refers to the initial configuration.

For a given force F applied on the support on the laminate, as shown in Fig. 5-6, a, $S_x$, $S_z$, $T_x$ and $T_z$ can be computed and the change in length $\Delta L_w$ can be evaluated. Following this procedure for increasing F, a relation between $\Delta L_w$ and the force F is developed. This relation can not be symbolically expressed. However, an approximate explicit expression can be obtained by computing an interpolation of the relation between $\Delta L_w$ and the force F. Thus, $\Delta L_w$ can be expressed as

$$\Delta L_w = AF + BF^2 + CF^3 + \ldots, \tag{5.43}$$

where the coefficients A, B, C,..., are computed by the interpolation. This is illustrated by an example. Consider a laminate of the same size and properties as in the numerical

example of chapter 3. These are

$$L_x=12 \text{ in.}$$
$$L_y=12 \text{ in.}$$
$$h=0.006 \text{ in.}$$
$$E_1=20.0 \text{ Msi}$$
$$E_2=1.3 \text{ Msi} \qquad (5.44)$$
$$G_{12}=1.03 \text{ Msi}$$
$$\nu_{12}=0.3$$
$$\alpha_1=-0.167\ 10\text{-}6\ /^{o}\text{F}$$
$$\alpha_2=15.6\ 10\text{-}6\ /^{o}\text{F}.$$

Supports are clamped at a distance $L_{xp}$ from the center of the laminate and a SMA wire is fastened at a distance e out the support, as depicted in Fig. 5-8. The lengths used are

$$e=0.275 \text{ in.}$$
$$L_{xp}=4 \text{ in.}$$

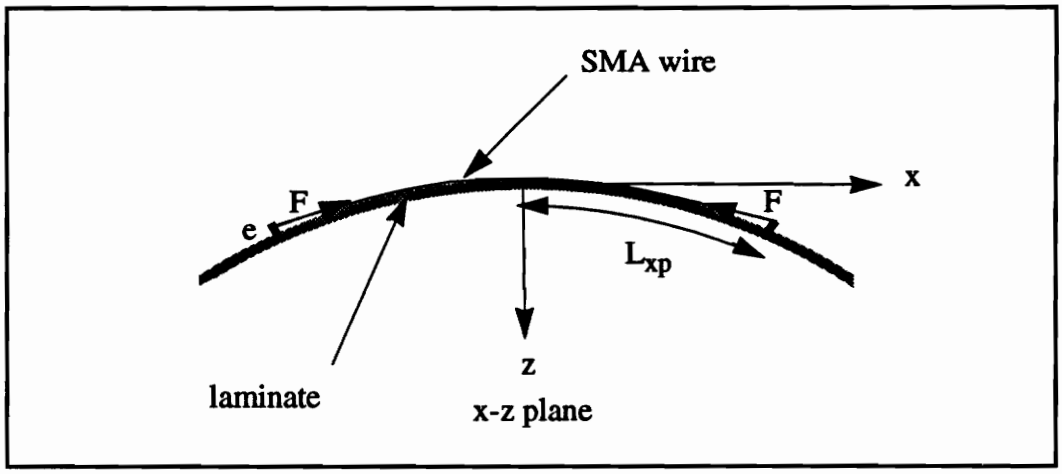


**FIG. 5-8. Description of the SMA wire-laminate system**

For increasing force level, the curvature a and the change in length $\Delta L_w$ are evaluated. Figure 5-9 represents the relation between the curvatures a and b, and the applied force F. It can be noted that the snapping force is 37.65 lb. The character of this force-curvature relation is somewhat different than the case of the force always remaining parallel with the x-axis, Fig. 3-10. The large value of the force to cause the laminate to snap, relative to the value in Fig. 3-10, is due to the smaller value of e used in the current SMA wire configuration. Figure 5-10 illustrates the relation between the change in length $\Delta L_w$ and the force F by a black line. By computing an interpolation of this relation, an approximate explicit function is obtained. This approximate function is represented by a dashed line in Fig. 5-10. In this case, a third order interpolating polynomial is obtained and,

$$\begin{aligned} &A=-2670\ 10^{-6}\text{in/lb} \\ &B=74.1\ 10\text{-}6\text{in/lb}^2 \\ &C=-1.34\ 10^{-6}\text{in/lb}^3. \end{aligned} \tag{5.45}$$

Thus, an approximate explicit function can relate the change in length $\Delta L_w$ to the applied force F. By substituting this approximate function in Eq. (5.32), a general force-temperature relation can be obtained and is expressed by

$$\begin{aligned} \frac{F}{s}-\frac{F_o}{s} = \frac{D}{L_w}\left(A\left(F-F_o\right)+B\left(F^2-F_o^2\right)+C\left(F^3-F_o^3\right)+\ldots\right) \\ +\Theta\left(T-T_o\right)+\Omega\left(\xi-\xi_o\right)\cdot \end{aligned} \tag{5.46}$$

This equation is general for every temperature range. To be efficiently used, Eq. (5.46) has to be handled the same way as for the restrained recovery case. That is, the transition temperature, $A_s^m$ and $A_f^m$, and the corresponding forces, $F_{As}$ and $F_{Af}$, have to be computed. The constitutive equation has to be rewritten and expressed as a function of these parameters.

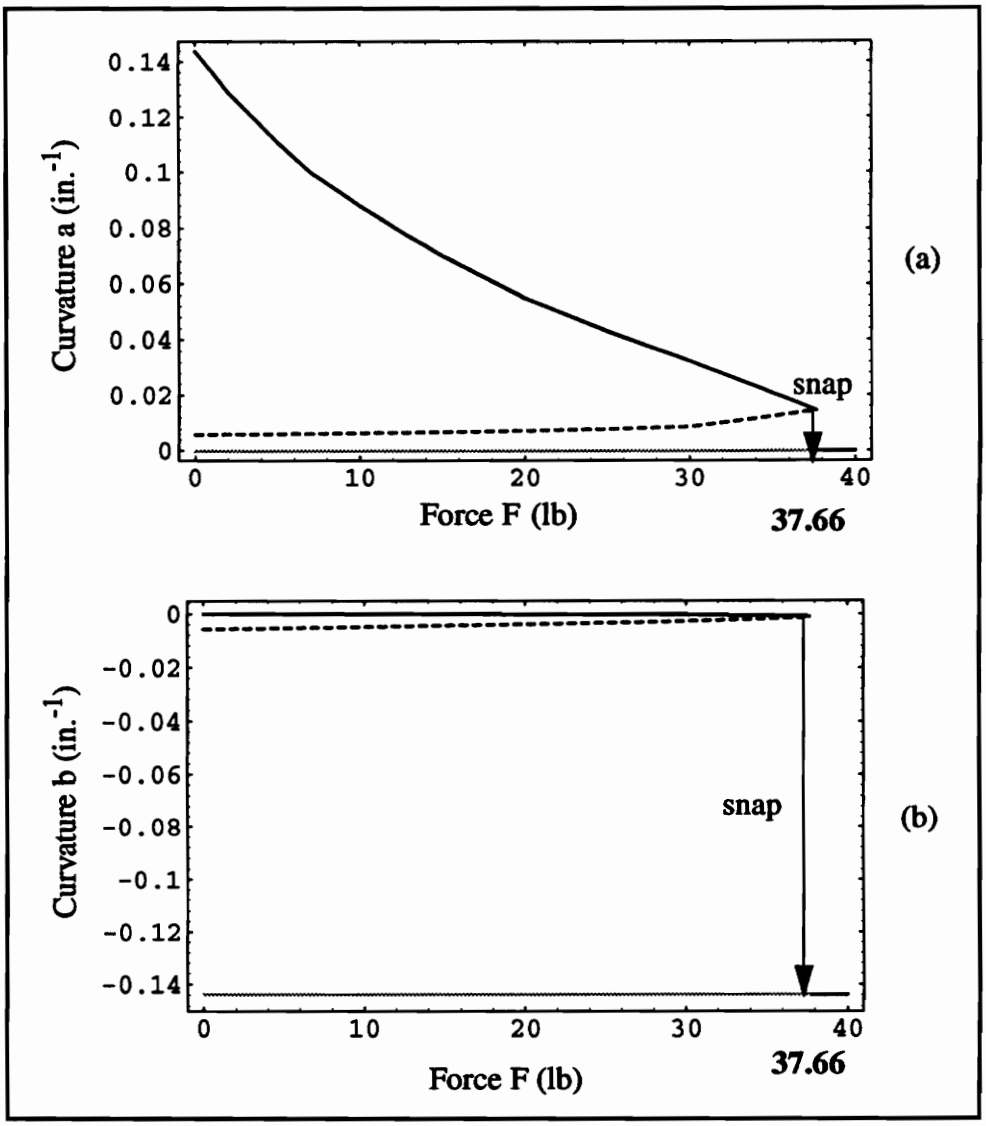


**FIG. 5-9. SMA-induced curvature change**

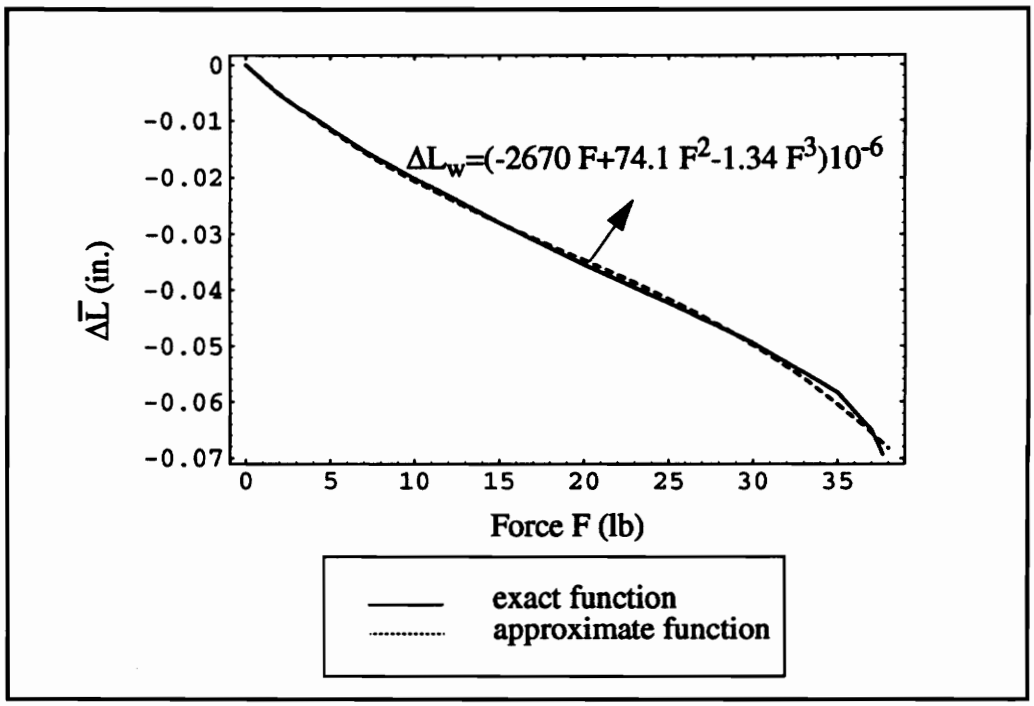


**FIG. 5-10. $\Delta L_w$ vs. the applied force F**

### 5.2.4 Computation of the force versus the temperature

In an actual application, the force is generated in the wire due to a temperature change, which in turn is caused by voltage in the wire and the resistance in the wire. Starting from room temperature, the temperature in the wire is increased until enough martensite is transformed to generate a force great enough to make the laminate snap. The relation between the force and the temperature can be expressed by

$$\frac{F}{s} = \begin{cases} \Theta(T-T_o) + \dfrac{F_o}{s} \\ \quad + \dfrac{D}{L_w}\left(A\left(F-F_{As}\right) + B\left(F^2-F_{As}^2\right) + \ldots\right) & T_o \le T \le A_s^m \\ \Theta\left(T-A_s^m\right) + \Omega\left(\xi-\xi_o\right) + \dfrac{F_{As}}{s} \\ \quad + \dfrac{D}{L_w}\left(A\left(F-F_{As}\right) + B\left(F^2-F_{As}^2\right) + \ldots\right) & A_s^m \le T \le A_f^m \\ \Theta\left(T-A_f^m\right) + \dfrac{F_{Af}}{s} \\ \quad + \dfrac{D}{L_w}\left(A\left(F-F_{Af}\right) + B\left(F^2-F_{Af}^2\right) + \ldots\right) & A_f^m \le T, \end{cases} \tag{5.47}$$

where $A_s^m$, $A_f^m$, $F_{As}$, $F_{Af}$ are respectively the transition temperatures and corresponding forces. These transition forces and temperatures can be computed following the exact procedure as in paragraph 5.1.3. However, simple symbolic expressions can not be obtained since the equations are not linear, but have square and cubic terms ($F^2$, $F^3$).

Equation (5.47) is not explicit since the martensite fraction $\xi$ depends on F. However, by assigning some values for the temperature, the force F can be determined by solving the following equation

$$y = -\frac{F}{s} + \begin{cases} \Theta(T-T_o) + \dfrac{F_o}{s} \\ \quad + \dfrac{D}{L_w}\left(A\left(F-F_{As}\right) + B\left(F^2-F_{As}^2\right) + \ldots\right) & T_o \le T \le A_s^m \\ \Theta\left(T-A_s^m\right) + \Omega\left(\xi-\xi_o\right) + \dfrac{F_{As}}{s} \\ \quad + \dfrac{D}{L_w}\left(A\left(F-F_{As}\right) + B\left(F^2-F_{As}^2\right) + \ldots\right) & A_s^m \le T \le A_f^m \\ \Theta\left(T-A_f^m\right) + \dfrac{F_{Af}}{s} \\ \quad + \dfrac{D}{L_w}\left(A\left(F-F_{Af}\right) + B\left(F^2-F_{Af}^2\right) + \ldots\right) & A_f^m \le T, \end{cases} = 0. \tag{5.48}$$

Repeating this procedure for increasing temperature, a force-temperature relation can be developed. This can be done for the SMA wire-laminate system just studied. The SMA wire attached to that laminate has the following properties

$$
\begin{aligned}
&L_w=8.09 \text{ in.}\\
&s=0.000628 \text{ in.}\\
&\Theta=0.005 \text{ Ksi/}^{o}\text{C}\\
&\Omega=-D_M\varepsilon_L\\
&D=D_A+\xi(D_M-D_A)\\
&D_A=9710 \text{ Ksi}\\
&D_M=3810 \text{ Ksi}\\
&\varepsilon_L=6.7\%\\
&\varepsilon_o=5\%\\
&\xi o=\varepsilon_o/\varepsilon_L\\
&C_A=1.5 \text{ Ksi/}^{o}\text{C}\\
&A_s=34.6\ ^{o}\text{C}\\
&A_f=49.0\ ^{o}\text{C}.
\end{aligned}
\tag{5.49}
$$

The initial conditions are

$$
\begin{aligned}
&F_o=0 \text{ lb}\\
&T_o=25\ ^{o}\text{C}.
\end{aligned}
$$

The transition temperature and forces are computed using Eq. (5.46) and following the same procedure as in paragraph 5.1.3.They are equal to

$$
\begin{aligned}
&A_s^{m}=34.615\ ^{o}\text{C}\\
&A_f^{m}=98.66\ ^{o}\text{C}
\end{aligned}
\tag{5.50}
$$

$F_{As}$=0.01436 lb

$F_{Af}$=46.22 lb.

By assigning values for the temperature, the associated force can be computed using Eq. (5.48). For example, at T=50°C, since $A_s^m \leq T \leq A_f^m$, the equation to be solved is

$$y = -\frac{F}{s} + \frac{D}{L_w}\left(A\left(F - F_{As}\right) + B\left(F^2 - F_{As}^2\right) + \ldots\right) + \Omega\left(\xi - \xi_o\right) + \Theta\left(T - A_s^m\right) + \frac{F_{As}}{s} = 0. \tag{5.51}$$

By plotting y as a function of F, the value F which cancels y can be determined as shown in Fig. 5-11. Following this procedure for different temperatures a relation is built between the force and the temperature, as illustrated in Fig. 5-12. Since the snapping force is 37.66 lb, the laminate should change its shape when the temperature in the SMA wire reaches 83.4 °C.

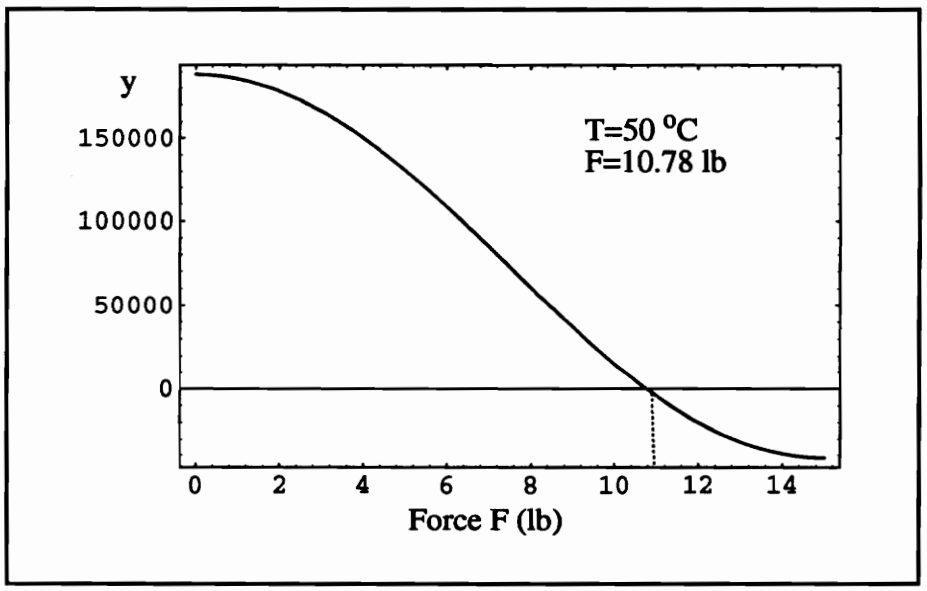


**FIG. 5-11. Function y for T=50 °C**

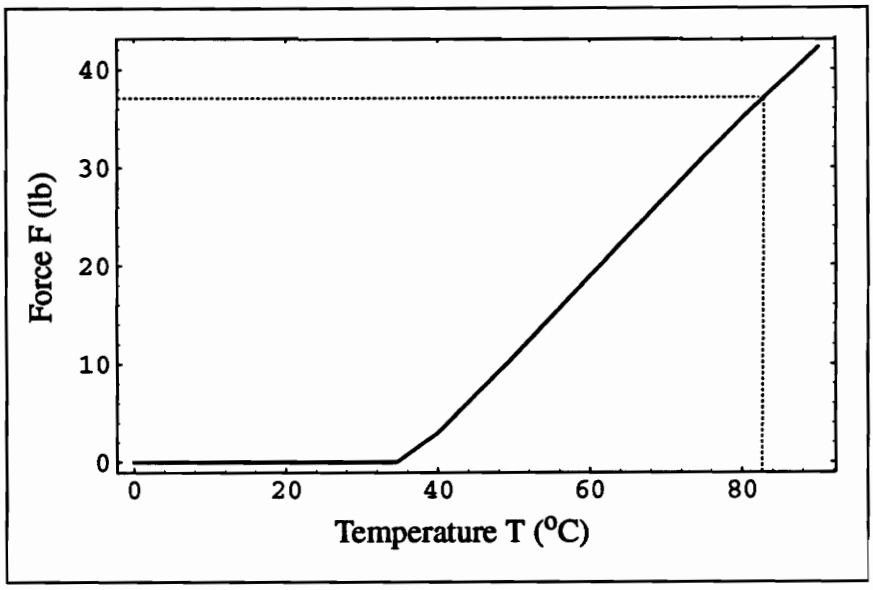


**FIG. 5-12. Relation between the SMA-induced force and the SMA temperature**

### 5.2.5 Computation of the curvature versus the temperature

Since the laminate curvature is related to the force, Fig. 5-9, and the force to the temperature, Fig. 5-12, the curvature can be easily related to the temperature. Figure 5-13 represents this relation for the example just studied.

Thus, constitutive equations, describing the mechanics involved when the laminate is subjected to SMA-induced force, have been derived. More specifically, the curvature of the laminate has been related to the temperature the SMA wire is heated to. Thus, experiments can now be conducted to study how the laminate responses to an SMA-induced force.

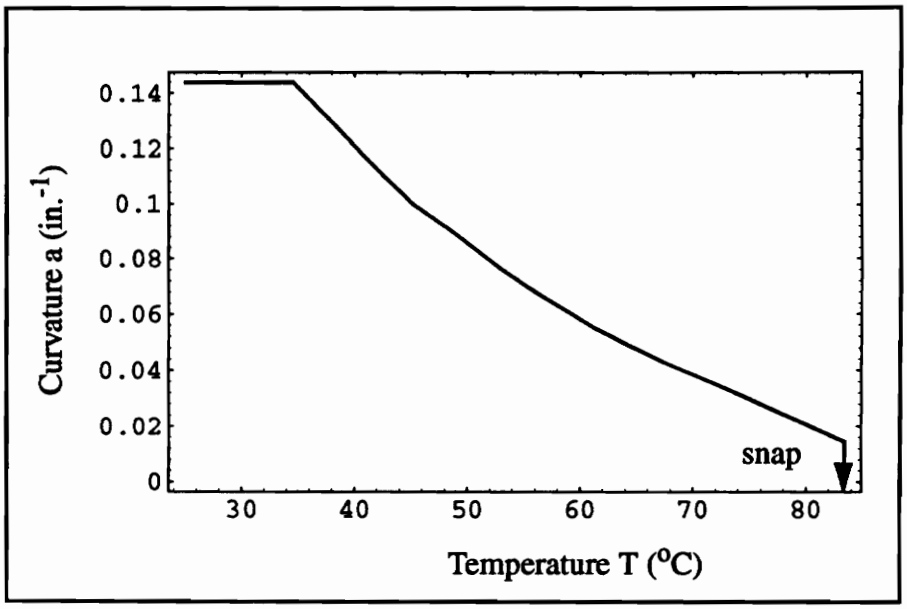


**FIG. 5-13. Curvature a as a function of the temperature**

# 6.0 Experiments with SMA induced-force

## *6.1 Experimental setup*

### 6.1.1 Description

The laminate tested is the one which has already been used in the experiments of chapter 4. The support locations are kept the same. However, new supports have to be designed. They have to be nonconducting and be able to maintain tightly the SMA wire during the strain recovery process. One support is simply a screw terminal where the SMA wire can be easily attached. The other support is just a bolt extending through the laminate. Thus, the SMA wire is attached to the screw terminal, around the bolt and back to the screw terminal, as shown in Fig. 6-1. In this configuration, the supports are not used to clamp the laminate to a table. The laminate simply lies on a flat surface.

Before being attached, the SMA wire is first elongated and then unloaded to generate 5% martensite residual strain. It is then attached to the supports. In fact the SMA wire is put under a small tension to prevent it from being slack. Due to this small initial force, the laminate curvature decreases. This curvature change is used to estimate the initial force.

Since the SMA wire is touching the laminate which is conductible, a piece of teflon coated fabric is between the SMA wire and the laminate surface. The SMA wire is connected to a power supply.

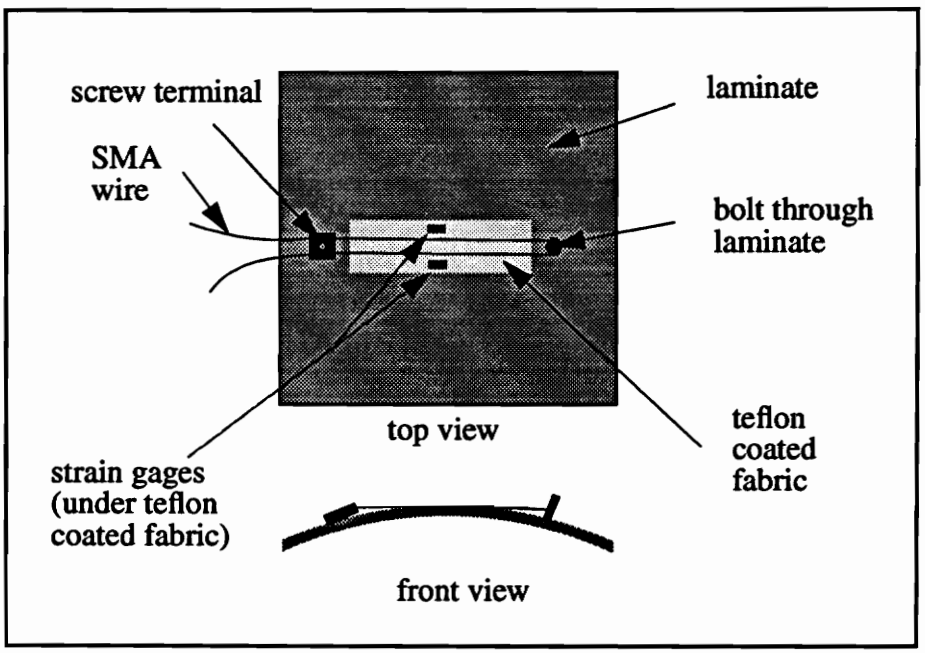


**FIG. 6-1. System description**

### 6.1.2 Measurements

A voltmeter and an ampmeter are used to measure, respectively, the voltage and the current in the SMA wire. Temperature is not measured. It is difficult to obtain reliable temperature measurements, since the temperature is not uniform through the radius of the wire, nor along the length. In addition, since the SMA wire is touching the laminate surface, the temperature dissipates indeed in the laminate.

Strains on the surfaces of the laminate are measured, as well as the laminate curvature. The curvature is determined by measuring the lengths $\bar{\lambda}$ and $\rho$, represented in Fig. 6-2. Using the expression derived in Appendix C, the curvature of the laminate can be related to $\rho$ and $\bar{\lambda}$ by

$$a = \frac{2\rho}{\rho^2 + \frac{\bar{\lambda}^2}{4}}. \tag{6.1}$$

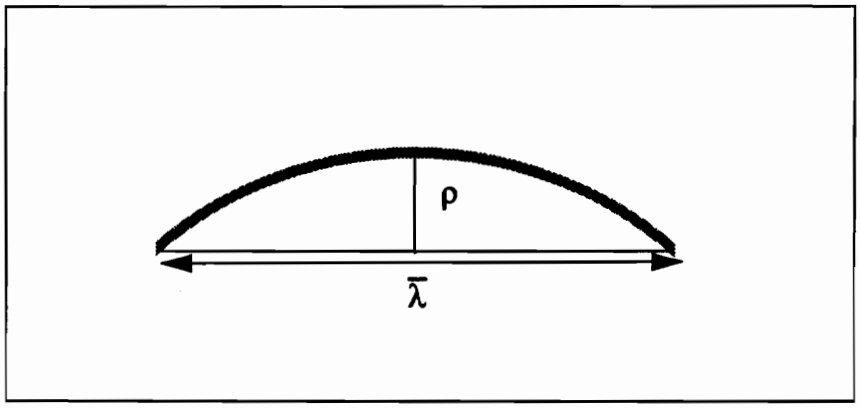


**FIG. 6-2. Laminate curvature measurement**

Thus, for increasing voltage, the current I, the SMA-induced-strains, and the curvature are measured. The experiments are conducted several times. Each time the laminate snaps under the SMA wire actuation, it is manually snapped back to its original shape. During this action, the SMA wire is stretched back and is ready to recover this strain for a repeat of the experiment.

## 6.2 *Experimental results*

Figure 6-3 represents the measured curvature as a function of the voltage. For a voltage less than 1 V, the curvature does not change. Thus, at this voltage the temperature in the SMA wire is not to be high enough to induce martensite transformation. For greater voltages, the curvature decreases very quickly. The SMA-induced force is large, which means that martensite is transforming into austenite. For a voltage of about 3 V, the SMA-induced force is large enough to make the laminate snap. Ideally the voltage could be related to the force and comparisons between the data of Fig. 6-3 and predictions similar to those of Fig. 5-9 (a) could be made. As mentioned, issues with the heat transfer of the problem prevent a direct comparison. It is noticed that the initial curvature slightly decreases from one repeat experiment to the other. The reason is that the laminate does not provide enough resistance to sufficiently elongate the SMA wire to its initially stretched length.

The measurement of the strains turns out not to be satisfactory. With a SMA-induced force, the local deformations and unwanted asymmetries in the response appear to be important enough that they affect the strains. Moreover, the strain gages may have been influenced by the heat radiating from the SMA wire to the laminate. Thus, the experimental strains are not presented.

The measurement of the current going through the SMA wire as a function of the voltage, Fig. 6-4, provides informations about the phase transformation. For low voltage, the current varies linearly. Then, when the voltage reaches about 1 V, the slope increases. Thus, the resistance of the SMA wire is changing. This change is strongly associated with the martensite transformation. In martensite phase, the SMA wire has more resistance than

in austenite phase.

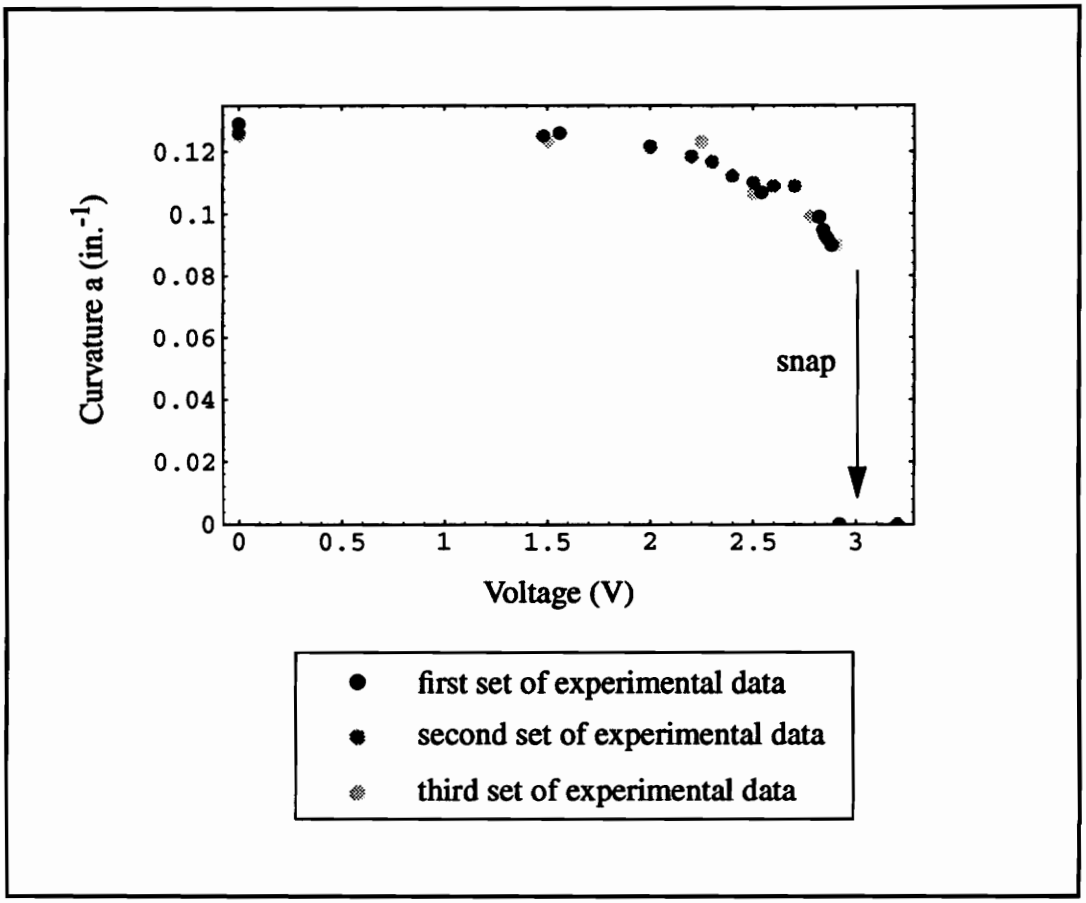


**FIG. 6-3. Measured curvature as a function of the applied voltage**

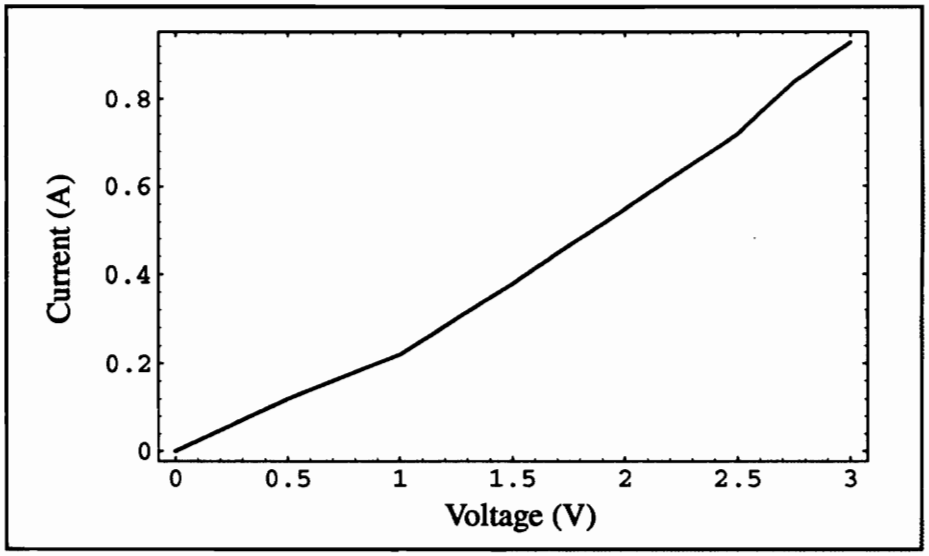


**FIG. 6-4. Current I as a function of the applied voltage**

## *6.3 Conclusion*

These experiments show that SMA material attached to an unsymmetric laminate can make the laminate curvature decrease and can even provide enough force to make the laminate change its shape. The experimental results can not directly be compared to the theory developed in chapter 5 since the curvature is measured as a function of the voltage, whereas the predicted curvature is related to the temperature. However, by studying the heat transfer occurring in the SMA, the temperature may be related to the voltage. That is beyond the scope of this study. The heat transfer problem is rather complicated (convection and radiation) and the thermal properties of the SMA wire are not precisely known. Thus, other experiments would be necessary to characterize the heat transfer and

the thermal properties of the SMA wire to be able to establish correlations between the experimental results and the predictions.

# 7.0 Closure

## *7.1 Summary*

After having presented a previously-developed theory predicting the room-temperature shape of cross-ply unsymmetric laminate, equations relating the shape of the laminate to an applied force have been derived. Force-induced strains and displacements have been predicted and checked by conducting experiments where the force was generated by a weight. Since very good correlations were obtained, SMA wires were introduced to generate the force. Equations describing the mechanics of the laminate subjected to SMA-induced forces have been derived. Relations were established between the SMA-induced force and the SMA temperature, and between the laminate curvature and the SMA temperature. Experiments were conducted and curvature was measured as a function of the applied voltage. Since a heat transfer study was required to be able to compare the experimental results to the predictions, comparisons could not be established. However, these experiments showed that SMA wires could be efficiently used as actuators to control the shape of unsymmetric laminates.

## 7.2 Conclusion

It can be concluded that

- Room temperature shapes of cross-ply unsymmetric laminates are predictable.
- The overall response of cross-ply laminates to applied forces is predictable. Forces required to snap the laminate can be predicted with high accuracy. However, near the snap condition, correlations with the theory are not as good since local deformations influence the strain and displacement measurements.
- The qualitative effects of SMA wires on unsymmetric laminates are predictable using established constitutive equations for SMA and the mechanics of unsymmetric laminates.
- Considerably more effort is needed to characterize SMA wires to achieve good quantitative correlation with predictions for this particular problem.

## 7.3 Recommendations for future work

Since local deformations were a problem in the experiments with the weight as well as in the experiments with the SMA wire, using a thicker laminate may provide better results.A thicker laminate has indeed a greater stiffness which may prevent local deformations from occurring. However, great force levels are required for producing laminate deformations. In conjunction with SMA wire, a thicker laminate would provide more resistance for the

SMA wire, which would be more completely stretched back to its initially stretched length. Moreover, a thicker laminate results a shallower curvature at room temperature. Thus, the supports displacements are smaller and the SMA wire may not touch the laminate to make it snap. Consequently, if the SMA wire does not touch the laminate, the heat does not radiate through the laminate and the heat transfer is simpler to model. Thus, it may be easier to correlate the temperature to the applied voltage, and comparisons of the experimental results to the theory may be established.

# References

1. PAGANO, N. J. and HAHN, H. T., *Evaluation of Composite Curing Stresses*, In J.G. Davis, Jr. (Ed), Composite Materials: Testing and Design, 4th Conference, American Society for Testing and Materials, Philadelphia, 317-329 p., 1977.

2. BERT, C. W. and MAYBERRY, B. L., *Free vibrations of Unsymmetrically Laminated Anisotropic Plates with Clamped Edges*, J. Composite Materials, Vol. 3, 282 p., 1969.

3. WHITNEY, J. M., *Bending-Extensional Coupling in Laminated Plates Under Transverse Loading*, J. Composite Materials, Vol. 3, 20 p., 1969.

4.WHITNEY, J. M., *Shear Buckling of Unsymmetrical Cross-Ply Plates*, J. Composite Materials, Vol. 3, 359 p., 1969.

5. HYER, M. W., *Some Observations on the Cured Shapes of Thin Unsymmetric Laminates*, J. Composite Materials, 15, 175-194 p., 1981.

6. HYER, M. W., *Calculations of the Room-Temperature Shapes of Unsymmetric Laminates*, J. Composite Materials, 15, 296-310 p., 1981.

7. HYER, M. W., *The Room-Temperature Shape of Four-Layer Unsymmetric Cross-Ply Laminates*, J. Composite Materials, 16, 318-340 p., 1982.

8. HAMAMOTO, A. and HYER, M.W., *Non-Linear Temperature-Curvature Relationships for Unsymmetric Graphite Epoxy Laminate*, Int. J. Solids Structures, 23, No 7, 919-935 p., 1987.

9. DANG, J., *Calculation of the Room-Temperature Shapes of Unsymmetric Laminates*, Proceedings of International Symposium on Composite Materials and Structures, Technomic, Lancaster, 201-206 p., 1986.

10. MÜLLER, L., *A Model for a Body with Shape Memory*, Arch. Rat. Mech. Anal., 70, 61-77 p., 1979.

11. TANAKA, K. and NAGASAKI, S., *A Thermomechanical Description of Materials with Internal Variables in the Process of Phase Transformation*, Ingenieur-Archiv, 51, 287-299 p., 1982.

12. LIANG, C. and ROGERS, C., *One Dimensional Thermomechanical Constitutive Relations for Shape Memory Materials*, AIAA Journal, 90, 1027 p., 1990.

13. LIANG,C. and ROGERS, C., *Design of shape memory alloy actuators*, Journal of Mechanical Design, 11, 223 p., 1992.

# Appendix A: Laminate elastic properties measurement

## Principle

The elastic properties of the laminate are determined experimentally by conducting tensile tests.

One tensile test is conducted on a composite specimen loaded in the fiber direction to evaluate the elastic modulus in the fiber direction, $E_1$, and the Poisson's ratio $\nu_{12}$. While the specimen is loaded, the stress, $\sigma_1$, the strain in the fiber direction, $\varepsilon_1$, and the stress across the fiber direction, $\varepsilon_2$, are recorded. From these data, linear functions relating the stress $\sigma_1$ and the strain $\varepsilon_2$, to the strain $\varepsilon_1$ are computed. These relations can be expressed as

$$\begin{aligned} \sigma_1 &= E_1\varepsilon_1 + \sigma_1^o \\ \varepsilon_2 &= \nu_{12}\varepsilon_1 + \varepsilon_2^o, \end{aligned} \tag{A.1}$$

where $\sigma_1{}^o$ and $\varepsilon_2{}^o$ are, respectively, the effective initial stress and strain resulting from experimental errors in the measurements. From these functions, $E_1$ and $\nu_{12}$ are determined.

Another test is conducted on a composite specimen loaded perpendicular to the fiber direction to determine the elastic modulus in the matrix direction $E_2$. While the specimen

is loaded, the stress $\sigma_2$ and the strain across the fiber direction, $\varepsilon_2$, are recorded. From these data, a linear function relating the force to the strain is computed and can be expressed as

$$\sigma_2 = E_2\varepsilon_2 + \sigma_2^o, \tag{A.2}$$

$\sigma_2^o$ representing the influence of experimental error. From this function, $E_2$ is determined.

## Experimental setup description

The tensile testing is done on a MTS load frame. The loading rate during the tests is 0.002 in/min. The maximum load level for the tensile test in the fiber direction is 1600 lb. For the tensile test perpendicular to the fiber direction, the load does not exceed 80 lb. The stress levels and the associated strains are recorded every second with an IBM data acquisition system. Two specimens of length l, width $\bar{w}$ and thickness $\bar{h}$, are tested. One, with the fibers along its length has four strain gages bonded to its surface. Two, back to back, in the fiber direction measure the elastic modulus $E_1$, and two, back to back, perpendicular to the fibers measure the Poisson's ratio, $\nu_{12}$, as shown in Fig. A-1.

The dimensions of this specimen are

l=5 in.

$\bar{h}$=0.0200 in.

$\bar{w}$=1.0008 in.

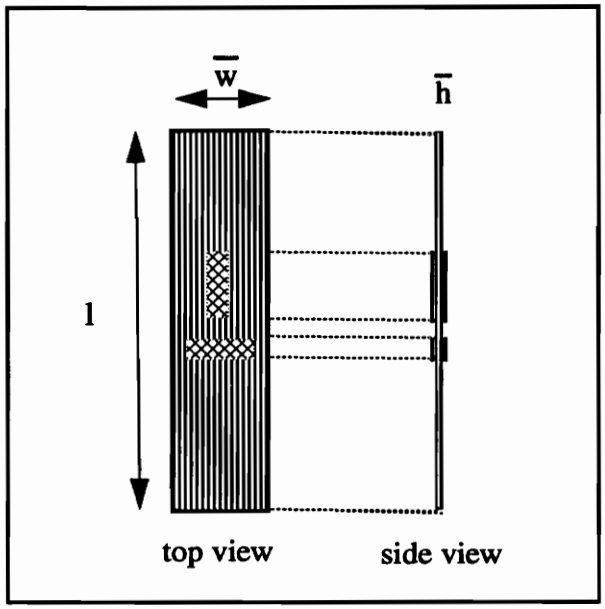


**FIG. A-1. Characteristics of the specimen with fibers along its length**

The other specimen, with the fibers perpendicular to the length, has only two back-to-back strain gages bonded on its surface to measure the elastic modulus $E_2$, as shown in Fig. A-2. The Poisson's ratio $\nu_{21}$ is not evaluated since it is very difficult to measure. The specimen dimensions are:

$l$=5 in.

$\bar{h}$=0.0212in.

$\bar{w}$=1.0060 in.

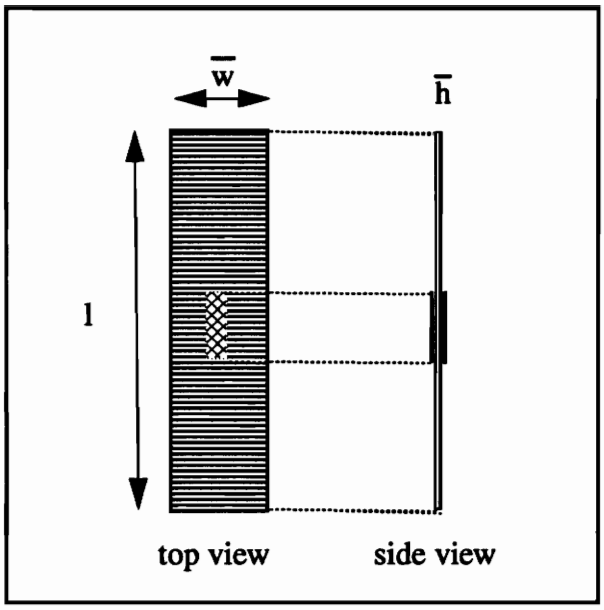


**FIG. A-2. Characteristics of the specimen with fibers perpendicular to length**

## Results

The data recorded during the tensile test on the composite specimen loaded in the fiber direction lead to two graphs, one for each set of two back-to-back strain gages. The plot of Fig. A-3 represents the stress $\sigma_1$ as a function of the strain in the loading direction, $\varepsilon_1$. Here $\varepsilon_1$ is the average of the two back-to-back gages in the fiber direction. The approximate linear function found to relate the stress to the strain is

$$\sigma_1 = 24.7710^6\varepsilon_1 + 118.44. \tag{A.3}$$

Thus,

$$E_1=24.77 \text{ Msi.} \tag{A.4}$$

Figure A-4 represents the strain perpendicular to the fibers, $\varepsilon_2$, as a function of the strain in the loading direction, $\varepsilon_1$. Here $\varepsilon_2$ is also the average of two back-to-back gages. The approximate linear function relating $\varepsilon_2$ to $\varepsilon_1$ is

$$\varepsilon_2 = 0.3353\varepsilon_1. \tag{A.5}$$

Thus, the Poisson's ratio is equal to

$$\nu_{12} = 0.3353. \tag{A.6}$$

The data from the second tensile test leads to another graph, corresponding to the set of two back-to-back strain gages measuring the strain in the fiber direction, $\varepsilon_2$, as a function of the stress $\sigma_2$. The stress $\sigma_2$ is presented in Fig. A-5 as a function of the strain $\varepsilon_2$. The linear function approximating the plot the best is

$$\sigma_2 = 1.27110^6\varepsilon_2 + 300.55. \tag{A.7}$$

Thus, the elastic modulus in the matrix direction is equal to

$$E_2=1.271 \text{ Msi}. \tag{A.8}$$

The elastic properties of the laminate are consequently

$$\begin{aligned} E_1&=24.77 \text{ Msi} \\ E_2&=1.271 \text{ Msi} \\ \nu_{12}&=0.3335. \end{aligned} \tag{A.9}$$

These values are used in the computation of the predictions in chapters 4 and 6.

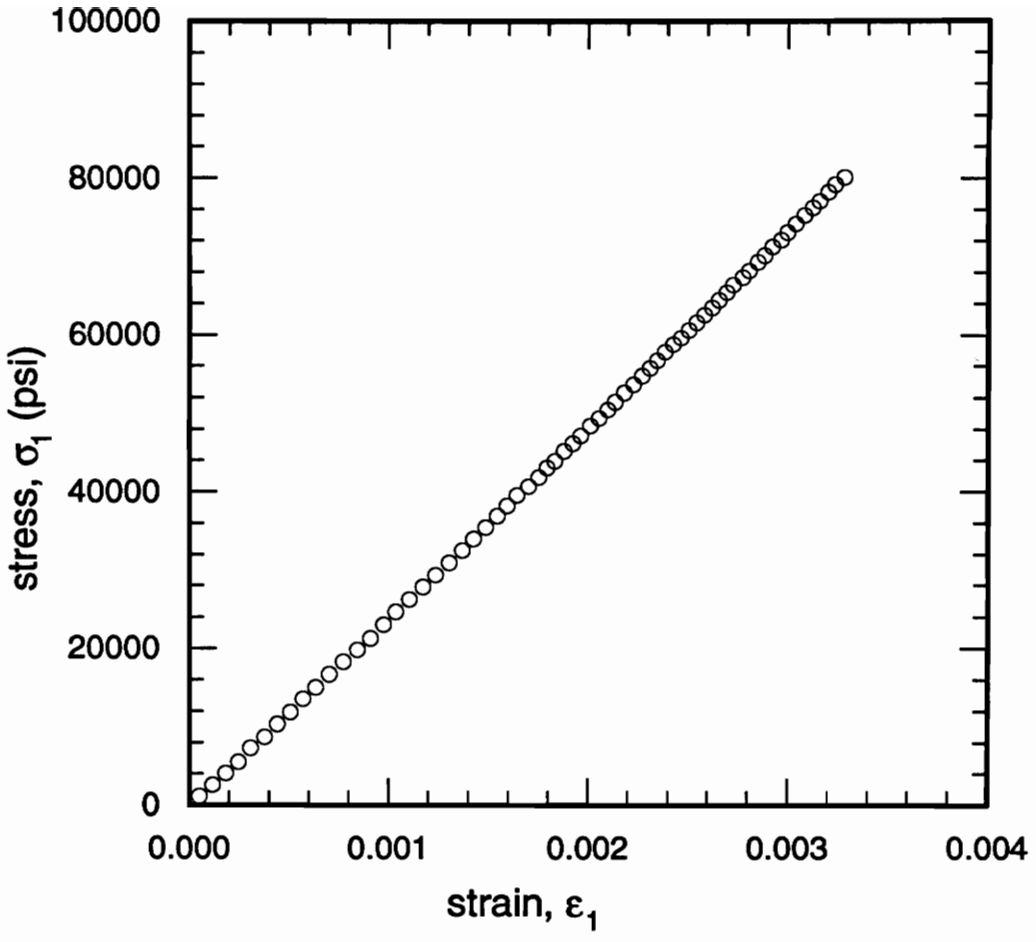


**FIG. A-3. Applied stress as a function of the strain in the fiber direction**

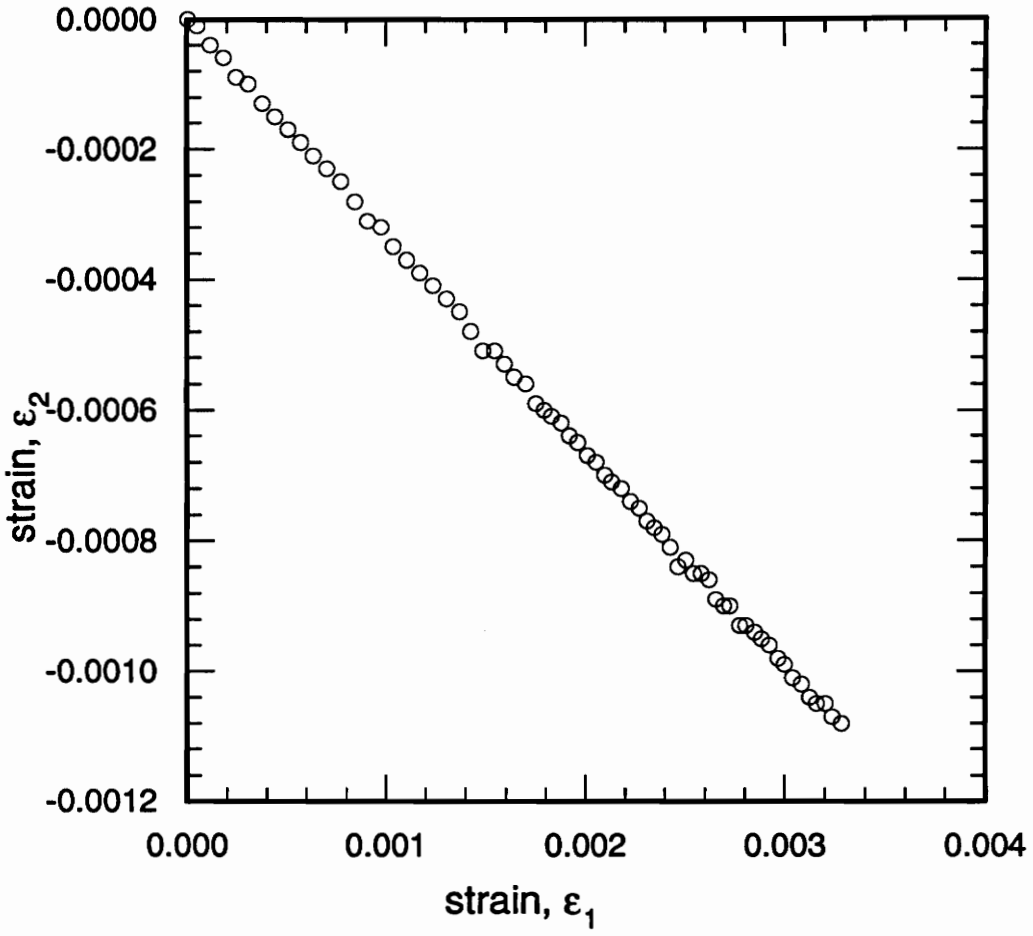


**FIG. A-4. Strain in the direction perpendicular to the fibers as a function of the strain in the fiber direction**

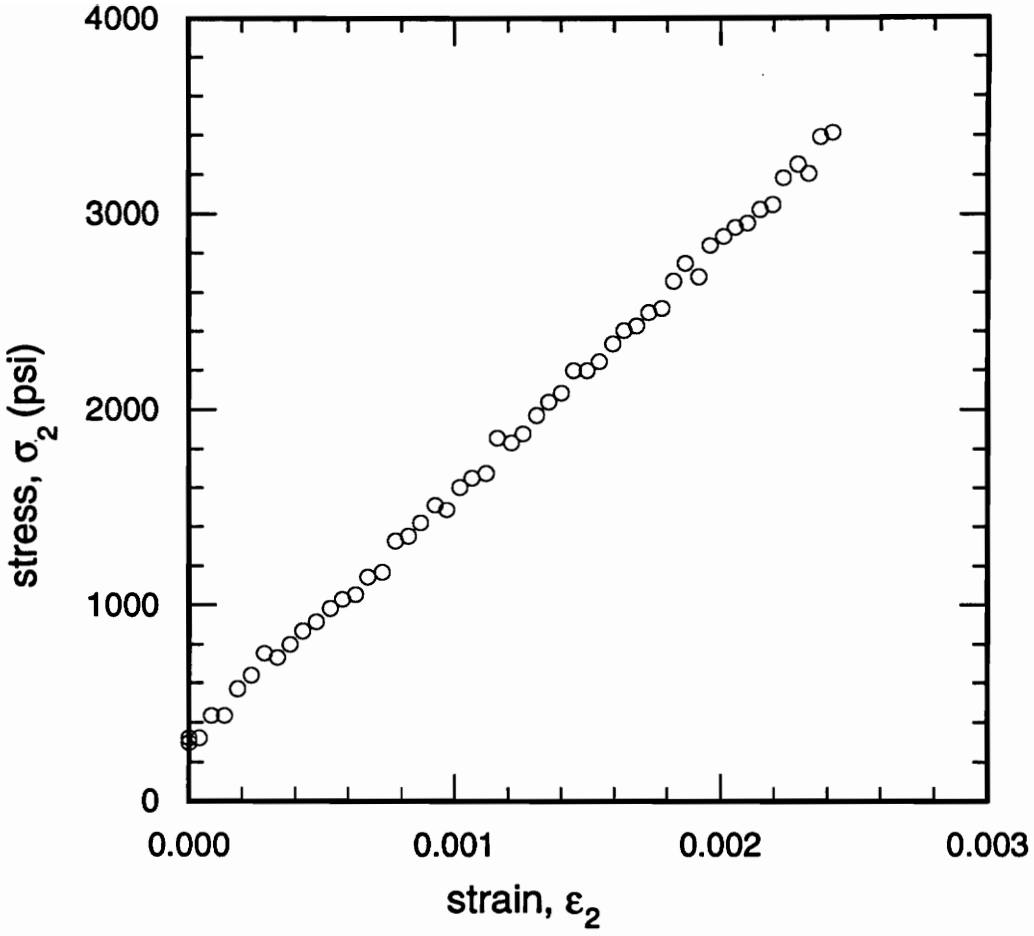


**FIG. A-5. Applied stress as a function of the strain in the direction perpendicular to the fibers**

# Appendix B: Laminate thermal expansion coefficients measurement

## Principle

The thermal expansion coefficients in the fiber direction, $\alpha_1$, and in the matrix direction, $\alpha_2$, are determined by measuring at different temperatures the strains in the fiber direction, $\varepsilon_1$, and perpendicular to the fiber direction, $\varepsilon_2$, of a unidirectional composite specimen. For a known temperature change $\Delta T$, and known strains $\varepsilon_1$ and $\varepsilon_2$, the thermal expansion coefficients $\alpha_1$and $\alpha_2$ are easily computed by

$$\alpha_1 = \frac{\varepsilon_1}{\Delta T}$$
$$\alpha_2 = \frac{\varepsilon_2}{\Delta T}. \qquad \text{(B.1)}$$

## Experimental setup description

Since the strain gages used to measure the strains responded to a temperature change, even though there is no actual change in strain level, a piece of titanium silicate with a coefficient of thermal expansion of negligible magnitude compared to those of composite

materials is used as a reference for the strains measurement. Indeed, the strain measured on the titanium silicate corresponds to the apparent thermal-induced strains of the strain gages. This strain, denoted $\varepsilon_T$ has to be subtracted from the strains measured by the gages on the composite specimen to obtain the actual thermal-induced strains in the composite. To check the validity of this experiment, a piece of aluminium, whose thermal expansion coefficient is well known, is also tested.

Four strain gages are bonded to the composite specimen, two, back-to-back, in the fiber direction, and two, back-to-back, perpendicular to the fiber direction, as shown in Fig. B-1. Two strain gages are bonded back-to-back on the aluminium specimen, whereas only one strain gage is used on the titanium silicate specimen.

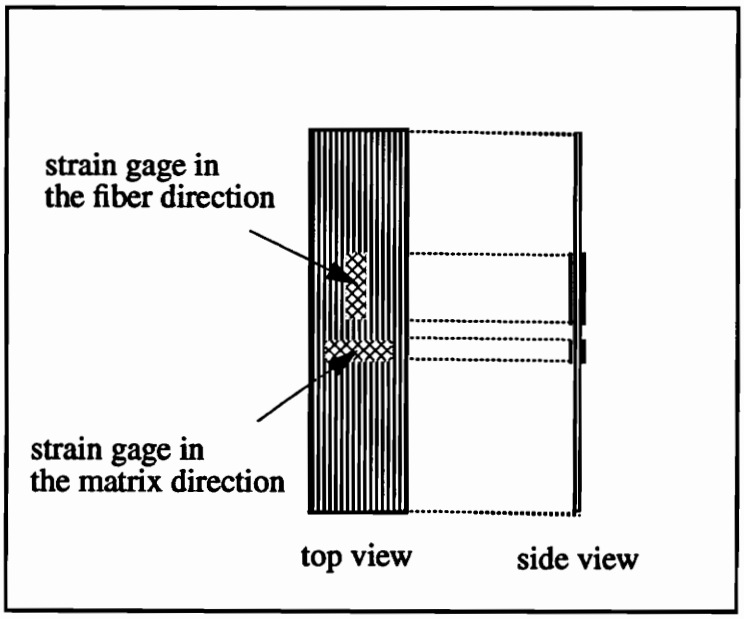


**FIG. B-1. Composite specimen characteristics**

A thermocouple taped to each of the three specimens, and two thermocouples in the oven chamber, one in the back and one in the front, are used to measure the temperature.

Moreover, a mercury thermometer is used as a check of temperatures measured by the thermocouples. Thus, for each temperature change, seven strains and six temperatures are recorded.

Starting with room temperature, the temperature is increased up to 175 °F. Strains and temperatures are measured five times, first at the initial temperature, i.e., room temperature, then four other times, at 100 °F, 125 °F, 150 °F and 175 °F.

## Results

The measured strains and temperatures are presented in Table B-1 where the notations used for the different temperatures and strains are given below.

$T_{th}$: temperature read on the mercury thermometer in the oven

$T_{ov1}$, $T_{ov2}$: temperatures of the thermocouples in the oven

$T_c$: temperature of the thermocouple on the composite specimen

$T_{al}$: temperature of the thermocouple on the aluminium specimen

$T_r$: temperature of the thermocouple on the titanium silicate specimen

$\varepsilon^t_{c_1}$ : strain in the fiber direction on the composite specimen, top surface

$\varepsilon^b_{c_1}$ : strain in the fiber direction on the composite specimen, bottom surface

$\varepsilon^t_{c_2}$ : strain in the matrix direction of the composite specimen, top surface

$\varepsilon^b_{c_2}$ : strain in the matrix direction of the composite specimen, bottom surface

$\varepsilon^t_{al}$ : strain of the aluminium specimen, top surface

$\varepsilon^b_{al}$ : strain of the aluminium specimen, bottom surface

$\varepsilon_r$ : strain of the titanium silicate specimen

**TAB. B-1. Experimental strains as a function of temperature**

| | | 1 | 2 | 3 | 4 | 5 |
|---|---|---|---|---|---|---|
| T ($^oF$) | $T_{th}$ | 83 | 99 | 125 | 149 | 175 |
| | $T_{ov1}$ | 83 | 99 | 125 | 150 | 176 |
| | $T_{ov2}$ | 83 | 99 | 125 | 149 | 175 |
| | $T_c$ | 83 | 99 | 125 | 150 | 175 |
| | $T_{al}$ | 83 | 100 | 125 | 149 | 174 |
| | $T_r$ | 83 | 99 | 125 | 149 | 174 |
| Strains ($10^{-6}$) | $\varepsilon^t_{c_1}$ | 0 | -112 | -298 | -481 | -675 |
| | $\varepsilon^b_{c_1}$ | 0 | -110 | -297 | -480 | -673 |
| | $\varepsilon^t_{c_2}$ | 0 | 123 | 335 | 527 | 720 |
| | $\varepsilon^b_{c_2}$ | 0 | 128 | 320 | 498 | 681 |
| | $\varepsilon^t_{al}$ | 0 | 94 | 235 | 366 | 505 |
| | $\varepsilon^b_{al}$ | 0 | 94 | 236 | 368 | 508 |
| | $\varepsilon_r$ | 0 | -122 | -319 | -507 | -707 |

To obtain the thermal-induced strains of the composite and aluminium specimens as a function of the temperature change $\Delta T$, the reference strain, $\varepsilon_r$, must be subtracted from the measured strains, and the initial temperature subtracted from the measured temperatures. Table B-2 presents, for the five temperatures, the corresponding temperature change and thermal-induced strains.

**TAB. B-2. Thermal-induced strains as a function of the temperature change**

| | | 1 | 2 | 3 | 4 | 5 |
|---|---|---|---|---|---|---|
| $\Delta T$ ($^oF$) | | 0 | 16.2 | 42 | 66.4 | 91.8 |
| Strains ($10^{-6}$) | $\varepsilon_{c_1} - \varepsilon_r$ | 0 | 11 | 21.5 | 26.5 | 33 |
| | $\varepsilon_{c_2} - \varepsilon_r$ | 0 | 247.5 | 646.5 | 1019.5 | 1407.5 |
| | $\varepsilon_{al} - \varepsilon_r$ | 0 | 216 | 554.5 | 874 | 1213.5 |

The temperature change, $\Delta T$, is the average of the six measured temperatures minus the average initial temperature, and the thermal-induced strains $\varepsilon_{c_1}$, $\varepsilon_{c_2}$, $\varepsilon_{al}$ are the average of the strains measured on the top and bottom surface of the specimens. Thus,

$$\begin{aligned} \Delta T &= \frac{T_r + T_{al} + T_c + T_{ov1} + T_{ov2} + T_{th}}{6} - 83 \\ \varepsilon_{c_1} &= \frac{\varepsilon_{c_1}^t + \varepsilon_{c_1}^b}{2} \\ \varepsilon_{c_2} &= \frac{\varepsilon_{c_2}^t + \varepsilon_{c_2}^b}{2} \\ \varepsilon_{al} &= \frac{\varepsilon_{al}^t + \varepsilon_{al}^b}{2}. \end{aligned} \tag{B.2}$$

The thermal-induced strains of the composite and the aluminium specimens are plotted as a function of the temperature change. An interpolation of the form

$$y = ax + b \tag{B.3}$$

is computed to find a linear approximation which fits the data the best. The thermal expansion coefficients are then evaluated by determining the derivative of the approximative function.

The plots obtained for the composite specimen are presented in Fig. B-2 and Fig. B-3. Figure B-2 illustrates the relation between the thermal-induced strains in the fiber direction and the temperature change, whereas Fig. B-3 represents the relation between the thermal-induced strains perpendicular to the fiber direction and the temperature change. For both figures, an interpolation is computed from which the thermal expansion coefficients are determined. As indicated on the figures, the thermal expansion coefficients in the fiber direction and the matrix direction are, respectively,

$$\begin{aligned} \alpha_1 &= 0.3435\ 10^{-6}\ /^{\circ}\mathrm{F} \\ \alpha_2 &= 15.34\ 10^{-6}\ /^{\circ}\mathrm{F}. \end{aligned} \tag{B.4}$$

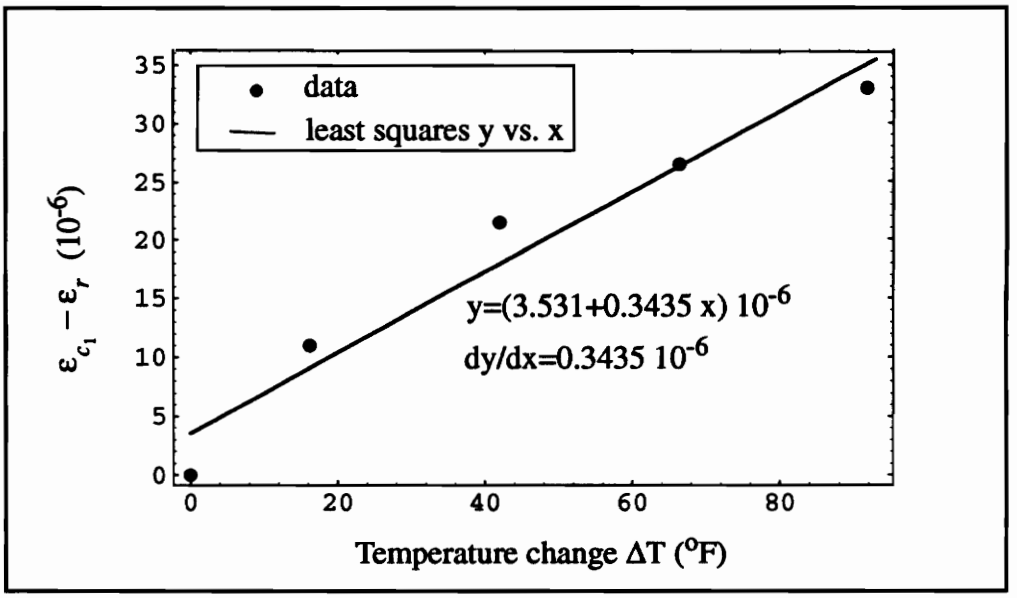


**FIG. B-2. Composite thermal-induced strain in the fiber direction vs. the temperature change**

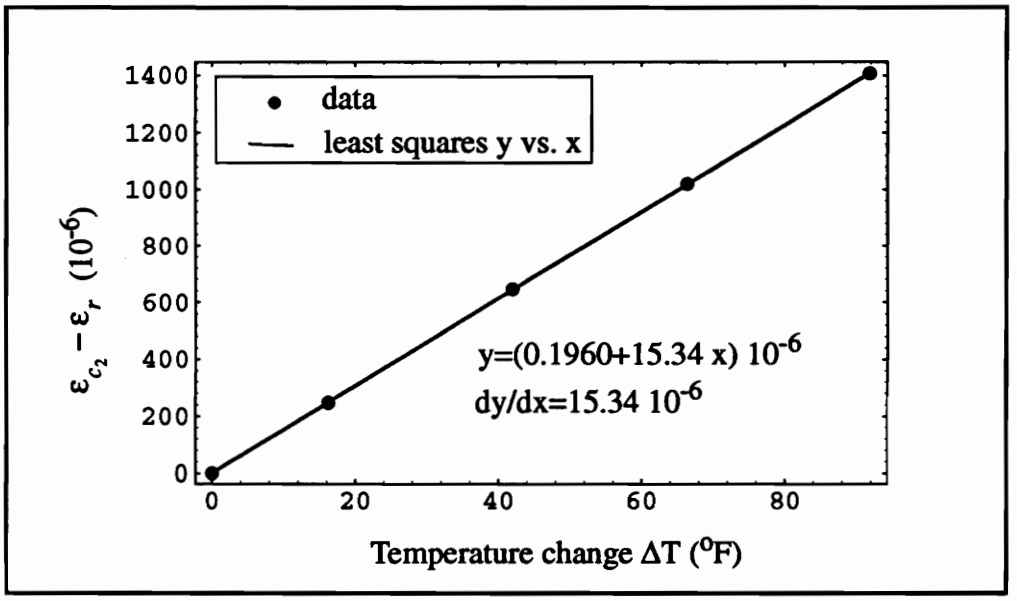


**FIG. B-3. Composite thermal-induced strain in the matrix direction vs. the temperature change**

Figure B-4, represents the relation between the thermal-induced strain and the temperature change obtained for the aluminium specimen. From the interpolation function, the thermal expansion coefficient is

$$\alpha=13.19\ 10^{-6}\ /^{o}F. \tag{B.5}$$

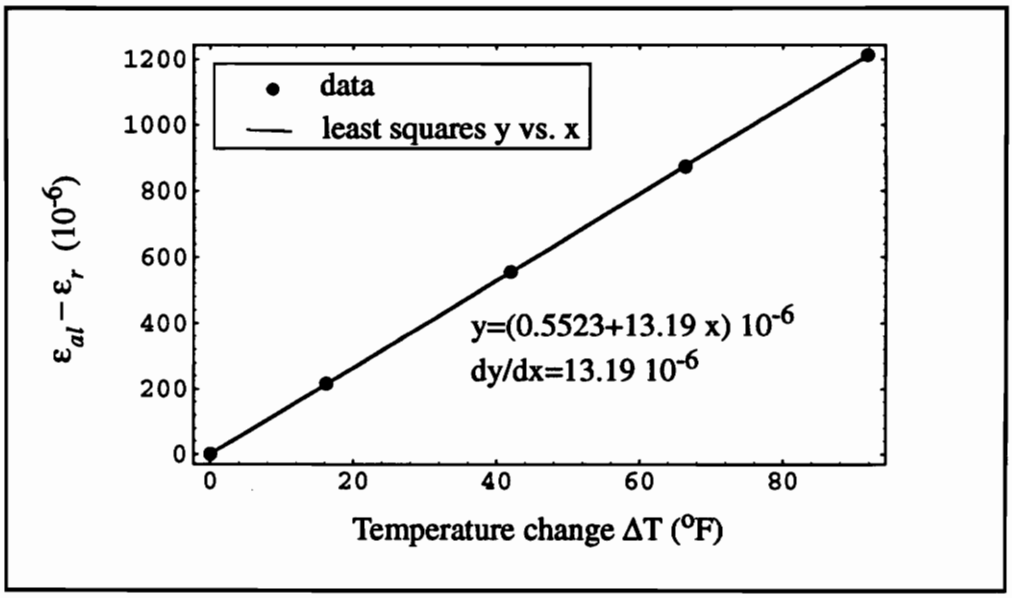


**FIG. B-4. Aluminium thermal-induced strain vs. the temperature change**

Since the value which is usually used for this coefficient is 13 $10^{-6}$, this experimental value is a very good measurement of the thermal expansion coefficient.

## Conclusion

Since the value found experimentally for the thermal expansion coefficient of the aluminium is very close to the theoretical one, the experimental setup seems to provide reliable experimental results. Thus, the experimental values found for the thermal

expansion coefficients of the composite specimen are assumed to be accurate.

# Appendix C: Laminate curvature measurement

The laminate curvature is experimentally determined by approximating the laminate's shape with a circle. Indeed, the curved contour of the laminate can be considered as a portion of a circle of radius R, as shown in Fig. C-1.

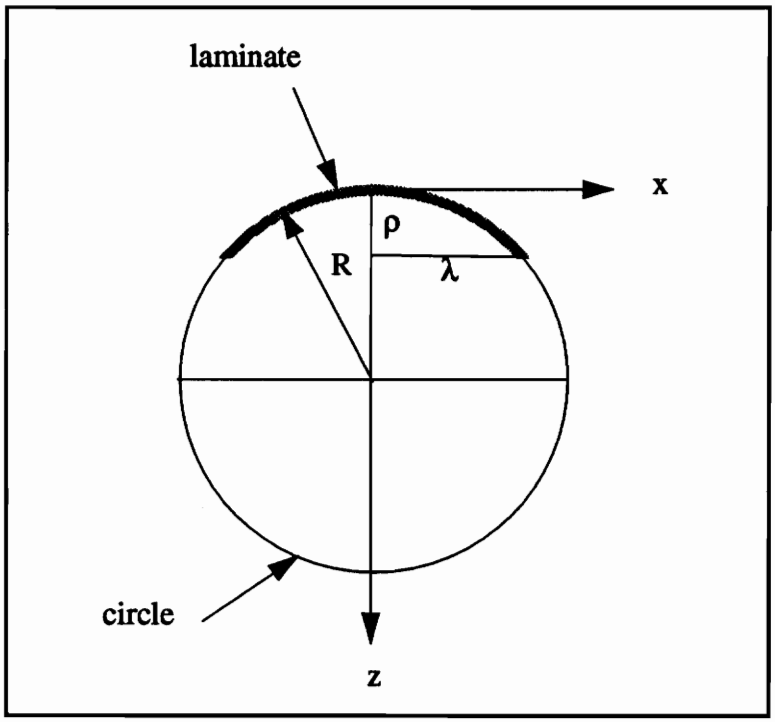


**FIG. C-1. Approximation of the laminate contour shape by a circle**

The equation of the upper half circle in the coordinate system represented in Fig. C-1 is

$$z = -\sqrt{R^2 - x^2} + R. \tag{C.1}$$

By substituting known values for x and z, the radius of the circle, R, is determined. From the laminate, values for x and z can be measured, which are represented in Fig. C-1 by, respectively, $\rho$ and $\lambda$.

Thus, Eq. (C.1) can be written as

$$\rho = -\sqrt{R^2 - \lambda^2} + R. \tag{C.2}$$

After some manipulations on the expression (C.2), the curvature 'a' of the laminate can be obtained,

$$a = R^{-1} = \frac{2\rho}{\rho^2 + \lambda^2}. \tag{C.3}$$

For any cross-ply unsymmetric laminate, the curvature of the laminate can be determined by measuring the lengths $\rho$ and $\lambda$ and by substituting these values in Eq. (C.3).

# Appendix D: Additional experiments checking the theory of chapter 3

The experiments which are presented in this appendix, Fig. D-1, were conducted on a laminate where the moisture absorbing was not controlled. Thus, the presence of moisture may have affected the initial curvature, and possibly the material properties. However, the experimental results confirm the predictions finally well. More importantly, Fig. D-1 illustrates the good repeatability of the experimental results.

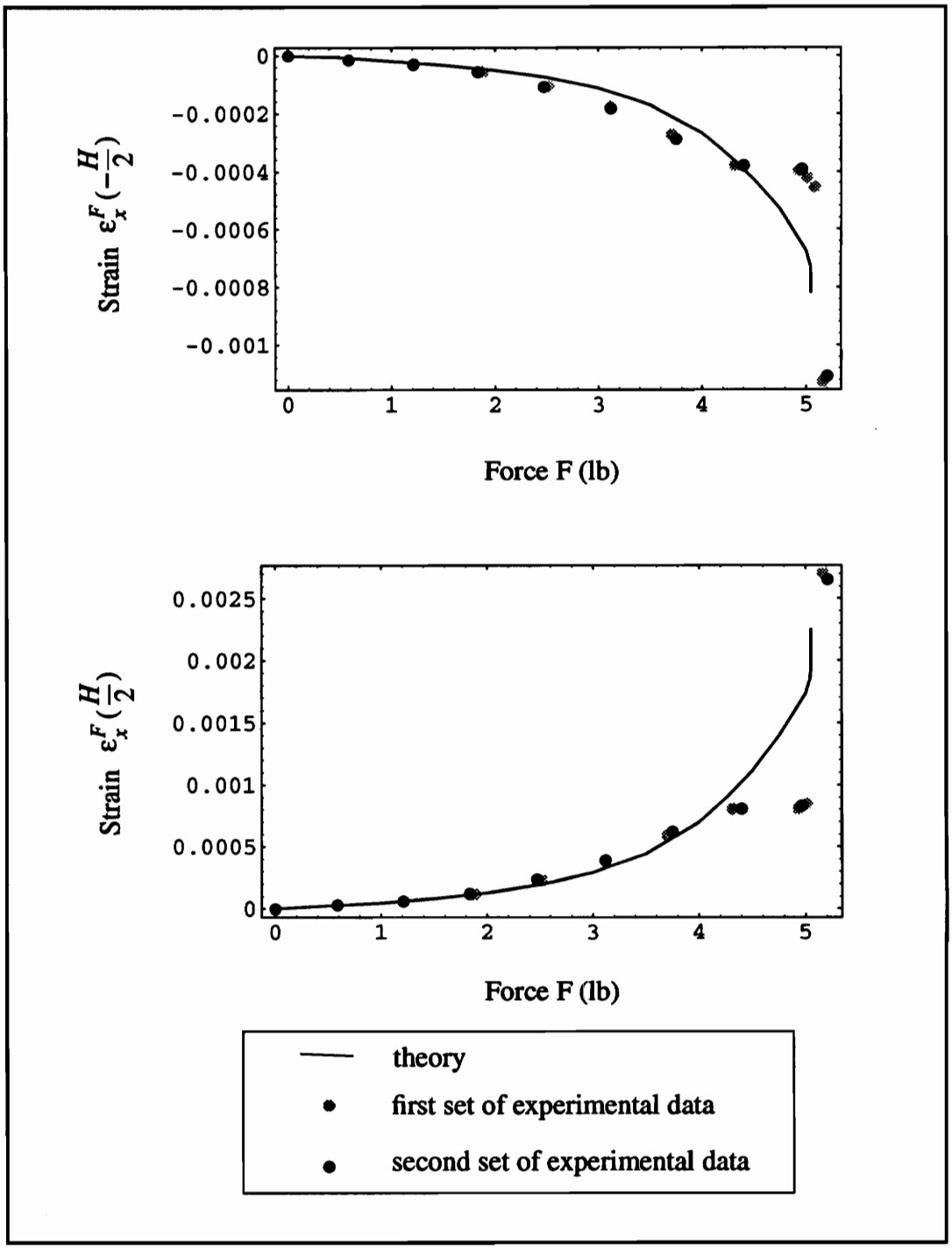


**FIG. D-1. Additional comparisons of experimental strains with theoretical strains**

# Appendix E: Computation of the support coordinates and of the tangent point coordinates

## Support coordinates computation

The coordinates ($S_x$,$S_z$) of the support end point S can be computed using the midplane field displacements, $u^o$ and $w^o$. From Figs. E-1 and E-2, the coordinates $S_x$, $S_z$ can be expressed by

$$\begin{aligned} S_x &= L_{xp} + u^o + u^R \\ &= L_{xp} + cL_{xp} - a^2\frac{L_{xp}^3}{6} + (e + \frac{H}{2}) \sin(aL_{xp}) \end{aligned} \tag{E.1}$$

$$\begin{aligned} S_z &= -(e + \frac{H}{2}) + w^o + w^R \\ &= -(e + \frac{H}{2}) + \frac{aL_{xp}^2}{2} + (e + \frac{H}{2})(1 - \cos(aL_{xp})) \cdot \end{aligned} \tag{E.2}$$

Thus, for a given shape, the coordinates $S_x$ and $S_z$ can be easily evaluated.

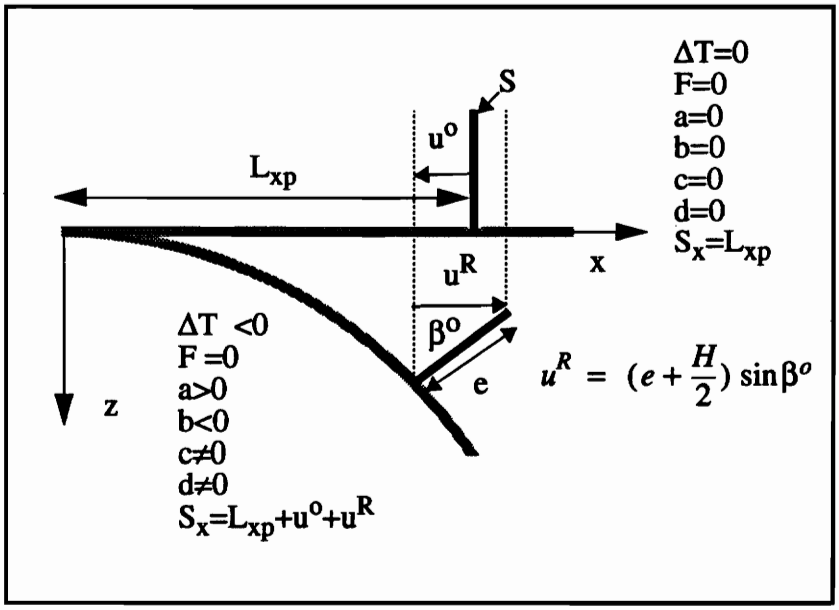


**FIG. E-1. Computation of the x coordinate of the support end**

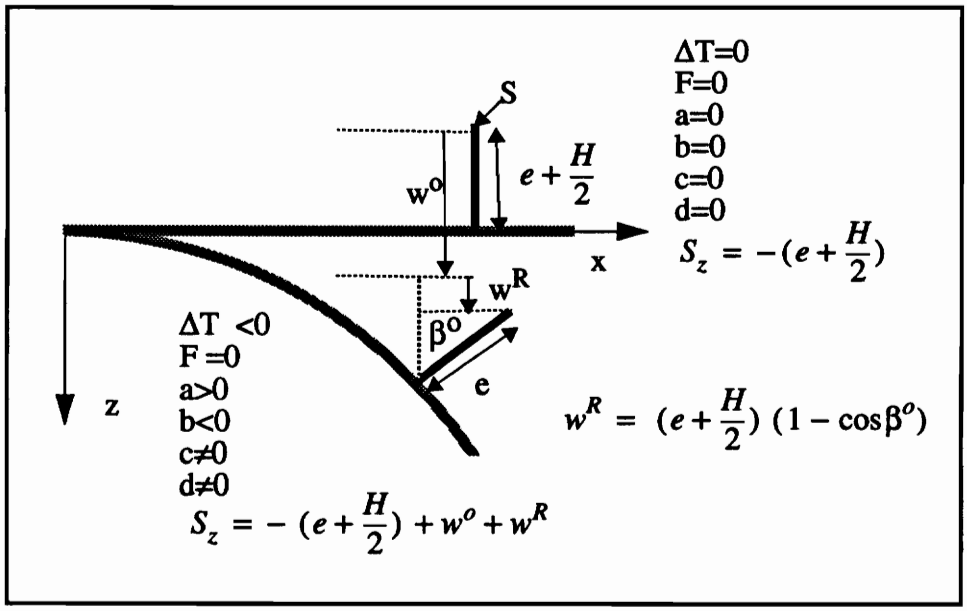


**FIG. E-2. Computation of the y coordinate of the support end**

## Computation of the tangent point coordinates

The coordinates of the point where the SMA wire becomes tangent to the laminate surface is computed using analytical equations for half-circle and straight line. In the coordinate system represented in Fig. E-3, the equation for the half-circle is

$$z = -\sqrt{r^2 - x^2} + r, \tag{E.3}$$

where r is the radius of the half-circle and is equal to

$$r = \frac{1}{a} + \frac{H}{2}, \tag{E.4}$$

a being the curvature of the laminate and H its thickness.

The slope at the point where the SMA wire becomes tangent to the laminate is

$$\left.\frac{dz}{dx}\right|_T = \frac{T_x}{\sqrt{r^2 - T^2{}_x}} = m, \tag{E.5}$$

where the point is denoted as $T(T_x, T_z)$. Thus, the equation of the straight line being tangent to the half-circle at point T can be expressed by

$$\begin{aligned} z - T_z &= m\,(x - T_x) \\ &= \frac{T_x}{\sqrt{r^2 - T^2{}_x}}\,(x - T_x) \end{aligned} \tag{E.6}$$

or

$$z = \frac{xT_x - T^2{}_x}{\sqrt{r^2 - T^2{}_x}} + T_z \cdot \tag{E.7}$$

Since point T is on the half-circle, its coordinates verify the half-circle equation and

$$T_z = -\sqrt{r^2 - T^2{}_x} + r \tag{E.8}$$

$$\sqrt{r^2 - T^2{}_x} = r - T_z \cdot \tag{E.9}$$

Substituting Eq. (E.9) into Eq. (E.7), Eq. (E.7) can be written as

$$\begin{aligned} z &= \frac{xT_x - T^2{}_x}{r - T_z} + T_z \\ &= \frac{xT_x - T^2{}_x + rT_z - T_z^2}{r - T_z} \\ &= \frac{xT_x - rT_z}{r - T_z} \\ &= \frac{xT_x - r^2}{r - T_z} + r \cdot \end{aligned} \tag{E.10}$$

Since the support end point S has to be on the tangent, its coordinates verify

$$S_z = \frac{S_x T_x - r^2}{r - T_z} + r. \tag{E.11}$$

By solving Eqs. (E.8) and (E.11) simultaneously, expressions relating the coordinates $T_x$, $T_z$ to $S_x$, $S_z$ are obtained.

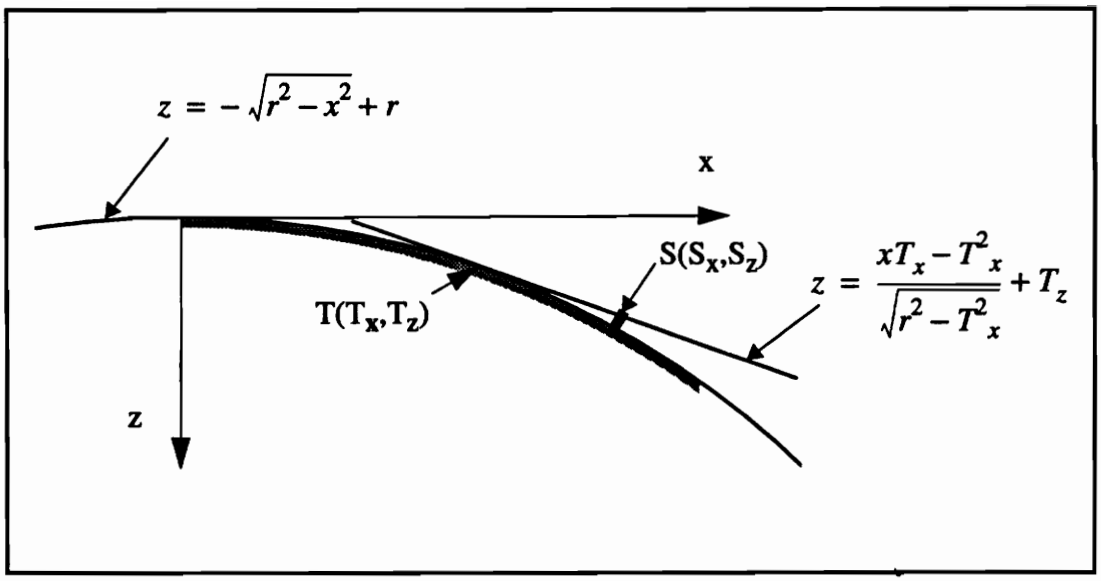


**FIG. E-3. Problem description**

Thus, for a given shape, corresponding to a certain force level, the coordinates of the support end are evaluated. Using these values, the coordinates of the point where the SMA wire becomes tangent to the laminate surface can be computed.

# Vitae

The author was born on March 18, 1970, in Saint Cloud, France. Upon completing high school, she pursued her studies at the "université de Technologie de Compiègne", (U.T.C.), France, in the department of Engineering Mechanics.While studying at the U.T.C., she participated in the U.T.C-Virginia Tech exchange program to enroll in the Master Program in Engineering Science and Mechanics at VPI&SU in August 1991. She received her french "Diplôme d'Ingénieur" in March 1993. After completing the requirements for a Master's Degree, she will pursue her studies at VPI&SU toward a Ph.D in the department of Engineering Science and Mechanics.

Marie-Laure Dano